Mathematical Modeling of Pathways Involved in Cell Cycle Regulation and Differentiation

Janani Ravi

Dissertation submitted to the faculty of the Virginia Polytechnic Institute and State University in partial fulfillment of the requirements for the degree of

Doctor of Philosophy

in

Genetics, Bioinformatics and Computational Biology

John J. Tyson, Chair

Kathy C. Chen

William T. Baumann

Carla V. Finkielstein

Kenneth B. Hannsgen

Jianhua Xing

01 December, 2011

Blacksburg, VA

Keywords: theoretical biology, bistability, START transition, cell size control, Wnt signaling

Mathematical Modeling of Pathways Involved in Cell Cycle Regulation and Differentiation

Janani Ravi

Abstract

Cellular processes critical to sustaining physiology, including growth, division and differentiation, are carefully governed by intricate control systems. Deregulations in these systems often result in complex diseases such as cancer. Hence, it is crucial to understand the interactions between molecular players of these control systems, their emergent network dynamics, and, ultimately, the overall contribution to cellular physiology. In this dissertation, we have developed a mathematical framework to understand two such cellular systems: an early checkpoint (START) in the budding yeast cell cycle (Chapter 1), and the canonical Wnt signaling pathway involved in cell proliferation and differentiation (Chapter 2). START transition is an important decision point where the cell commits to one round DNA replication followed by cell division. Several years of experimental research have gone into uncovering molecular details of this process, but a unified understanding is yet to emerge. In chapter one, we have developed a comprehensive mathematical model of START transition that incorporates several findings including information about the phosphorylation state of key START proteins and their subcellular localization. In the second chapter, we focus on modeling the canonical Wnt signaling pathway, a cellular circuit that plays a key role in cell proliferation and differentiation. The Wnt pathway is often deregulated in colon cancers. Based on some evidence of bistability in the Wnt signaling pathway, we proposed the existence of a positive feedback loop underlying the activation and inactivation of the core protein complex of the pathway. Bistability is a common feature of biological systems that toggle between ON and OFF states because it ensures robust switching back and forth between the two states. To study and explain the behavior of this dynamical system, we developed a mathematical model. Based on experimentally determined interactions, our simple model recapitulates the observed phenomena of bimodality (bistability) and hysteresis under the effects of the physiological signal (Wnt), a Wnt-mimic (LiCl), and a stabilizer of one of the key members of core complex (IWR-1). Overall, we believe that cell biologists and molecular geneticists can benefit from our work by using our model to make novel quantitative predictions for experimental verification.

Acknowledgements

I extend my sincere thanks to my advisor, Dr. John Tyson, for giving me this opportunity to be a part of his group. I'm immensely grateful to Dr. Kathy Chen for her constant mentorship, colleagueship, and care that she extended throughout during these five years. Members of my graduate research committee – Drs. Bill Baumann, Carla Finkielstein, Kenneth Hannsgen, and Jianhua Xing – have been patient and supportive to come to several committee meetings and offer useful guidance, and I'm very thankful to them for that. Thanks to Drs. Ethan Lee and Curtis Thorne for their fruitful collaboration and constant willingness to discuss and reconsider their experimental findings in the light of our mathematical model, and do more experiments when needed. It has been great to interact with the vibrant yeast research community during several meetings and conferences, and I wish to thank all its members, especially Drs. Fred Cross, Rob de Bruin, Jan Skotheim, Frank Uhlmann and Carlos Igual, for their valuable feedback.

Coming to the GBCB program at Virginia Tech opened up a wonderful vista of opportunities for learning from scholars in the field and meeting peers from a diverse background. I'm grateful to the program faculty and staff for having me here and making that time memorable. I thank the GBCB program director Dr. David Bevan for making this possible and constantly nurturing the program. No words of gratitude can match the contributions of Dennie Munson, our program coordinator, to the life of every GBCB student. Being our mother away from home, all of us religiously believe in Dennie's omnipresence and omnipotence in making things happen for us with a snap of her fingers!

I have had a great time in the Tyson lab during these five years thanks to several friendly and cheerful members. Many cheers to Jason Zwolak for not only writing the software PET and

JigCell that make up the invisible machines behind my day-to-day work building complex models, but also making them work! I'm grateful to: Tongli Zhang, Sandip Kar, Debashis Barik, Anael Verdugo and Baris Hancioglu for stimulating discussions; Cihan Oguz and Pavel Kraikivski for helpful feedback on the model and my presentations; and my buddies Oak, Kartik, Yan and Tian for their friendship and making the lab a wonderful place to work in.

My love and gratitude go to Arjun – my friend, philosopher and guide (incidentally my husband) – for always being there. Many thanks to my dear friends from Chennai – Viveka, Shailaja, Premal, Krishnan, Udaya, Archana and Samhita – and Blacksburg – Yamuna, Vandana, Naresh, Kartik, Satya, PK and friends from Asha for Education – for making our lives outside work special.

Finally, my family – parents Ravi and Jayanthi, sister Harshini, and grandparents – has been the nurturer, teacher, pamperer, selfless patron, critique and cheerleader. They have stood with me all along as I have taken my baby-steps to come to this stage. Naturally, with no words to thank, I dedicate this dissertation to them.

Table of Contents

List of Figures

Chapter 1

Chapter 2

List of Tables

Chapter 1

Introduction

Dynamical processes in the cell including growth, division and differentiation are carefully governed by intricate control systems. Deregulations in these systems often result in complex diseases such as cancer. Hence, it is crucial to understand the interactions between molecular players of these control systems, their emergent network dynamics, and, ultimately, the overall contribution to cellular physiology.

In this thesis, we have developed a mathematical framework to understand two such cellular systems: an early checkpoint in the budding yeast cell cycle (Chapter 1), and the canonical Wnt signaling pathway involved in cell proliferation and differentiation (Chapter 2).

The restriction point (R-point) is an important early checkpoint occurring in the G1 phase of the mammalian cell cycle, and passing this point serves as an irreversible commitment to enter S phase (DNA synthesis). An analogous checkpoint, called the START transition, governs the entry into S phase in the budding yeast cell cycle. Similarities between the mammalian R-point and the yeast START transition are manifold. Similar to the loss of sensitivity to mitogenic stimuli following passage through the R-point, START is marked by the loss of sensitivity to pheromones. The R-point and START are also mediated by very similar molecular mechanisms involving positive feedback loops that abruptly activate important transcription factors needed for the onset of S-phase. These S-phase molecules have other important downstream effects, such as relieving mitotic factors of repression by stoichiometric inhibitors and proteosomal degradation machinery.

A distinctive feature of START is size control. The irreversible transition from G1 into S phase in budding yeast cells requires, in addition to the absence of inhibitory pheromones (mating factors) that the cells grow to a minimal (threshold) size. Also, interestingly, the critical

size for passing through START in budding yeast cells depends on the nutrient media in which the cells are growing.

Motivated by the afore-mentioned similarities and differences between mammalian and yeast cells, we focus in the first chapter of this dissertation on the molecular details underlying START. We have incorporated many molecular details of this process into a comprehensive mathematical model, including information about the phosphorylation state of key START proteins and their subcellular localization.

In the second chapter, we focus on modeling the canonical Wnt signaling pathway, which plays a key role in cell proliferation and differentiation. The Wnt pathway is often deregulated in colon cancers. The most important downstream effect of this pathway is the nuclear accumulation of an activator, β-catenin (for a transcription factor, TCF). In unstimulated cells, the level of β-catenin is kept low by a destruction core complex present in the cytoplasm that targets it for proteasome-mediated degradation. In response to external stimuli, Wnt, β-catenin level rises and it enters the nucleus where it regulates the expression of several genes involved in cell proliferation and/or differentiation. This occurs because Wnt-bound transmembrane receptors disrupt the destruction core complex by recruiting most of its components to the membrane. Inactivation of the destruction core complex allows β-catenin to accumulate. In colon cancer cells, the function of the destruction core complex is often compromised by mutations of some of its components, such as scaffold proteins (Axin and APC), kinases (GSK3β and CK1α), and a phosphatase (PP2A).

Based on some initial evidence of bistability in the Wnt signaling pathway, Lee and Tyson (personal communication) proposed the existence of a positive feedback loop underlying the activation and inactivation of the destruction core complex. Our collaborators at Vanderbilt

University (Thorne and Lee) have provided additional experimental evidence for the existence of bistability in Wnt signaling. Bistability is a common feature of biological systems that toggle between ON and OFF states because it ensures robust switching back and forth between the two states. We, therefore, developed a mathematical model to explain this behavior in the Wnt signaling pathway. Based on experimentally determined interactions, our simple model recapitulates the observed phenomena of bimodality (bistability) and hysteresis under the effects of the physiological signal (Wnt), a Wnt-mimic (LiCl), and a stabilizer of one of the key members of destruction core complex (IWR-1, which stabilizes Axin).

Modeling the START transition in the Budding Yeast Cell Cycle

Abstract

In the budding yeast cell cycle, the START transition is a crucial cell cycle decision point, where the cell becomes (irreversibly) committed to DNA replication (S phase) and cell division, as it leaves G1. It is characterized by rapid degradation and inactivation of cyclin dependent kinase inhibitors. A key requirement for START is the growth of the yeast cell to a critical size threshold. Prior to START, yeast cells undergo cell cycle arrest in response to mating factors. However, once the cell has passed START, its further progression through the cell cycle is unresponsive to mating-factor-mediated arrest.

Physiologically, these properties of START are reminiscent of the Restriction point (R-point) in the mammalian cell cycle wherein cells become non-responsive to the removal of growth factors once they pass the R-point. Interestingly, this similarity arises due to the intrinsic wiring of the underlying molecular network. Similar to the pRb-E2F system operating at the R-point in mammals, the Whi5-SBF (inhibitor–transcription factor) complex operates at the START transition in yeast ensuring irreversible commitment.

Several studies have extensively delineated the molecular mechanism of the START transition in yeast. Together with cyclin dependent kinase, the Cln cyclins (Cln1 and Cln2) are responsible for bud formation, and the Clb cyclins (Clb5 and Clb6) initiate DNA synthesis. Cyclin Cln3 plays a significant role in triggering START by activating two transcription factors SBF and MBF. SBF (a heterodimer of Swi4/Swi6) promotes the production of Cln1, 2, whereas MBF (a heterodimer of Mbp1/Swi6) promotes the production of Clb5, 6.

Earlier, it was thought that (similar to CyclinD phosphorylation of pRb) Cln3 phosphorylation of Whi5 causes Whi5 export from the nucleus, thereby removing its inhibition on SBF. However, recent evidence shows that the mechanism is more complicated. Mutant studies indicate that SBF activation requires the phosphorylation of either Whi5 or Swi6 but not necessarily both. Also, the timing and mechanism of Whi5 nuclear export have been shown to be important, but not critical for the timing and execution of START. Therefore, a consolidated model for the START transition that reconciles all the discovered regulatory and spatial dynamics is highly desirable.

We have built a detailed mathematical model for the START transition based on all known molecular interactions and experimental phenotypes. Using this model, we are able to recapitulate the phenotypes of over 150 known mutants, including regulation of size control and localization of inhibitor/transcription factor complexes. Further, the model also lays a foundation for incorporation and understanding of the nutritional effects on size control.

Introduction

Most cells, whether unicellular or part of a multicellular organism, have to grow and divide and propagate life. The underlying process controlling DNA synthesis and cell division is the **cell cycle**. The dynamics and mechanism of the cell cycle have intrigued molecular biologists and computational biologists alike making it one of the most well studied cellular processes over the past 3–4 decades (Novak & Tyson, 1993; Tyson & Sachsenmaier, 1978).

Mammalian cell cycle

The mammalian cell cycle is typically divided into 4 phases: DNA synthesis or replication (**S**) and mitosis/cell division (**M**) phases, separated by two gap phases (**G1** and **G2**) (Figure 1). During **G1**, the cell is responsive to external signals like growth factors/inhibitors, survival factors, and other cell-cell contact signals that control and drive the cell into one of the cell fates: a) one round of DNA replication, b) differentiation to perform specialized functions, or c) quiescence, until new signals leading to other fates appear. **The Restriction point** is an important checkpoint in the mammalian cell cycle that occurs in late G1. The passage through the Restriction point marks the cell's commitment to one round of DNA replication in response to mitogenic stimuli. Beyond this point, cells are not sensitive to mitogenic stimuli anymore; even when mitogens are removed (as shown in Figure 1), the cell completes the committed round of DNA replication before pausing again in G1 (Pardee, 1974).

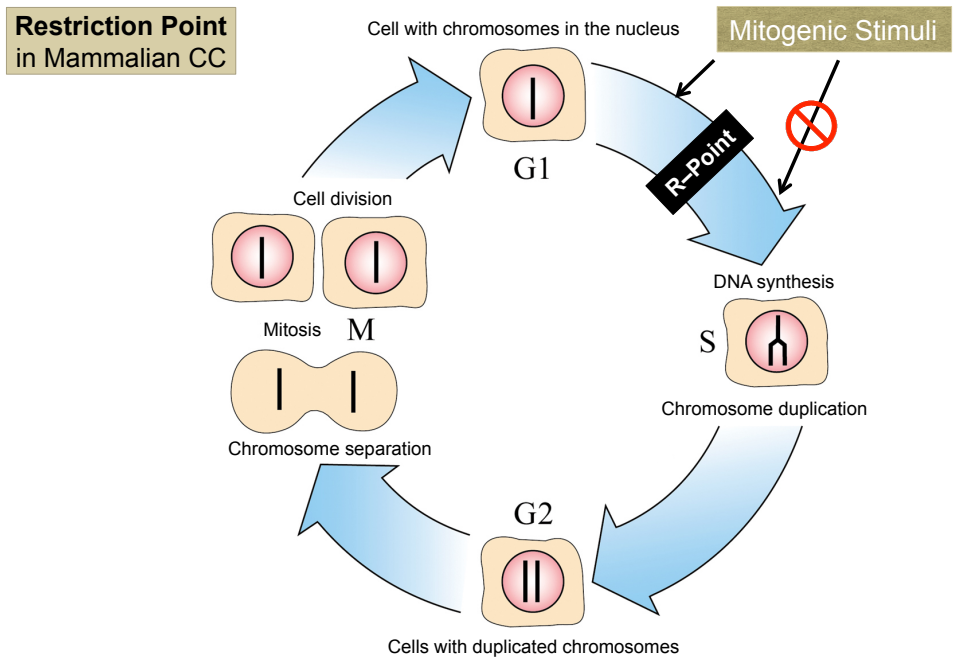

Figure 1. Mammalian cell cycle

(Adapted from: http://nobelprize.org/nobel_prizes/medicine/laureates/2001/press.html)

The most important molecular players in the cell cycle are the Cyclin/CDK heterodimers. Cyclins, as their name suggests, are proteins whose concentration goes up and down periodically, corresponding to progression through the cell cycle. They are tightly regulated through their synthesis, degradation and sequestration by the cyclin dependent kinase inhibitor (CKI) complexes. In contrast, the levels of cyclin dependent kinases (CDKs) that bind to cyclin proteins remain constant throughout the cell cycle. It is only in the presence of obligatory cyclin partners that CDKs can function. Thus, the activity and substrate specificity of CDKs are governed by the availability and nature of the cyclin partner. Each species of eukaryotic organism has a set of cyclins that interact with their corresponding CDK partners to perform certain crucial phosphorylations important for the transition between phases and progress through the cell cycle. There are

several cyclins and CDKs involved in the mammalian cell cycle. For instance, CyclinD-CDK4/6 complexes are involved in G1, followed by CyclinE-CDK2 driving the G1/S transition, leading to the accumulation of S-phase and mitotic cyclins, CyclinA-CDC2 and CyclinB-CDC2, driving DNA synthesis and mitosis, respectively (Alberts et al, 2002).

Our model system, budding yeast

The simplest and the best model system that has been employed to study the cell cycle is the unicellular eukaryote, budding yeast (*Saccharomyces cerevisiae*) (Figure 2). The molecular details of the cell cycle have been systematically worked out in budding yeast for three principal reasons. First, and most importantly, cell cycle control genes are highly conserved across species all the way from yeast cells through mammalian cells. Secondly, the budding yeast system offers much lower redundancy and complexity in the regulation network when compared to higher eukaryotes. For instance, budding yeast cells have only one cyclin dependent kinase (Cdc28, standing for 28^{th} cell division cycle (CDC) mutant isolated by Hartwell et al, (1970)) as against several CDKs in mammalian systems. Finally, these unicellular eukaryotes can exist as haploids making them amenable to genetic manipulation and easy to work with.

In this thesis, we concentrate on modeling the START transition in yeast, which is analogous to the Restriction point control in mammalian cells, with the hope that a clear understanding of the former regulation would lead to a better understanding of the latter control in mammalian cells.

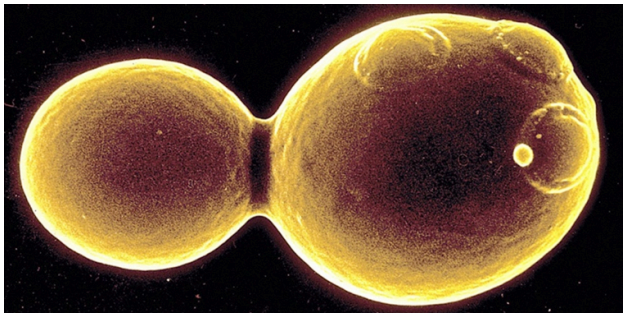

Figure 2. Budding yeast with bud scars

(http://ppdictionary.com/fungi.htm)

START transition vs. Restriction point

START transition in budding yeast and Restriction point control in mammalian cell cycles share similarity at several levels of organization from high-level physiology to the underlying molecular interaction network. Akin to the abrupt change in growth factor sensitivity of mammalian cells before and after the restriction point, yeast cells actively respond to mating factors (pheromones), which are inhibitors of cell cycle, only prior to START and lose their sensitivity right after START (Chang & Herskowitz, 1990; Peter & Herskowitz, 1994; Wittenberg & Reed, 1996).

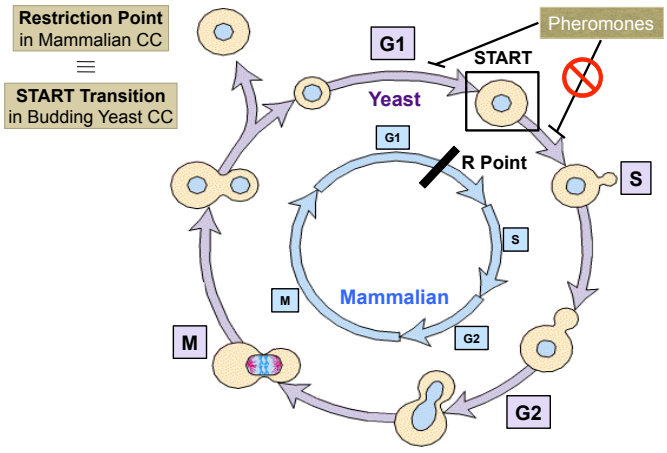

Figure 3A. Budding yeast cell cycle in comparison to the Mammalian cell cycle (Lodish et al, 2000).

The framework for the molecular players underlying the START transition in yeast and R-point transition in mammalian cells and their dynamical behavior are very similar (Figure 3B). In both cases, the cells start in G1 with a minor G1 species (CyclinD for mammalian cells and Cln3 for yeast cells) that is present at constant level throughout the cell cycle. These minor G1 cyclins progressively phosphorylate and turn off the inhibitors (pRb and Whi5, respectively) of the transcription factors (E2F and SBF/MBF, respectively) resulting in activation of transcription factors and accumulation of major G1 cyclins (CyclinE and Cln1,2, respectively) and S phase cyclins (CyclinA and Clb5,6, respectively). Furthermore, these G1/S cyclins are able to phosphorylate and inactive the TF inhibitors. As a result, this positive feedback allows G1/S cyclins to rise and inhibitor levels to drop sharply. The complete activation of G1 and S-phase cyclins triggers the Restriction point in mammalian cells and START transition in yeast.

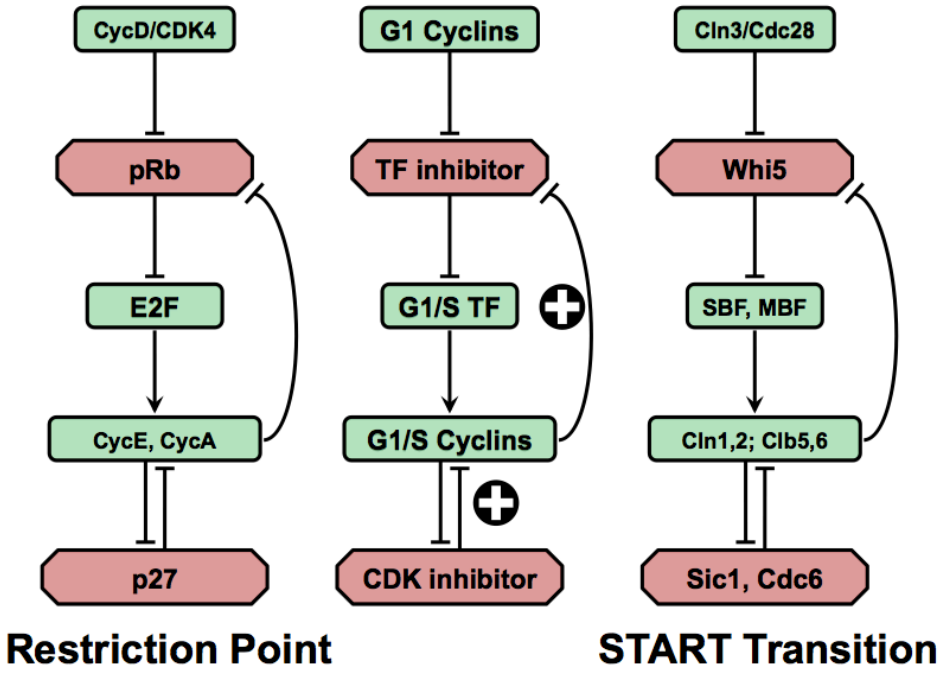

Figure 3B. Highly similar molecular wiring underlying the Restriction point and START transition. The central panel captures the conserved mechanism across mammalian and yeast G1/S transitions, while the panels to the left and right represent specific pathways in mammalian and yeast systems respectively.

The positive feedbacks ensure bistability in the START transition, as well as in the Restriction point. The existence and significance of the positive feedback involving G1/S cyclins for the timing and irreversibility of START have been experimentally determined (Charvin et al, 2010; Skotheim et al, 2008). Similar phenomena are demonstrated in the dynamical behavior of the restriction point (Yao et al, 2008).

Size Control in budding yeast

Despite these similarities, there exists a distinctive mechanism of size control that operates in budding yeast cells (Johnston, 1977); in comparison, (although debatably)

there is a relatively weak size control that operates in the mammalian cells (Conlon & Raff, 2003; Sveiczer et al, 2004).

During development in metazoans and other multicellular organisms, cells undergo dramatic changes in size and shape, yet each of the diverse cell types attains a characteristic size upon differentiation, indicating that cell size must be under stringent social control. While social constraints apply in multicellular organisms, lower single celled eukaryotes such as budding yeast do not depend on cell-cell interactions or cues from neighbors in their decision to grow and divide. They continue to proliferate as long as they have nutrient supply. Nevertheless, budding yeast has stringent control for maintaining size homeostasis generation after generation. This is achieved through a tight coupling of cell growth and division. A mechanism for this phenomenon is emerging in budding yeast, but is far from complete.

Cell size has been known for several decades to be tightly controlled in yeast cells. In budding yeast, the cell size checkpoint acts prior to START (G1/S) transition (Johnston, 1977), whereas in fission yeast, at the G2/M transition (Fantes, 1977). This checkpoint ensures that cells grow to a critical size threshold prior to making a commitment to either DNA synthesis (S) or cell division (M), respectively. Classic studies on size control in budding yeast (Johnston, 1977) have shown that small newborn cells tend to have longer lag periods than larger newborn cells before they make the START transition (first appearance of bud) even if they are genetically identical and placed under identical physiological conditions. This delay allows the small cells to grow large enough (to attain their *size threshold*) before START.

Cells modulate their critical size depending on the growth medium

The critical size to which a cell has to grow is dependent on the nutrient medium (Johnston et al, 1979). When shifting from a poor to rich growth medium, cells previously initiating buds at a small size, now accumulate in G1 and grow to a new larger critical size before initiating a bud (Johnston et al, 1979). In the experiment, cells did not increase in number immediately as expected when switched to rich medium from a minimal medium. During this delay, the percentage of unbudded cells goes up, suggesting a possible scenario where the cells, now in a richer medium, have to grow larger, before they form a bud. This experiment laid the evidence for an increase in cell size threshold for budding with a richer growth medium. Similar observation was made by (Jagadish & Carter, 1977), that the size threshold for DNA synthesis also increases with a richer growth medium. Tyers and group proposed a molecular mechanism for the control of critical size threshold by the growth medium (Jorgensen & Tyers, 2004; Tyers, 2004). The Chen2004 model does not include such a mechanism. Therefore, one of our primary aims is to build a detailed model for the START transition with a size control mechanism that would allow for future incorporation of the dependence of size control on the growth medium.

These intriguing aspects of START – the molecular control network and size requirements, the irreversibility of the transition, and the abrupt change in the physiological behavior following the transition – make it an excellent dynamical system to study in detail.

Molecular mechanisms underlying START transition

As described previously, the key proteins involved in the cell cycle are the cyclins, CDKs and the cyclin antagonists. Yeast has only one CDK, Cdc28, and since it is abundant and its activity requires the binding of a cyclin partner, we usually only refer to the cyclin partner it binds to (during different phases of the cell cycle) when we are referring to the heterodimer. Table 1 below lists the most important cyclins that are involved in the different phases of a budding yeast cell cycle.

Table 1. Functions of different cyclins in budding yeast cell cycle

Cyclin	Function
Cln1,2	- Bud emergence, START - Inhibiting kinase inhibitors Sic1, Cdc6 and Cdh1 (which inhibit Clbs)
Cln3	- Activates SBF (TF for Cln1,2), MBF (TF for Clb5,6) in response to cell size
Clb1,2	- Late mitotic events including elongation of short mitotic spindle - Promotes cell cycle transition into mitosis
Clb3,4	- Early mitotic events including formation of short mitotic spindle - Involved in DNA synthesis, spindle assembly as well as G2/M transition
Clb5,6	- DNA Synthesis - Inhibiting kinase inhibitors Sic1, Cdc6 and Cdh1

In yeast, START depends on the activation of the transcription factors SBF (SCB-binding factor complex – a heterodimer of Swi4 and Swi6) and MBF (MCB-binding factor complex – a heterodimer of Mbp1 and Swi6). These transcription factors are primarily responsible for the transcription of the G1 cyclins Cln1,2 and S-phase cyclins, Clb5,6 (Koch et al, 1993; Nasmyth & Dirick, 1991). Activation of these transcription factors is triggered when the cell attains a critical size (that is influenced by nutrient conditions), by the action of Cln3. Bck2 also activates these transcription factors in response to cell size. In the absence of Cln3, Bck2 plays a role in activation of SBF and MBF (Koch et al, 1993; Nasmyth & Dirick, 1991). SBF and MBF have a large functional overlap (Bean et al, 2005). In the absence of SBF, MBF can activate Cln1,2 synthesis. Likewise, in the absence of MBF, SBF can activate Clb5,6. The mechanism of Cln3 and Bck2 activation of SBF and MBF will be described in later sections.

At the end of S-phase, SBF is turned off by mitotic cyclins Clb1,2 (Amon et al, 1993; Siegmund & Nasmyth, 1996) and MBF is turned off by Clb1,2 and Nrm1 (de Bruin et al, 2008).

Cln1,2 and Clb5,6 are primarily transcribed by SBF and MBF respectively. However, Clb5,6 are not active initially in late G1, as they are inhibited by Sic1, a CDK inhibitor (Mendenhall, 1993). Since Cln1,2 can phosphorylate Sic1 and Cdc6 (another CKI) and the phosphorylated Sic1 and Cdc6 are rapidly degraded by SCF (Verma et al, 1997), Clb5,6 becomes activated soon after Cln1,2 activation. So, at START transition, as SBF and MBF are activated, Cln1,2 accumulates first, leading to bud emergence, followed closely by Clb5,6 activation leading to initiation of DNA synthesis (Figure 4).

In wild type cells, these two events occur nearly simultaneously – a characteristic of START transition described by Hartwell (1974).

Another consequence of the START transition is that the progression of the cell cycle to the G2/M phase is facilitated. Clb5,6 activated at the START transition inhibit Cdh1 (a protein important for Clb1,2 degradation). Thus, Clb1,2 are able to accumulate when their synthesis is turned on later in G2 phase. The accumulation of Clb1,2 marks the entry into mitosis (Figure 4).

At the end of mitosis, when all sister chromosome pairs are attached to opposite poles of the spindle (spindle assembly checkpoint is inactivated), Cdc20 gets activated. Cdc20, acting together with the anaphase promoting complex (APC), causes the dissolution of cohesin that holds the sister chromatids together. This enables the sister chromatids to move apart to the opposite poles of the spindle. The dissolution of sister chromatids triggers activation of a phosphatase, Cdc14. Cdc14 plays three important roles: (i) activation of the synthesis of CKI, (ii) dephosphorylation and stabilization of CKI and (iii) activation of Cdh1 with the help of Cdc20, leading to the degradation of Clb1,2. Degradation of mitotic cyclins enables the cell to exit from mitosis and reenter G1 (Alberts et al, 2002).

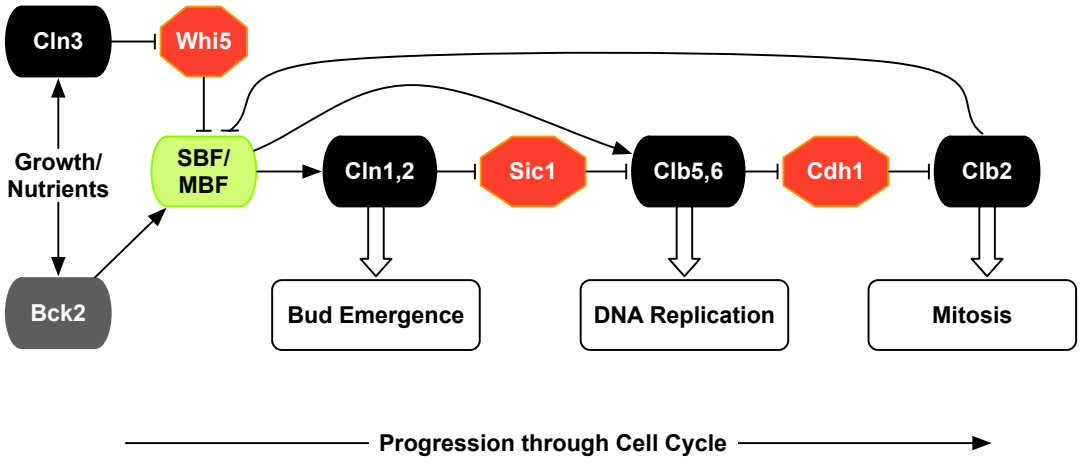

Figure 4. A simplified mechanism underlying the progression through the cell cycle in budding yeast. Cln3 and Bck2 are activators of START (turn on SBF, MBF needed for Cln1,2; Clb5,6). Cln1,2 phosphorylates and inhibit Sic1, a stoichiometric inhibitor of Clb5,6, thus allowing DNA replication to occur. S-phase cyclins, Clb5,6, inhibit Cdh1, an antagonist of the mitotic cyclins, Clb1,2, thus allowing progression through the mitotic events, and finally exit from mitosis leading back to G1.

Early hypothesis of SBF activation

Figure 5A shows the consensus picture of SBF activation at the end of 2008. SBF is bound to and inactivated by inhibitor Whi5 (Costanzo et al, 2004; de Bruin et al, 2004). Cln3 (Cln3/Cdc28) phosphorylates Whi5, which causes Whi5 to dissociate from SBF, thereby activating it. Thus, as Cln3 levels accumulate, by late G1, most of the Whi5 proteins get phosphorylated and move to the cytoplasm leaving SBF free for transcription. In late S phase, SBF is again phosphorylated and turned off by Clb2 (Amon et al, 1993; Siegmund & Nasmyth, 1996) and Clb6 (Geymonat et al, 2004). The Whi5-SBF (inhibitor–transcription factor) complex that operates at the START transition in yeast is thus reminiscent of the pRb-E2F system operating at the restriction point in

mammals ([Cln3 –| Whi5 –| SBF → Cln1,2 → START] vs. [CycD –| pRb –| E2F → CycE → R-point]; refer to Figure 3B).

In addition to Cln3, Bck2 is another known activator of START. It is believed to act by a mechanism independent of CDK and Whi5 (Wijnen & Futcher, 1999). In the absence of Cln3, cells are very large and have prolonged G1 (Dirick et al, 1995). Additional deletion of Bck2 in the *cln3*Δ strain makes the cells inviable (Wijnen & Futcher, 1999). These observations suggest that although delayed, SBF activation in *cln3*Δ cells still occurs by Bck2. The details of Bck2 regulation of SBF are described in a later section under Results and Discussion.

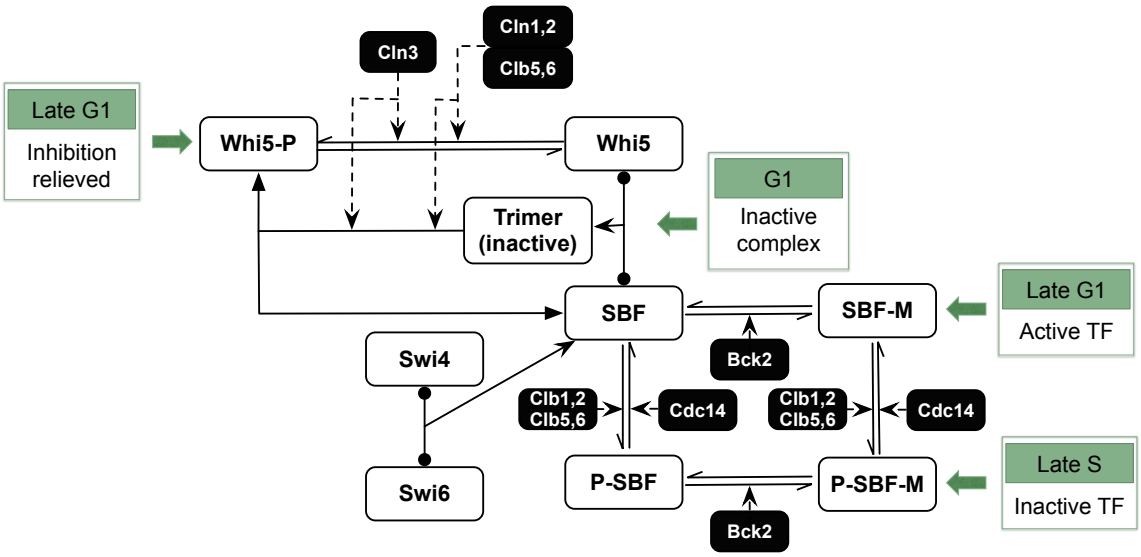

Figure 5A. Earlier hypothesis that Whi5 phosphorylation is crucial for SBF activation.

This model for START includes (i) activation of SBF by Clns (Cln3, Cln1,2, Clb5,6) by inactivation of Whi5 (by phosphorylating free and SBF-bound Whi5) in late G1, (ii) activation of SBF by Bck2 to an alternate form independent of Whi5 and CDK, and (iii) inactivation of SBF by Clb1,2 in late S phase.

In essence, SBF activation associated with START was believed to depend solely on the phosphorylation of Whi5, its dissociation from the SBF complex and subsequent export to the cytoplasm (Figure 5B). According to the experiments shown by Di Talia and group (2007), as cells progress through START, Whi5 gets progressively phosphorylated and inactivated. Consequently, it becomes cytoplasmic in late G1, leaving SBF in the active state for Cln1,2 transcription. The authors also showed that Whi5 moves back to the nucleus (to inhibit SBF) only at mitotic exit. In addition to phosphorylation and inactivation of Whi5, Wijnen et al. (2002) showed that part of the mechanism of Cln3 activation of the START transition is through its action on phosphorylation of Swi6. The cytoplasmic localization of Swi6 was also related to a phosphorylation event, specifically the S160 site on Swi6 (Sidorova et al, 1995). These observations together made up the simple story of the activation of SBF and relocalization of the inhibitor (Figure 5B).

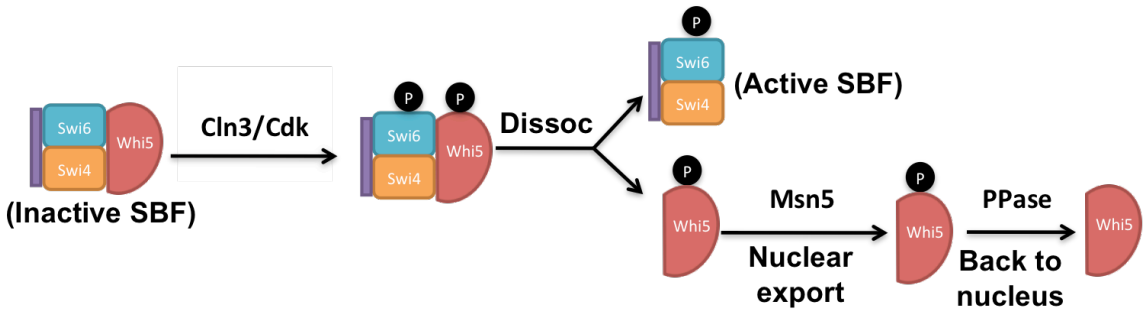

Figure 5B. Earlier hypothesis on association, dissociation and translocation events underlying SBF activation.

Inactive SBF-Whi5 trimer gets phosphorylated by Cln/CDK on both Swi6 and Whi5, followed by the trimer dissociation to give active SBF (with Swi6 phosphorylated) and phosphorylated Whi5 that can get exported ot the cytoplasm (by transport protein, Msn5).

Current hypothesis of START transition: Phosphorylation of Whi5 is not crucial for SBF activation

Contrary to previous beliefs, recent evidence showed that the regulation of SBF is not as simple as this. If the phosphorylation of Whi5 were key to its export and SBF activation, then mutating all the phosphorylation sites should retain Whi5 in the nucleus, delaying SBF activation, and hence resulting in larger cells. However, the non-phosphorylable mutant *WHI5-12A* (or *WHI5-18A*) with all known CDK (and non-CDK sites included) phosphorylation sites mutated to Alanine showed no difference in size compared to wild type (Wagner et al, 2009). Likewise, we would expect mutation of the phosphorylation sites on Swi6 (to Alanine), which causes Swi6 retention in the nucleus (Sidorova et al, 1995), thereby advancing START resulting in smaller cells. However, it has been known that *SWI6-SA4* too shows a wild type size (Wagner et al, 2009). Most surprisingly, only the double non-phosphorylable mutant *WHI5-12A SWI6-SA4* shows a 40% increase in size (Wagner et al, 2009) (Figure 6). These observations suggest that either Whi5 or Swi6 needs to be phosphorylated (if not both), for timely activation of SBF (so that there is no difference in size).

In this respect, the working of the START transition differs significantly from that of the restriction point. Whi5 phosphorylation for activation of SBF in budding yeast was not required, in contrast to pRb phosphorylation being absolutely crucial for the activation of E2F in mammalian cell cycle (Brown et al, 1999; Costanzo et al, 2004).

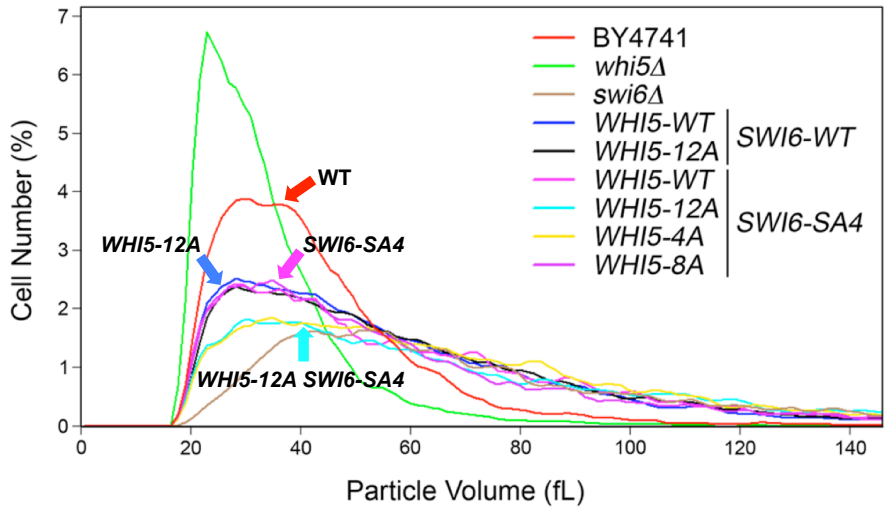

Figure 6. Experimental phenotypes of non-phosphorylable mutants.

(Adapted from Figure 7c of (Wagner et al, 2009)). Cell size distribution of wild type and three non-phosphorylable mutants are shown using arrows drawn with corresponding colors (Red=WT; Blue=*WHI5-12A*; Pink=*SWI6-SA4*; Cyan: *WHI5-12A SWI6-SA4*) to indicate mutant genotypes.

Building a comprehensive START model

Due to unavailability of details related to the mechanism involving Whi5 at START until 2004, our previous models of the budding yeast cell cycle have a very simplistic mechanism for START (Chen et al, 2004; Chen et al, 2000). These models only consider SBF/MBF activation by Cln3 and Bck2 and inactivation by Clb2 in a condensed phenomenological abstraction (using an ultra-sensitive Goldbeter-Koshland switch (Goldbeter & Koshland, 1981)).

In light of all the recent findings about the role of Whi5 phosphorylation and their discrepancies with the previously held consensus mechanisms, there is a need to reconcile all the details into a coherent model for the START transition in budding yeast. We have developed a comprehensive model that, i) contains a detailed mechanism for the activation and inactivation of SBF, along with the inhibitor Whi5, that is compliant with

the recently determined experimental phenotypes, ii) contains a mechanism for activation and inactivation of MBF (de Bruin et al, 2008; de Bruin et al, 2004; Koch et al, 1993), iii) explains the role of Bck2 in the START transition, iv) explains critical aspects of the localization of the monomers in the transcription-factor/inhibitor complex (Whi5, Swi6 and Swi4) (Baetz & Andrews, 1999; Di Talia et al, 2007; Sidorova et al, 1995), and, v) explains size control operating at the START transition (Johnston et al, 1979). We have also taken into account the specific contribution of Cln3 in setting the cell size threshold (Verges et al, 2007). These specificities in the model have set the stage for future incorporation of more detailed mechanisms that could explain nutritional effects on size control (Tyers, 2004).

We have then transformed this qualitative wiring diagram into a mathematical model based on nonlinear ordinary differential equations. Our model explains wild type cell cycle dynamics, timely localization of monomers and size control, and additionally, explains experimentally observed phenotypes of over 150 mutants.

Results and Discussion

Model for START Transition

We used the detailed mathematical model of budding yeast cell cycle published by our group (Chen et al, 2004) – hereafter referred to as 'Chen2004 model' – as a starting point upon which to build a model for START transition (Figure 7). The Chen2004 model incorporates several aspects of the cell cycle mechanism from START transition through mitotic exit, and is able to explain ~120 cell cycle mutants. However, since many details pertaining to START were published later, the Chen2004 model only considers a very simplified mechanism for the activation and inactivation of SBF (jointly with MBF) in the form of an ultrasensitive, "Goldbeter-Koshland" (GK) switch (Goldbeter & Koshland, 1981). In our current model, reconciling several recent studies (Table 2; detailed below) we have expanded the model for START to include events like association/dissociation of various components of SBF, MBF, their phosphorylation/dephosphorylation, and their import/export to describe in detail the mechanisms for the regulation of both SBF and MBF (Figure 8).

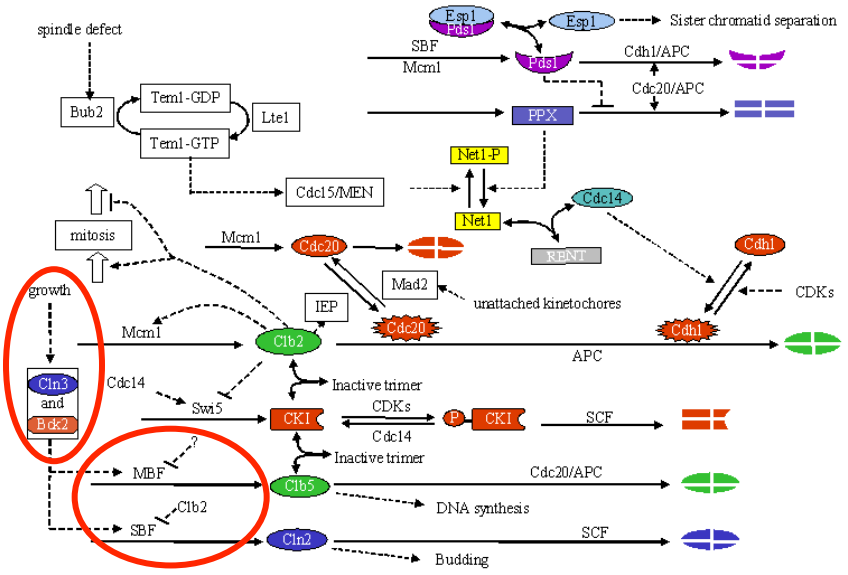

Figure 7. Chen2004 model of the budding yeast cell cycle.

(Reproduced with permission from (Chen et al, 2004)). The model considers key molecular players and interactions from G1, START, S-phase, M-phase and mitotic exit. It takes into account the key cyclins involved in G1 (Cln3), G1/S (Cln2 that represents Cln1, Cln2), S (Clb5 that represents Clb5, Clb6) and M-phases (Clb2 that represents Clb1, Clb2), the cyclin dependent kinase inhibitors, Sic1 and Cdc6 and the cyclin degradation proteins, Cdh1/APC, Cdc20/APC. The two red circles enclose components pertaining to START in the Chen2004 model. In the current work, this part of the model has been substituted with detailed mechanisms for the regulation of SBF and MBF by Cln3 and Bck2, which are illustrated in Figure 8, 13 and 17.

The main focuses of our model are the description, of activation and inactivation of G1-S transcription factors SBF and MBF. Accordingly, at its core, the model contains the SBF and MBF monomers Swi4, Swi6 and Mbp1, and the inhibitor protein, Whi5. Additionally, we consider two promoters for the two sets of genes involved in budding and DNA synthesis that are turned on by SBF and MBF, respectively. In our model, we take into account all possible pools of monomers and protein complexes that are either bound or unbound to promoter. Additionally, we incorporate all the pertinent

phosphorylation states for each these components based on whether they are Cln/CDK or Clb/CDK targets. We further include any available information on cellular compartmentalization of these molecules in the model.

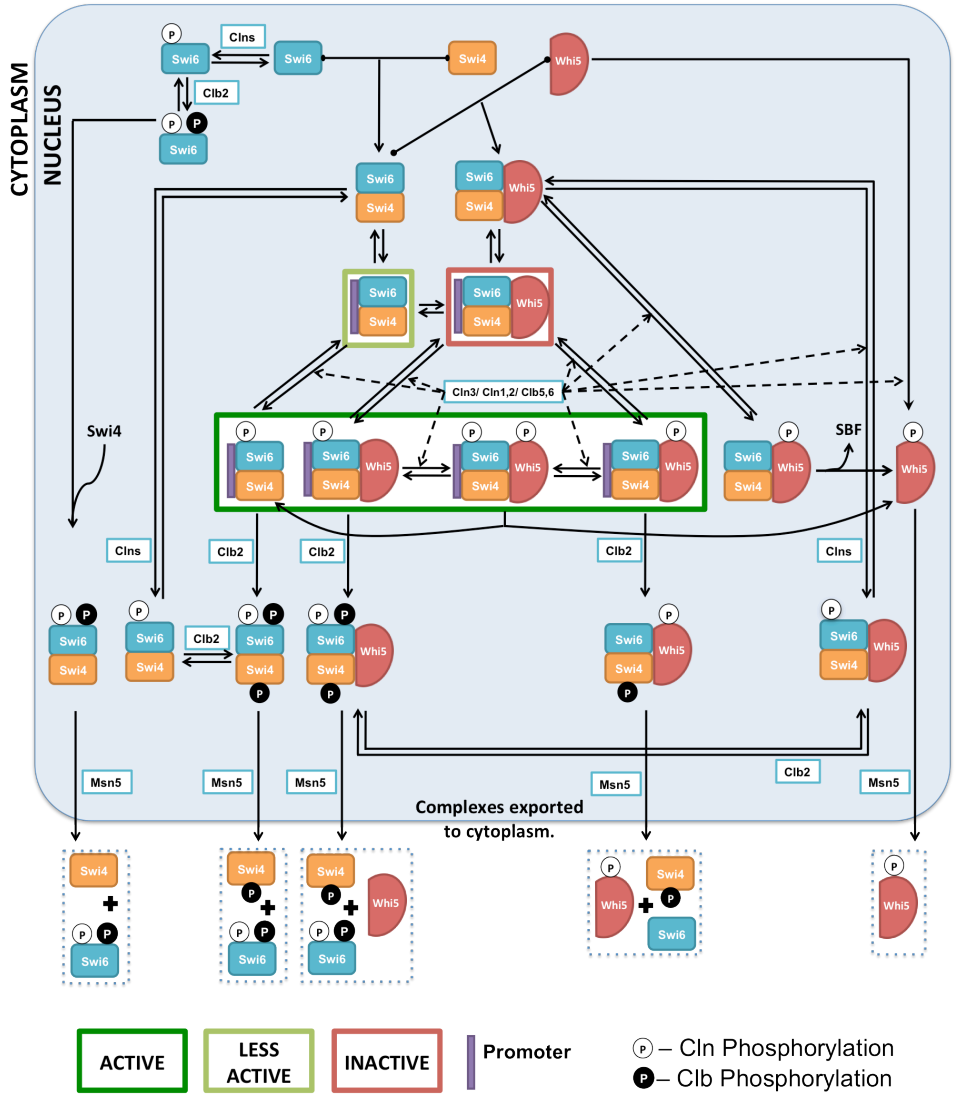

Figure 8. Core model for SBF activation and inactivation.

Presented in the figure are the most important interactions considered in our model for SBF activation and inactivation. The core components are Swi4 (orange icon), Swi6 (turquoise icon), Whi5 (red icon), the promoter (purple bar), kinases (Cln3, Cln1,2, Clb5,6, Clb1,2) and export protein (Msn5) (white box). The nucleus is represented with bluish-gray background, while the rest corresponds to cytoplasm. Promoter-

bound complexes enclosed in boxes with borders in dark green, light green and red represent complexes with maximal, residual and no activity respectively. White-filled circles represent activatory phosphorylations done by Cln3, Cln1,2, and Clb5,6; whereas the black-filled circles represent the inactivating phosphorylations by Clbs (Clb5,6 & Clb1,2 for Swi6 phosphorylation and Clb1,2 for Swi4 phosphorylation). The Cln (white) phosphorylation on Whi5, and Clb (black) phosphorylation on Swi6 (S160) are needed for export to cytoplasm. To avoid overcrowding, remaining complexes corresponding to modifications on other free forms are not included in the figure. All the concerned equations are given in the Materials and Methods section. Key facts about abundance, regulation and localization of all the components are described in Table 2.

Table 2. Description of START components in the model

Protein / Component	Description/Regulation
Whi5	***Description*** - Whi5 is a stoichiometric inhibitor of the transcription factor complexes, SBF (Costanzo et al, 2004; de Bruin et al, 2004) and MBF (Costanzo et al, 2004). ***Abundance*** - The abundance of Whi5 is roughly 1500 protein molecules per cell in an asynchronous culture (Ghaemmaghami et al, 2003), although Whi5 is known to be transcriptionally regulated showing a 3-fold variation, peaking in late G1 phase (Pramila et al, 2006). Therefore, we assume available Whi5 (for inhibition) in G1 to be 1000 molecules. - For simplicity, we assume total Whi5 to be conserved in the model. ***Regulation & Localization*** - Whi5 has 12 known CDK phosphorylation sites and 6 other non-CDK sites (Wagner et al, 2009). We assume Hill kinetics (with Hill's coefficient=5) for CDK phosphorylation of Whi5 to capture the non-linearity resulting from multi-site phosphorylation (compared and tested for smaller version of model). - We assume that Whi5 is phosphorylated by Cln3, Cln2 and Clb5 (with

	different efficiencies) and dephosphorylate by Cdc14 at mitotic exit (Costanzo et al, 2004; de Bruin et al, 2004; Taberner et al, 2009). We also assume that all forms of Whi5 (either free, or SBF-bound or SBF-promoter-bound) are subjected to phosphorylation and dephosphorylation. - Whi5 is nuclear until late G1, and moves to cytoplasm prior to START, and stays cytoplasmic until mitotic exit (Di Talia et al, 2007). This localization is dependent on phosphorylation of specific CDK phosphorylation sites on Whi5, and the transport protein Msn5.
Swi6	***Description*** - Swi6 is a **component** of the transcription factor, **SBF** and **MBF** (Koch et al, 1993; Moll et al, 1993). ***Abundance*** - It is 3 times more abundant than Whi5 (Ghaemmaghami et al, 2003). - We assume total Swi6 to be conserved in the model. ***Regulation & Localization*** - Swi6 has 5 consensus CDK phosphorylation sites (Wijnen et al, 2002). - We assume that the Cln kinase phosphorylation on Whi5 and its phosphorylation on Swi6 have the same dynamics. That is, we use the same Hill function to describe the phosphorylation of Cln kinase on Whi5 as well as on Swi6. - In the model, the sites bearing the P-form – the activatory phosphorylations are done by Cln3, Cln2 and Clb5 with different efficiencies, and the dephosphorylation is by unspecified phosphatase. - Phosphorylation at the S160 site, is known to be responsible for the cytoplasmic localization of Swi6 from mid-S phase until mitotic exit (Sidorova et al, 1995). This is considered to be the Q-form (inactivated form) in the model and is required for cytoplasmic localization. The Q-form phosphorylation is carried out by Clbs (Clb5 and Clb2 in our model), and dephosphorylated by Cdc14 at mitotic exit (Geymonat et al, 2004). Transport of Q-forms to the cytoplasm requires Msn5 and Swi4 (Queralt & Igual, 2003). - We assume phosphorylation (P- and Q-forms) occurs for all forms of Swi6 (either free or promoter bound forms).

Swi4	***Description*** - Swi4 is a component of the transcription factor, SBF (Koch et al, 1993; Moll et al, 1993). ***Abundance*** - Based on observed protein abundances, we consider the relative abundance of Swi4 and Mbp1 to be ~0.55x as abundant as Whi5 (Ghaemmaghami et al, 2003). Therefore, Swi4 is the limiting component of the SBF complex. - We assume total Swi4 to be conserved in the model. ***Regulation and Localization*** - We assume that phosphorylation of Swi4 is necessary for SBF inactivation (based on (Siegmund & Nasmyth, 1996)). Phosphorylation of Swi4 subunit of SBF causes SBF to dissociate from the promoter. - Swi4 is nuclear at all times (Baetz & Andrews, 1999). In the model, phosphorylated Swi4 gets dephosphorylated by a constitutively active phosphatase, PP2A. The unphosphorylated form remains nuclear at all times. - Since *swi6*Δ mutant is viable, but *swi6*Δ *bck2*Δ is inviable, we assume that Swi4 has some residual activity in the absence of SBF (Koch et al, 1993; Nasmyth & Dirick, 1991), but it requires Bck2 for its activity. The active Swi4 complex is also assumed to be inactivated by Clb2.
Mbp1	***Description*** - Mbp1 is a component of the transcription factor, MBF (Koch et al, 1993; Moll et al, 1993). ***Abundance*** - As mentioned above, we assume Mbp1 to have a relative abundance of 0.55x w.r.t Whi5. Mbp1 is, therefore, a limiting component of MBF (Ghaemmaghami et al, 2003). - We assume total Mbp1 to be conserved in the model. ***Regulation and Localization*** - MBF regulation is driven by Cln3 and Bck2 for activation (Koch et al, 1993), and Nrm1 (de Bruin et al, 2008) and Clb2 (to a much lesser extent) for inactivation.

	- Since little information is available about the modification or localization of Mbp1, they are not considered in the model.
Msn5	***Description*** - Msn5 is a transport protein that exports phosphoproteins (Swi6 and Whi5 in our model) from the nucleus to the cytoplasm (Queralt & Igual, 2003; Taberner et al, 2009). ***Regulation*** - We do not consider the regulation of Msn5. It is assumed to be constant in our model.
Cln3 & Bck2 (Modification from Chen2004)	***Regulation & Localization*** - **Activation** of Cln3, which is by nuclear import, depends on chaperone protein, Ydj1, which is proposed to be the sensor of cell size (Verges et al, 2007). In the model, Ydj1 depends on mass. We also assume that the abundance of Cln3 depends on mass. This assumption is necessary for mutant cells with longer G1 to have shorter G2/M so that the total cycle time (G1 + S/G2/M) is the same as wild type cells. Thus, mutant cells can maintain their size homeostasis generation after generation. - **Inactivation** of Cln3 is done by Ssa1 (Verges et al, 2007). To explain the change of Cln3 localization during the cell cycle, (being nuclear in late G1, just prior to START and become cytoplasmic from late S phase on), we assume that Ssa1 is activated by Clb2 and Swi5, both of which accumulate during M-phase. - Currently, there is no evidence for Bck2 being regulated the same way as Cln3. But since Bck2 is known to be a cell size regulator too (Wijnen & Futcher, 1999), we assume that its activation and inactivation depend on similar mechanisms that are contingent on mass and Clb2, Swi5 (instead of Ydj1 and Ssa1).
Promoters	- We assume the promoter concentration to be 0.2 relative to Whi5 abundance, corresponding to 200 of SBF regulated genes. - We consider two species, Prom2 and Prom5 corresponding to genes regulated by SBF and MBF, respectively.

The rest of the results and discussion is presented as subsections addressing the following aspects of START transition: i) the mechanistic model in wild type cells, ii) the role of phosphorylation in START transition, iii) the mechanism for cellular size control and nutritional effects, iv) the timing and localization of different monomers corresponding to activation and inactivation of SBF, and v) the cell cycle dynamics/phenotypes of relevant mutants presented as time-course simulations. In our model simulations, we use the firing of the origin of replication, ORI=1, to be the marker for START.

Regulation of START in wild type cells in the model

Important assumptions made in the model

1. The SBF-Whi5 complex that gets doubly phosphorylated on Swi6 and Whi5 is unstable and dissociates to give active SBF (phosphorylated on Swi6) and phosphorylated Whi5, which can be exported to the cytoplasm by Msn5 (highlighted in Figure 10).

2. We only consider the activity of the different promoter-bound SBF-Whi5 complexes. They are defined as follows:

Fully active forms

- SBF phosphorylated by Swi6 (SBFB6P, SBFB6PQ; SBFa3 = 1 * (SBFB6P + SBFB6PQ))
- SBF-Whi5 complex phosphorylated on either Swi6 or Whi5 (SBFa4 = 1 * (WSB6P + WSB6PQ), SBFa5 = 1 * (WSB5P))

- SBF modified by Bck2 is more active than SBF with no modifications, and as active as SBF phosphorylated on Swi6, but does not contribute as much as the Cln forms because there is only one Bck2 modified form as against three Cln-activated forms (SBF phosphorylated on Swi6, and SBF-Whi5 complex phosphorylated on either Swi6 or Whi5 (SBFa2=1*BSB).

Less active forms

- SBF with no modifications has lesser activity than any of the Cln/Bck2 modified forms (SBFa1=0.2*SBFB).
- Swi4 (dimers) activated by Bck2 has very low activity (even lower than SBF with no modifications) (SBFa6 = 0.16 * SWI4B).

Inactive form

SBF bound by Whi5 is inactive, when present without any modifications.

3. Msn5 export: Complexes or monomers that are phosphorylated on Whi5 are exported to the cytoplasm with the help of Msn5. The Q-form of Swi6 in complex with Swi4 is exported by Msn5 (Q-form of monomeric Swi6 is not exported).

4. Cln3 regulation: We assume that Cln3 is translocated from ER to the nucleus by the chaperone protein, Ydj1 in response to cell size (Verges et al, 2007). We also assume that the reverse of this reaction (export from the nucleus) takes place, facilitated by Ssa1 in response to late mitotic factors (see section on Size Control for greater detail). Furthermore, we assume that Cln3 increases with cell size.

5. Bck2 regulation: Since little is known about the regulation of Bck2, we assume that the regulation is very similar to that of Cln3.

Complex formation

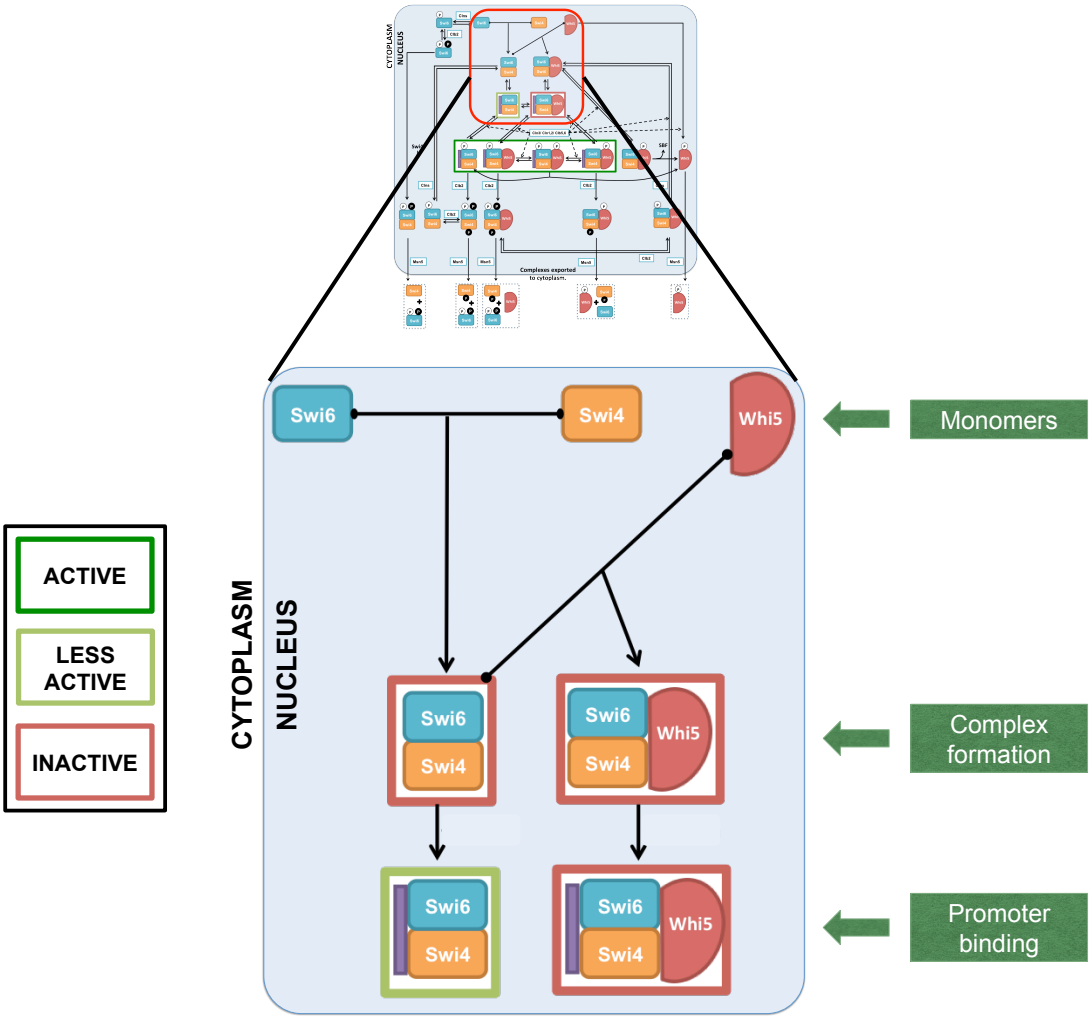

Figure 9A. Complex formation & promoter binding.

Initial flow of events in G1 starting from monomers. The top panel is the core model for SBF activation and inactivation as appeared in Figure 8. The red box containing reactions involving in the complex formation and promoter binding is expanded and shown in the lower panel.

Figure 9B. Ratios of promoter to Swi4/Mbp1, Swi6, and Whi5.

(Roughly based on (Ghaemmaghami et al, 2003)).

In our model (Figure 9A), we begin with Swi4 Swi6 and Whi5 monomers and unbound promoters that bind together rapidly to form SBF complexes based on their stoichiometry and starting concentrations, which are based on known relative protein levels (Ghaemmaghami et al, 2003) (Figure 9B).

Because of the protein abundances (Swi6 : Whi5 : Swi4/Mbp1 : promoter = 3 : 1 : 0.55 : 0.2), there are free Swi6 and Whi5 molecules in the cell. Most of Swi4 is bound by Swi6 and Whi5 (i.e. most SBF is in the Swi4/Swi6/Whi5 form), and most of Mbp1 is bound to Swi6 forming MBF complexes. Since promoter is the limiting factor, most promoters are bound by either Swi4/Swi6/Whi5 (inactive SBF) or by Mbp1/Swi6 (inactive MBF). The remaining SBF and MBF complexes are free and unbound to promoters.

SBF activation by Cln kinases and Whi5 nuclear export

In the following discussion, we focus on these promoter bound SBF complexes, and describe their activation by Cln kinase inactivation by Clb kinases. The same kind of regulation is assumed to occur on the promoter free complexes, but we will not describe them here.

When the cell is in G1, most of the promoter bound SBF complexes are in a Whi5-bound state and are hence inactive. When Cln3 and Bck2 accumulate in the nucleus in late G1, they activate SBF by different mechanisms (Wijnen & Futcher, 1999). Cln3/CDK activates SBF by phosphorylating Whi5 and Swi6 at several residues (Costanzo et al, 2004; de Bruin et al, 2004) resulting in the formation of the doubly phosphorylated form. We assume that the doubly phosphorylated form is unstable and it

dissociates into phosphorylated SBF that is active and phosphorylated Whi5 (Figure 10). Phosphorylated Whi5 subsequently moves to the cytoplasm with the help of export protein Msn5 (Wagner et al, 2009). Whi5 stays cytoplasmic until exit from mitosis when the phosphatase Cdc14 comes up and dephosphorylates it, thus allowing it to move back to the nucleus. This picture is consistent with known observations about Whi5 localization throughout the cell cycle (Di Talia et al, 2007), wherein Whi5 is predominantly nuclear from the beginning of the cell cycle until late G1 and predominantly cytoplasmic for the rest of the cycle.

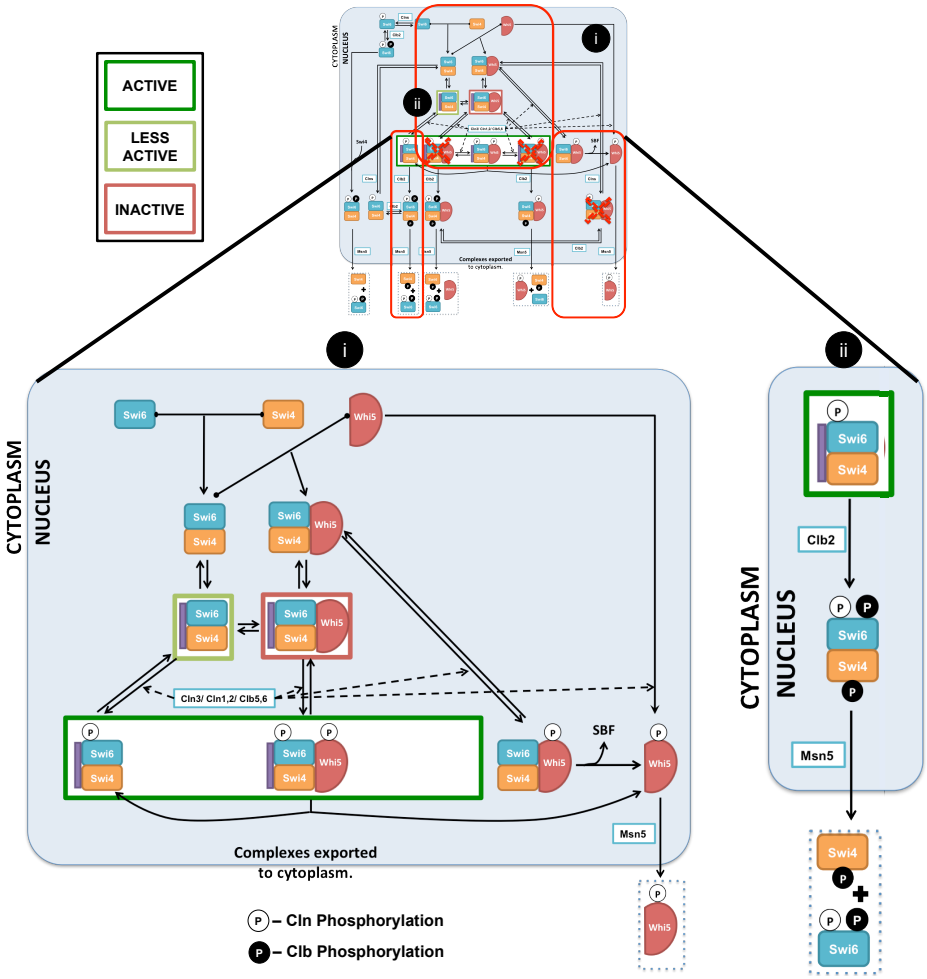

Figure 10. SBF regulation in wild type cells.

The primary course of events that wild type cells would follow is highlighted in red boxes in the top panel (same as Figure 8) (i) SBF activation and Whi5 export. In the figure, the cells start with monomers, which proceed to form complexes and bind to the promoter. In WT cells, both Swi6 (P-form) and Whi5 get phosphorylated by Clns (Cln3, Cln1,2 and Clb5,6). We assume that this doubly phosphorylated form is unstable and dissociates to yield active SBF (with Swi6 phosphorylated) and phosphorylated Whi5 that is free to move to the cytoplasm with the help of export protein, Msn5. (ii) SBF inactivation and export. SBF gets inactivated by two sets of Clb phosphorylations (black-filled circles): Q-form on S160 site of Swi6 by Clb5,6 and Clb1,2, and on Swi4 by Clb1,2, leading to dissociation of SBF from promoter. Msn5 recognizes the Q-form of Swi6 phosphorylation (that is in complex with Swi4) for export to the cytoplasm. Complex dissociates in the cytoplasm soon after export. Phosphate groups are indicated as white-filled circles (activatory phosphorylations) or with black-filled circles (inhibitory phosphorylations).

SBF inactivation

SBF is inactivated by mitotic cyclins (Clb1,2; Clb6) (Geymonat et al, 2004) in late S phase (Figure 10 (ii)). We assume that this second round of phosphorylation happens on Swi4 (Siegmund & Nasmyth, 1996) and on a different site on Swi6 (S160) (Sidorova et al, 1995) leading to dissociation of the complex from the promoter and cytoplasmic localization of Swi6, respectively. Transport of the complex to the cytoplasm is facilitated by the export protein, Msn5, which recognizes phosphorylated forms of Whi5 (Wagner et al, 2009) and Swi6 in complex with Swi4 (Queralt & Igual, 2003).

Figure 11 depicts the steps of inactivation and export for the important active forms of SBF (enclosed in dark green boxes). The usefulness of considering these distinct intermediates (active complexes) is described in the subsection on non-phosphorylable mutants. Although we do not expect to see these intermediates in significant portions in wild type cells, the regulatory logic and flow of molecular events going from active to

inactive complexes and export are assumed to be the same. In each of the cases, following Clb phosphorylation, the intermediate complexes dissociate from the promoter. Clb2 phosphorylation on the Swi4 moiety of SBF causes dissociation of the complex from promoter, hence turning off SBF-regulated genes. The free SBF forms (promoter-unbound) then move to the cytoplasm if the Swi6 moiety is phosphorylated (with the help of Msn5). We assume that these complexes dissociate once they are in the cytoplasm, and remain there until their corresponding phosphatases reverse their modifications: PP2A for undoing of Swi4 phosphorylation and a nonspecific phosphatase for Cln phosphorylations on Swi6, and Cdc14 (that accumulates prior to mitotic exit) for undoing Clb phosphorylation on Swi6 (S160) and Cln phosphorylation on Whi5 in the cytoplasm. This assumption maintains consistency with the following three experimental observations: a) Swi4 is always nuclear (Baetz & Andrews, 1999)), b) Swi6 is cytoplasmic only for the time window from late S phase to exit from mitosis (Sidorova et al, 1995) and the phosphorylation of the S160 residue is associated with Swi6 localization, and c) Whi5 is localized in the cytoplasm from late G1 to mitotic exit (Di Talia et al, 2007).

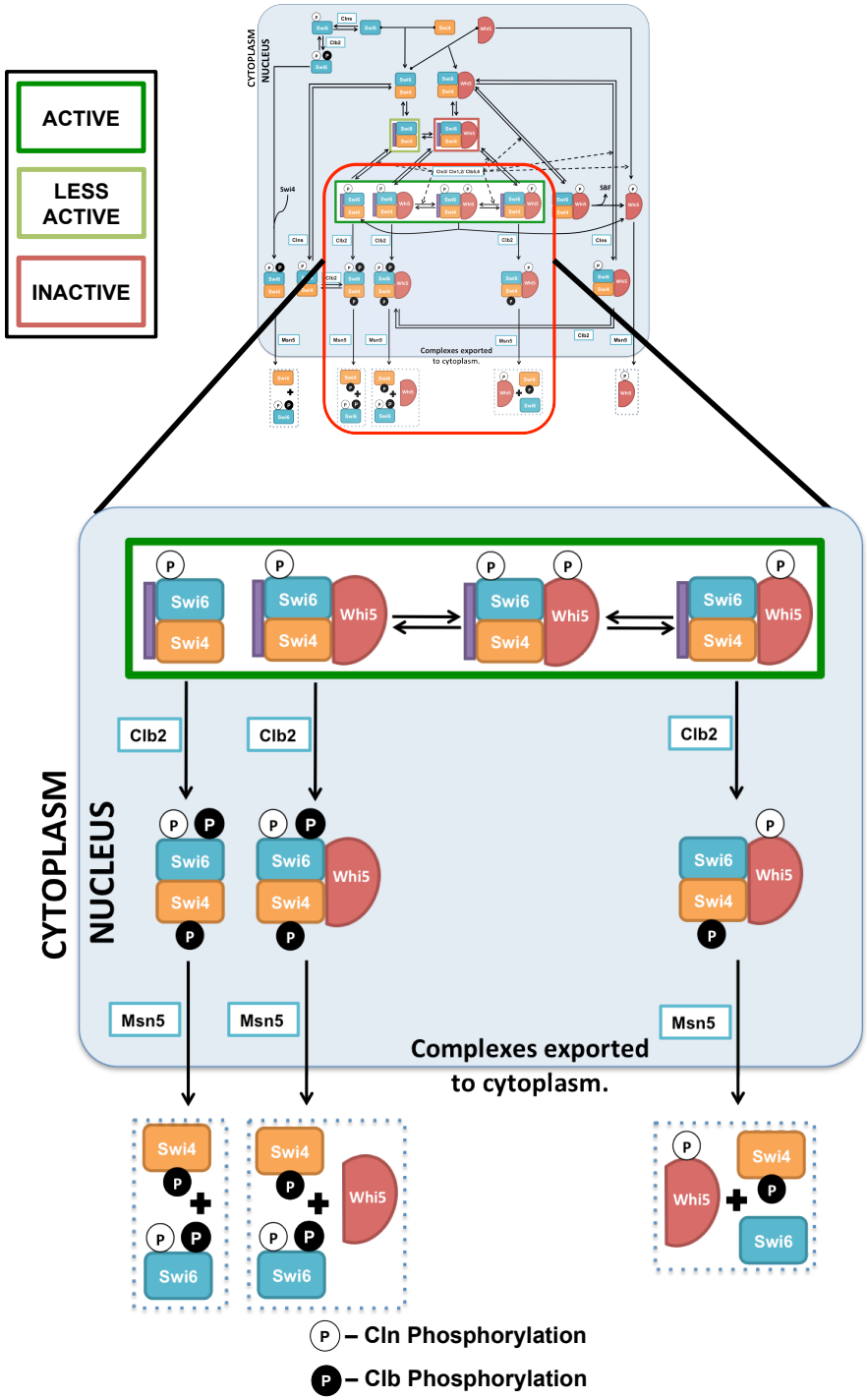

Figure 11. SBF inactivation in wild type cells.

The transition from active to inactive SBF complexes, followed by export is highlighted in red boxes in the top panel (same as Figure 8). We assume that either Clb phosphorylation on Swi6 (S160) (Q-form), or Cln phosphorylation on Whi5 is necessary for recognition by transport protein, Msn5, and

subsequent export to the cytoplasm. Additionally, we assume that in promoter-bound complexes, Clb phosphorylation of Swi4 is necessary and sufficient for the complexes to dissociate from the promoter necessary to turn off gene transcription and to facilitate SBF export. Similar to SBF inactivation in Figure 10, SBF complexes dissociate in the cytoplasm soon after export.

The mechanism described in Figure 10 corresponds to the typical set of biomolecular interactions that occur in a wild type cell through the cell cycle. In addition to these interactions, we have incorporated in the model several other intermediate reactions that could potentially occur in the cellular scenarios with overexpression and knockout mutants. For example, Figure 11 considers intermediates that we expect to observe only in non-phosphorylable mutants. The model considers different pools of complexes (free and promoter-bound) and monomers, and mechanisms for their modification and localization (Figure 8; Table 2). The levels (and significance) of each of these complexes/intermediates depend on the amounts of starting monomers, the nature of the mutant, and the growth rate (reflected in the mass doubling time).

A typical time-course simulation of a wild type cell (solved numerically with the equations, parameters and initial conditions in Tables 6,7) is shown in Figure 12. The cyclin concentration (in arbitrary units) is tracked for ~2.8 cell cycles spanning 300 min for cells growing in glucose (mass doubling time of 90 min). The total cycle time for the daughter corresponds to 107 min and the G1 length is 58 min. Similar to the Chen2004 model (Chen et al, 2004), our expanded model captures the cellular dynamics of cyclins, cyclin antagonists, transcription factor complexes, checkpoint proteins and distribution between various active SBF and MBF forms (Figure 12A, B, C, D, E). As mentioned before, in our model simulations, we use the firing of the origin of replication, ORI=1, to

be the marker for START. Also, in all cases (wild type as well as other mutant phenotypes shown through the course of the chapter), we designate the observed phenotypic size of the mutants relative to wild type and for viable cells, we show cycles after the cell has reached steady state. We compare the active SBF and MBF complexes present in each of the mutants to predict their size.

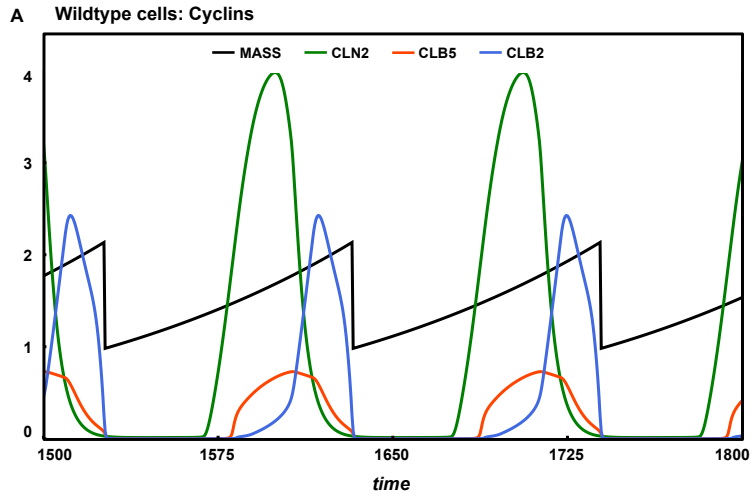

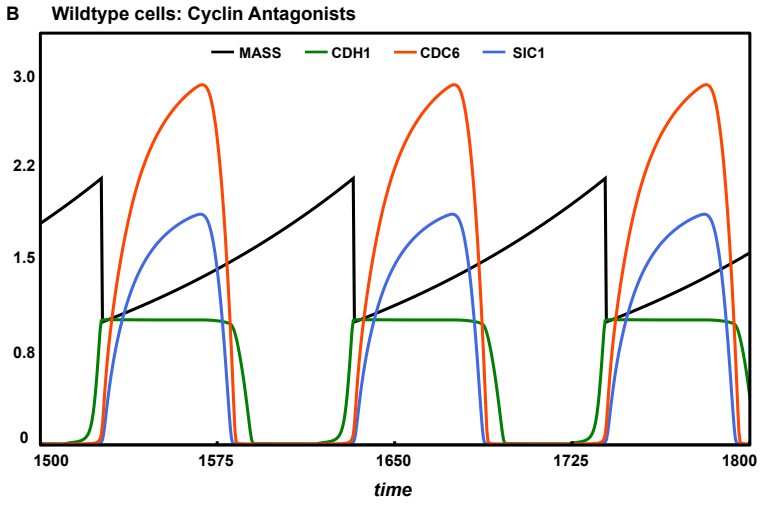

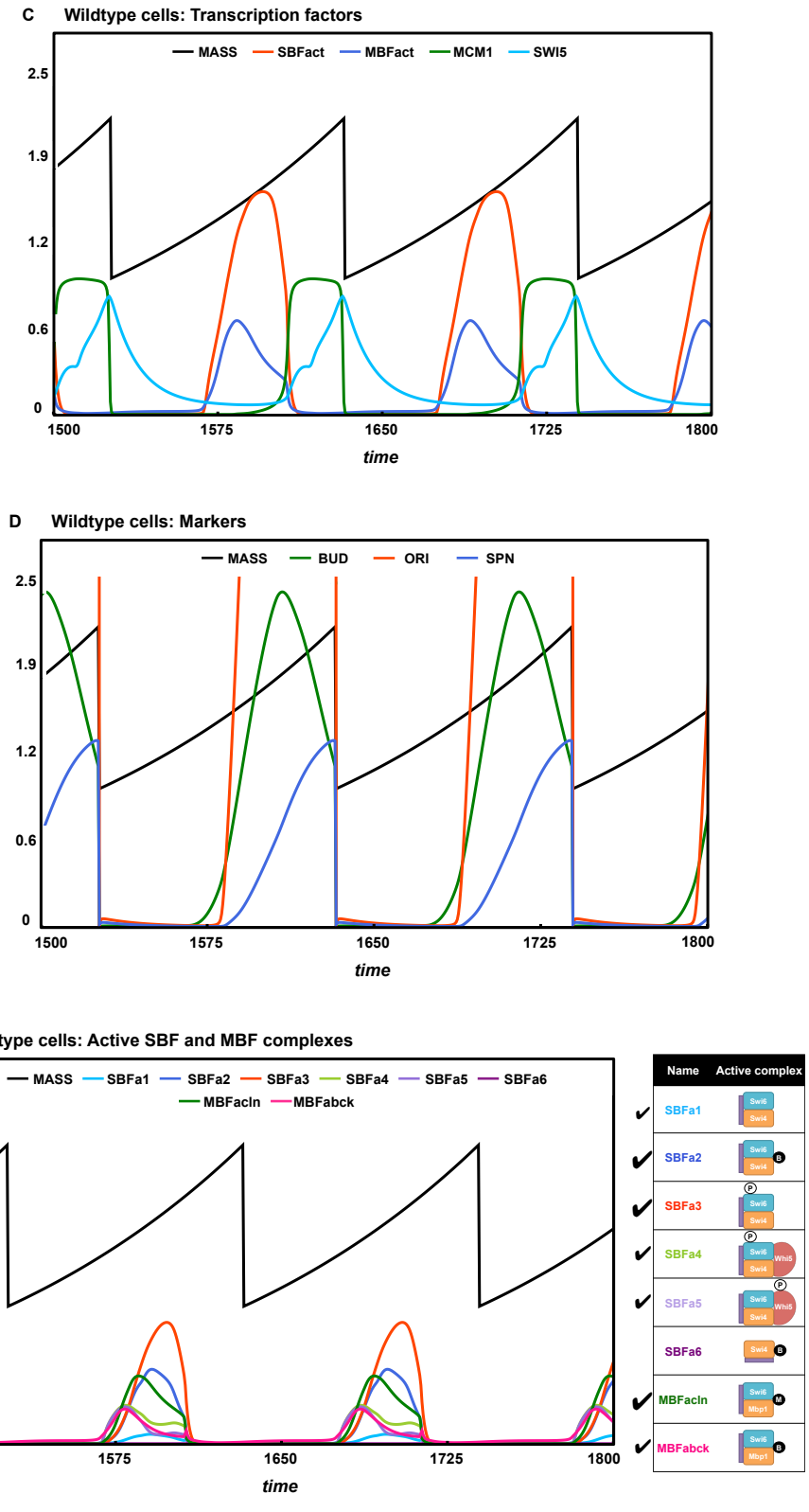

Figure 12. Simulation of wild type cells in glucose.

In each of the panels, the following proteins/components are tracked for ~2 cell cycles in glucose with a mass doubling time of 90 min and daughter cycle time of ~107 min. (A) Cyclins (Cln2, Clb5 (active), Clb2 (active)), (B) Cyclin antagonists (Cdh1, Sic1 (active), Cdc6 (active)), (C) Transcription factors (SBF, MBF, MCM1, Swi5), (D) Markers (CDK targets (BUD, ORI, SPN) that are used to indicate the occurrence of physiological events when their accumulated levels have reached a threshold (BUD=1 (bud emergence), ORI=1 (DNA synthesis initiation), SPN=1 (spindle alignment in metaphase)), (E) Active SBF and MBF complexes. Each form (SBFa1-a6, MBFacln, MBFabck) shown is the activity of SBF or MBF contributed by a particular form. The complexes that contribute to the different forms (all bound to promoter) are as follows: SBFa1= unmodified SBF (SBFB in the model); SBFa2=SBF activated by Bck2 (BSB); SBFa3=SBF phosphorylated on Swi6 (SBFB6P+SBFB6PQ); SBFa4=SBF-Whi5 complex phosphorylated on Swi6 (WSB6P+WSB6PQ); SBFa5=SBF-Whi5 complex phosphorylated on Whi5 (WSB5P); SBFa6=Swi4dimers activated by Bck2 (Swi4B); MBFacln=MBF activated by Clns; MBFabck=MBF activated by Bck2. The presence/absence of these complexes has been represented in an iconic form in the adjoining table. Check and cross marks are used to denote presence or absence (due to mutation) of specific complexes. Absence of any sign denotes that the specified complex is absent in the simulation of that strain. Black curve in all panels denotes mass (corresponding to exponential cell growth and division). As shown in (E), for wild type cells, the dominant form of SBF is SBFa3, the form of SBF phosphorylated on Swi6, whereas the dominant form of MBF is the Cln-activated MBF.

Activation of SBF by Bck2

In addition to activation by cyclins, SBF and MBF are also activated by Bck2 (Wijnen & Futcher, 1999). The mechanism of Bck2 activation of these transcription factors is not very clear, but it is believed to be independent of CDK phosphorylation and the inhibitor protein, Whi5 (Costanzo et al, 2004; Wijnen & Futcher, 1999). Hence, we consider a mechanism by which Bck2 modifies SBF to alternate forms that are active (BSB, Swi4B in Figure 13). The double mutant *cln3*Δ *bck2*Δ is inviable, emphasizing the

importance of Cln3 and Bck2 in the model (Figure 26C). From the relative sizes of *cln3*Δ and *bck2*Δ mutants (*cln3*Δ >> *bck2*Δ >> WT; Figure 26A, B; (Dirick et al, 1995; Wijnen & Futcher, 1999)), we determine the relative contributions of Cln3 and Bck2 to SBF/MBF activation in the model. We assume the complexes activated by Bck2 to be active but not as active as the Cln-activated forms. These less-active forms are enclosed with light green boxes in Figure 13.

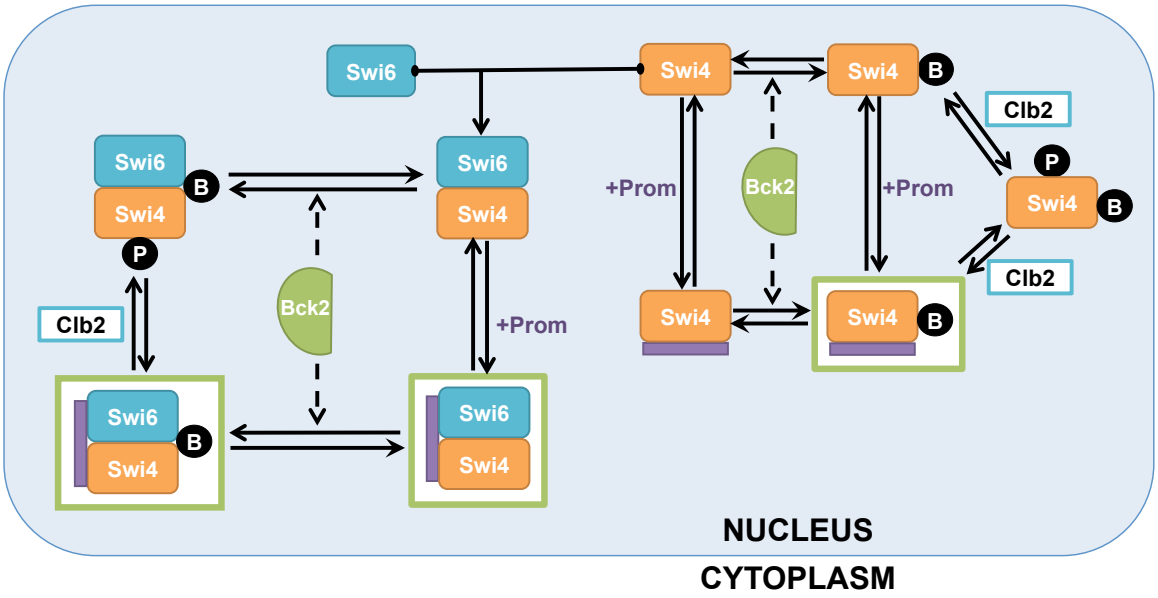

Figure 13. Role of Bck2 in activation of SBF.

Bck2 activates SBF by modifying it to an alternate form independent of CDK activity and Whi5. Bck2 also acts on Swi4 and modifies it to an active form. The cartoon is a concise representation (not including all the intermediate steps), but as depicted, activation by Bck2 and promoter-binding is required for the complex to be active. Black-filled circles with 'B' represent the Bck2-induced modification and active forms are enclosed in a light green box (since these complexes are not as active as Cln-activated forms). Clb2 causes complex inactivation (see equations in Materials and Methods for details).

We also assume that Swi4 has some residual activity (in the absence of Swi6) and that the Swi4 homodimeric complex is activated by Bck2. This assumption is important to understand the mutants *swi6*Δ, *swi4*Δ *swi6*Δ and *swi6*Δ in the background of *cln3*Δ and *bck2*Δ. The significance of the assumption and the behavior of these mutants is described in the section on mutants pertaining to regulation of Bck2.

Regulation of MBF

Alongside SBF, the other important transcription factor operating at START is MBF, comprising a heterodimer of Mbp1 and Swi6. One of the primary cell cycle targets of MBF considered in our model is Clb5. Due to functional overlap between SBF and MBF transcription factors and their targets, we also consider transcription of Cln2 by MBF and Clb5,6 by SBF (Bean et al, 2005).

MBF is activated by both Cln3 (and Cln2, Clb5 to a lesser extent) and Bck2 by independent mechanisms, and inactivated by Clb2 and by Nrm1, one of MBF's own targets (de Bruin et al, 2006). Nrm1 plays a more important role than Clb2 in the inactivation of MBF. In our model, we have incorporated the positive feedbacks in activation and the negative feedback in inactivation of MBF as depicted in Figure 14.

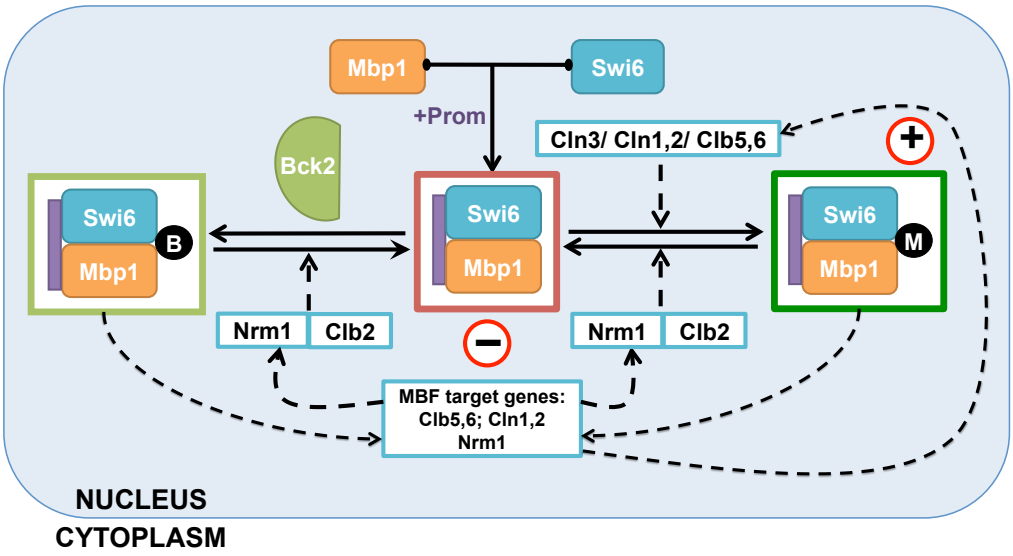

Figure 14. MBF regulation.

MBF, by itself, is inactive in a repressed state (indicated by enclosing red box). It is activated either by cyclins (Cln3, Cln1,2, Clb5,6) or by Bck2 independently (these forms are more and less active, as indicated by the dark and light green boxes, respectively). MBF is primarily inactivated by its own transcriptional target, Nrm1, resulting in a negative feedback highlighted by the '–' sign.

Additionally, we have also considered inactivation of MBF by Whi5 (Costanzo et al, 2004), even though de Bruin *et al.* (2004) show that Whi5 does not bind to and negatively regulate MBF (Whi5 binding is not shown in our cartoon of MBF regulation, but is included in the model).

Size control

During the cell cycle, budding yeast has stringent control for maintaining size homeostasis (Johnston, 1977). The yeast cells must grow to a critical size to start budding and initiate S phase. This control is achieved through a tight coupling of cell growth and

division, and the underlying mechanism is emerging. We consider the following molecular details of this size control mechanism in our model of the cell cycle.

Cln3 activation of SBF, MBF

The involvement of Cln3 in size threshold became evident from over-expression and knockout studies. Cln3 deletion mutants or mutants with increased cytoplasmic export are larger in size compared to WT, while mutants over-expressing Cln3 or with increased Cln3 nuclear import are smaller than WT (Cross et al, 2002; Cross, 2001). Cln3 had thus been thought to be a nuclear sensor of cell size, triggering START only when the threshold had been reached. Also, although Cln3 has been observed to be an important regulator of START, Cln3 knockout mutants are still viable due to the activity of Bck2. Bck2 is known to be activated by glucose and to promote START by an unknown mechanism that is independent of Cdc28 and Whi5 (Costanzo et al, 2004; Wijnen & Futcher, 1999). However, the mechanism of action of Bck2 is not understood.

Earlier models of the cell cycle (Chen et al, 2004; Chen et al, 2000) account for these mutant phenotypes in the following way: as cells grow in volume, total Cln3 protein level in the cell increases in parallel (its concentration is constant). It is assumed that Cln3 migrates to the nucleus and it becomes concentrated there (assuming the nuclear volume does not change significantly). Therefore, nuclear concentration of Cln3 is proportional to cell size. This nuclear Cln3 (& Bck2) accumulation triggers START and activates SBF by an ultrasensitive GK switch (Goldbeter & Koshland, 1981) when a threshold level is reached. Thus START transition behaves like a switch in the Chen2004 model (Chen et al, 2004; Chen et al, 2000). This hypothesis is questionable in the light of

recent experiments about the proportionate growth of the nucleus in relation to the cell (Jorgensen et al, 2007).

Size control in our current model

In our current model, cell size control is an outcome of the regulation and nuclear import of Cln3 (and Bck2) prior to START. It has been experimentally determined that in early G1, the Cln3/Cdc28 complex is sequestered to the endoplasmic reticulum (ER) membrane by Ssa1/2, Whi3 and other proteins. In late G1, the accumulation of Ydj1, a J-chaperone protein that responds to cell size, relieves the inhibition on Cln3 by translocating the Cln3/Cdc28 complex to the nucleus (Verges et al, 2007). Thus, Ydj1 is believed to be the cell size sensor, upstream of Cln3.

In our model, we assume that Ydj1, in response to mass, moves Cln3 from ER into the nucleus abruptly in late G1. Once Cln3 translocates to the nucleus in response to size, its downstream effects are mediated by Whi5, which, in its unphosphorylated form, binds to and inhibits SBF (Costanzo et al, 2004; de Bruin et al, 2004). Nuclear Cln3 phosphorylates Whi5, making the latter cytoplasmic and inactive, thus activating SBF. Since Ssa1 is the protein that retains (and thus inhibits) Cln3 in the ER, we assume that Ssa1 inactivates Cln3 (Verges et al, 2007). In order to explain the observation that Cln3 is nuclear from late G1 to late S/G2, we propose that Ssa1 is activated by Clb2 and Swi5 (Figure 15). This regulatory model explains the localization of in the nucleus from late G1 until the onset of mitotic events (late S-phase). Since little is known about Bck2 regulation, we assume that it is regulated similar to Cln3.

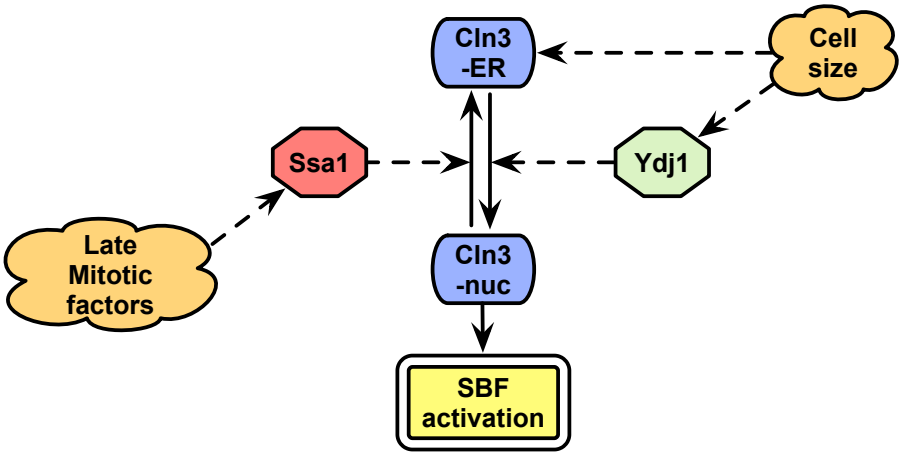

Figure 15. Cartoon of Cln3 regulation by Ydj1/Ssa1.

The nuclear form of Cln3 is the active form. Nuclear import is controlled by Ydj1 in response to cell size, whereas sequestration of Cln3 in the ER (inhibiting Cln3) is done by Ssa1, probably, in response to late mitotic factors. (See text above for details) We assume that Bck2 is regulated in a similar fashion.

We have thus modified the size control mechanism from the Chen2004 model, but still retain Cln3 (and Bck2) as the ultimate size sensor. We have also removed the dependence of G1/S and S-phase cyclins on mass from Chen2004 model, thereby, making Ydj1 and hence Cln3, Bck2 the key players in size control. Such a detailed mechanism for the START module would also allow for incorporation of the nutritional effects on size control in the future (described in the subsection below).

We have shown in our model that daughter cells are in compliance with a progressive G1 delay (activation of ORI/BUD in the model) in response to slower growth rates (poorer nutrient media) that is characteristic of strong size control. We tested this by varying the mass doubling times from 90 to 240 minutes (Figure 16). The daughter and mother cycle times were in perfect agreement with results from Lord and Wheals (1980). Also, in line with our expectations, our simulation showed that the longer cycle times in

slower growth media were mostly due to a delay in G1, wherein slower growing and smaller cells wait to reach the size threshold, leaving the budded phase almost constant (data not shown). The budded period was, however, close to 50 and almost constant over the wide range, differing quantitatively from the corresponding curve in the experiments (Figure 16).

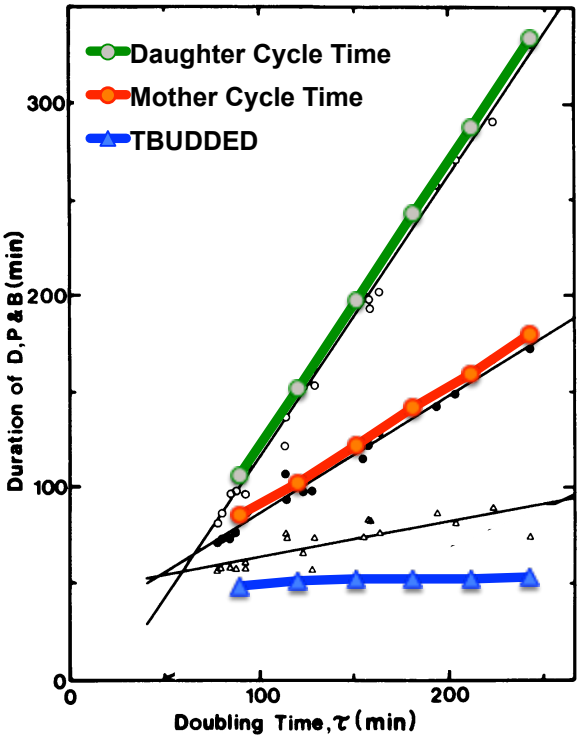

Figure 16. Duration of daughter and mother cycle times as function of mass doubling time.

Comparison with experiment by Lord and Wheals (1980) (used with permission). Green and red lines with filled circles are daughter and mother cycle times computed for mass doubling times 90-240min in our simulation. They are compared with daughter (black open circles) and mother cycle (black filled circles) times in the experimental graph. Blue lines with filled triangles correspond to budded period (simulations) and they are compared with black open triangles representing budded period (both mother and daughter) in

experiments. (Note: 90min mass doubling time (MDT) corresponds to glucose and 150min MDT to galactose).

The cell size distribution for different growth rates compares well with experiments by Lord and Wheals (1980) (Figure 17). Slower growth rates result in smaller cell volumes (taken to be mass at division in our model simulations) and higher growth rates (richer nutrient media) have a higher median cell volume.

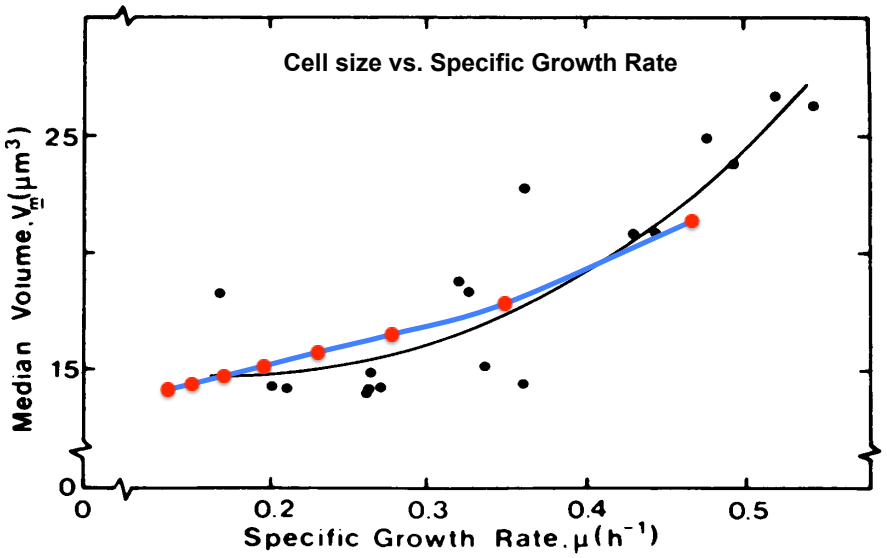

Figure 17. Cell size as a function of growth rate in budding yeast (daughter cells).

Comparison with experiment by Lord and Wheals (1980) (used with permission). Blue curve connecting red circles shows cell size at division at specific mass doubling times (MDT) from 90-300min (30min interval) and corresponding specific growth rates (ln2/MDT) from our model simulations. This curve is overlaid upon the experimental graph where median cell volumes for populations at different growth rates are plotted. The experimental curve was fitted by eye.

Single-cell experiments have shown a clear negative correlation between the time spent in G1 and mass at birth (Di Talia et al, 2007). The exact slopes and nature of these correlations depend on whether we are looking at mother or daughter cells. Mother cells

show a single slope of -0.1, indicating that mother G1 is controlled by a timer. Daughter cells show 2 slopes: the slope for the small newborn daughters is -0.7, indicating that the G1 for small daughters is controlled by a sizer; the slope for larger newborn daughter cells is 0.3, indicating a much less dependence on size. Although our model is continuous and deterministic in nature, owing to no variability between cells, we generated some preliminary results to be compared to experimentally determined cell sizes in single-cell assays (Figure 18). In the study of Di Talia (2007), the smaller daughter cells were observed to show stronger size control in comparison to larger ones. We checked this in our model by altering the initial mass at birth and following the time taken to pass through START (firing of origin of replication, ORI, in the model; Figure 18). Our simulation result shows a slope of -0.96 for small daughters and a slope of -0.36 for larger daughter cells. In the model, the small daughter cells have a strong size control, which is an artifact of the way size control has been implemented in the model. Concurrent with the experimental findings (Di Talia et al, 2007), we find that the part of G1 that is responsible for the delay in smaller cells comes from the time it takes for Whi5 to exit the nucleus (T1) and not the time between Whi5 export and bud emergence (T2) or firing of ORI (Figure 18). Although, we observe the negative correlation and important contribution of T1 to TG1, our results do not fit perfectly with the two-slope model observed in the experiments. This might be due to the manner in which we have performed the simulations. Our cells have identical genetic make-up (levels of different cell cycle proteins) independent of the starting cell size. In contrast, the experimentally observed cell populations might have protein levels scaled to their mean cell size.

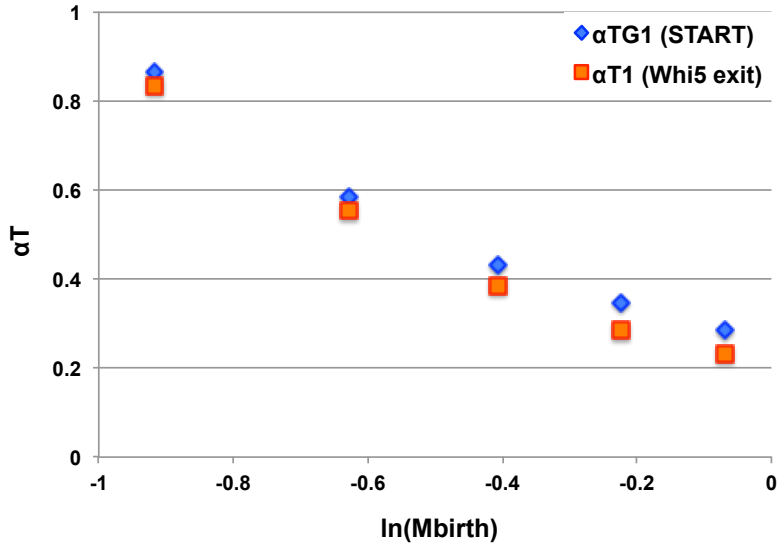

Figure 18. Correlation between cell size and residence in time in G1 for daughter cells (particularly time until Whi5 exits nucleus).

Dependence of length of G1 (TG1, from birth to ORI=1) and time taken for Whi5 export (T1, from birth to 50% of Whi5 export to the cytoplasm) are plotted with respect to mass at birth (on a log scale).

Our proposed molecular model for the nutritional effects on size control: Glucose-dependent Cln3 inactivation

Previously described shift-up experiments demonstrate that the critical size requirement for making the START transition depend on the nutrient medium that the yeast cells are growing in (Johnston et al, 1979). Although Cln3 seems to be an important sensor of cell size, it has been observed that despite higher Cln3 levels in a rich medium, cells make the START transition at a higher size threshold (Hall et al, 1998). In this section, we analyze the role of Cln3 in sensing cell size and setting the size threshold for START in response to nutrients.

Presence of glucose causes an increase in the rate of ribosome biosynthesis, and also an increase in protein synthesis efficiency (because of an increase in the number of ribosomes) by the TOR, Ras/cAMP, and Gpr1/Gpa2 pathways (Hall et al, 1998; Jorgensen & Tyers, 2004; Tokiwa et al, 1994; Wang et al, 2004).

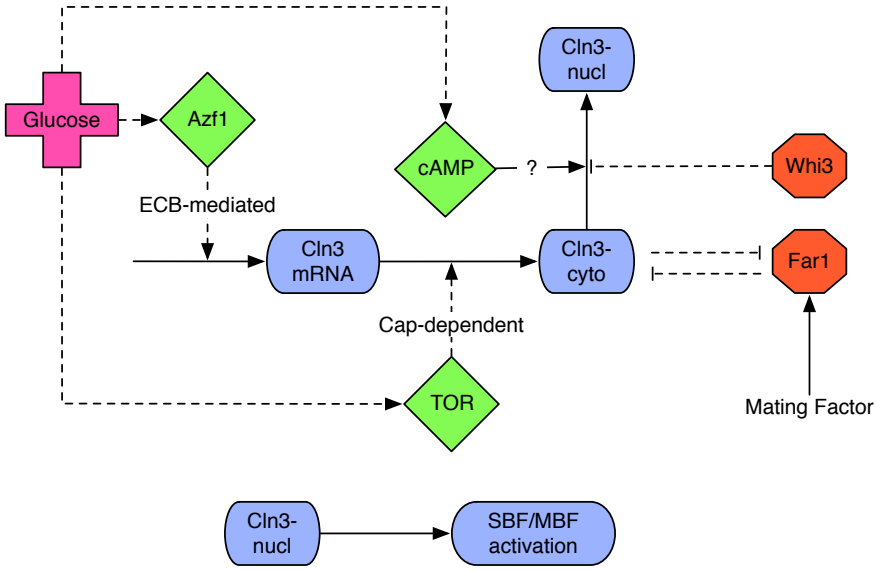

Figure 19. Regulation of Cln3.

The regulation includes the following interactions: 1. Inhibition of nuclear localization by Whi3, 2. Mutual inhibition between Cln3 and mating factor induced Far1, 3. Transcriptional regulation of Cln3 by Azf1 in response to glucose, 4. ECB-mediated transcription, 5. Translational regulation by TOR (cap-dependent initiation) of G1-cyclins, 6. Increase of Cln3 protein level/activity by cAMP through the Ras/cAMP/PKA pathway. Finally, activation of SBF, MBF by nuclear Cln3 is shown.

Cln3, now established as an important regulator of START, is activated by glucose in more than one way (Figure 19). Glucose upregulates Cln3 transcriptionally by activating a transcription factor Azf1 (Newcomb et al, 2002), translationally by the TOR pathway, and also post-translationally by an unknown mechanism involving cAMP

driving Cln3 to the nucleus where it is active. Among the inhibitors of Cln3 are Whi3, which drives it back to the cytoplasm (Gari et al, 2001), and Far1, a protein in the pheromone pathway that is an inhibitor of G1 cyclins (Alberghina et al, 2004).

From what is known about glucose regulation of Cln3, increase in Cln3 level due to rich carbon source (glucose) in the medium is expected to cause a corresponding decrease in size threshold. However, a higher critical size is observed in glucose than in poor carbon source like raffinose or ethanol (Johnston et al, 1979). In different growth media, growth rates are different. If the size threshold is modified by Cln3 and Bck2, the cell has to reach a critical size to export Whi5. The time after Whi5 export until budding, T2, is constant, so for faster growth rate, the size is bigger. This could be the reason for different size distribution for different nutrient sources (even for *cln3*Δ cells) (Jorgensen & Tyers, 2004). Hence, there must be another sensor of glucose that causes repression of SBF, and its inhibitory effect on SBF overpowers the activatory effect of Cln3. (Costanzo et al, 2004).

Two downstream nutrient modulators of TOR/PKA pathway, Sch9 (an AKT- like kinase) and Sfp1 (a zinc-finger transcription factor) are considered to be candidate intermediates in this mechanism (Jorgensen & Tyers, 2004). The nuclear concentration of Sfp1 is regulated by multiple nutrient and stress signals. Sfp1 is localized predominantly in the nucleus in fast growing cells. Carbon starvation or rapamycin treatment causes it to redistribute uniformly between nucleus and cytoplasm. The abundance of Sch9 correlates with cell growth rate and cell size (more Sch9, and larger size in rich medium). These experiments suggest that nuclear Sfp1 and Sch9 are repressors of START transition. Sch9 and Sfp1 single deletion mutants are smaller than WT cells (since SBF is not repressed

and START occurs early resulting in cells smaller than WT) in the presence of glucose, and these mutants are insensitive to glucose (Jorgensen et al, 2002). This observation supports the roles of Sfp1 and Sch9 in glucose regulation of START transition (Figure 20). However, the mechanism whereby Sfp1 and Sch9 repress SBF is unknown.

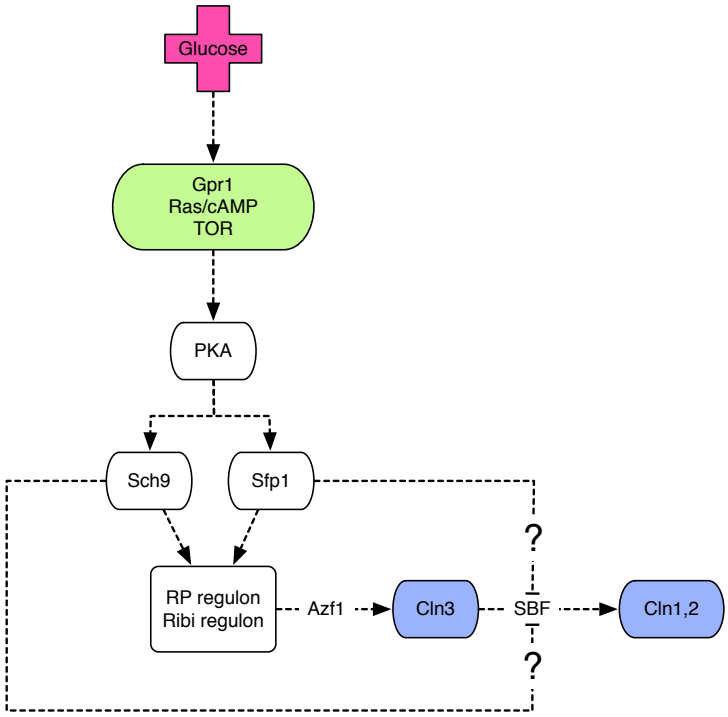

Figure 20. Model for effect of nutrient on size control through SBF.

Glucose activates the Gpr1, Ras/cAMP, TOR pathways that independently activate their downstream target PKA. PKA activates an AKT-like kinase, Sch9, and a Myc-like transcription factor, Sfp1 downstream of it. Sch9 and Sfp1, subsequently, turn on the ribosome proteins and the ribosome biogenesis regulons that lead to the activation of transcription factor, Azf1, necessary for the accumulation of Cln3. Cln3 activates SBF whereas Sch9 and Sfp1 inhibit SBF by an unknown mechanism. The inhibitory effect of Sch9 and Sfp1 is stronger than the activatory effect of Cln3 leading to an increase in size threshold in rich media.

Export and localization of START proteins

Localization of the core proteins (in their various modified/complexed forms) plays a crucial role in START transition (Di Talia et al, 2007; Sidorova et al, 1995; Wagner et al, 2009). We consider export and localization of the START monomers by building a compartmentalized model (nucleus, cytoplasm inside a single cell; Figure 21). The ratio of the sizes of these two cellular compartments is predefined (0.2:0.8 in our case) and remains constant throughout the cell cycle (Jorgensen et al, 2007). We assume that SBF complexes that have been phosphorylated on Whi5 or the S160 site of Swi6 are transported to the cytoplasm by Msn5, and dissociated immediately, and phosphorylated Whi5 monomers can be exported by Msn5 as well (Figure 21, Step 1). Unphosphorylated monomers move back to the nucleus (regardless of the phase of the cell cycle) (Figure 21, Step 2). Phosphorylated Whi5, Swi6 and Swi4 wait for corresponding phosphatases to remove the phosphate groups and be able to reenter the nucleus (described below) (Figure 21, Steps 3, 4).

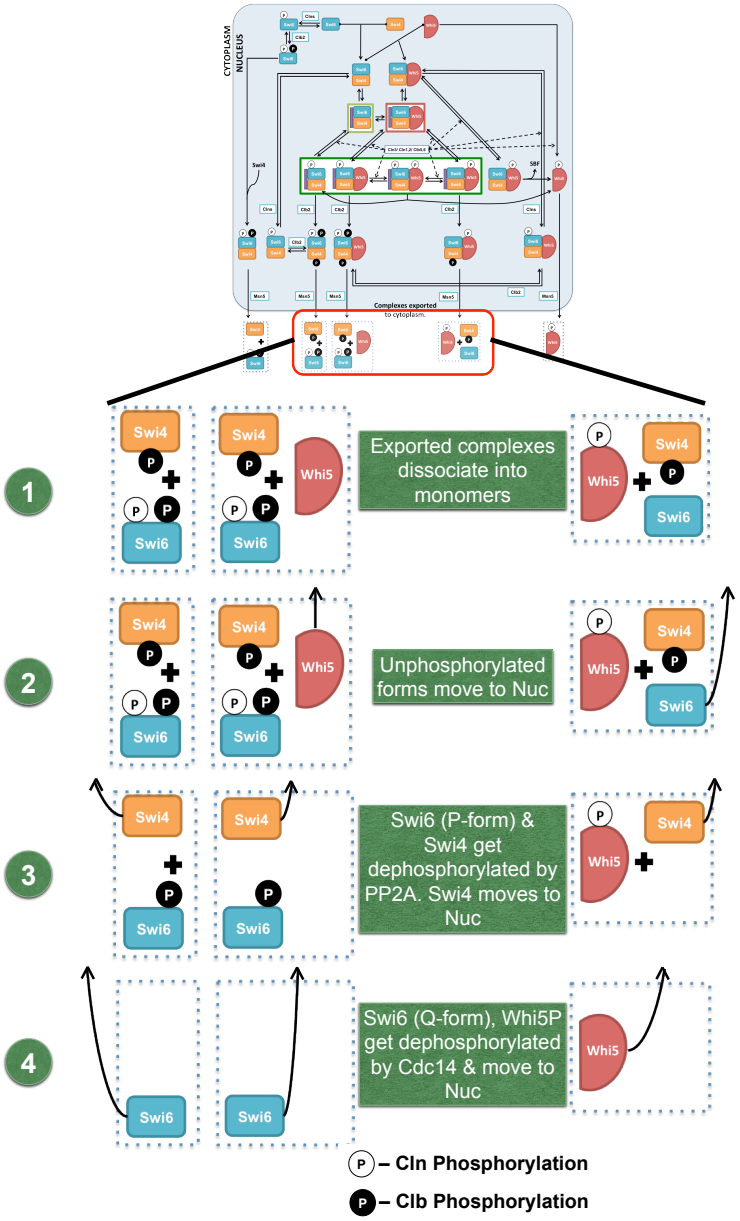

Figure 21. Localization of different monomers.

Following from Figure 10, all SBF complexes with appropriate phosphorylation states move to the cytoplasm following Clb phosphorylations. This figure describes the timing of re-import and hence overall temporal localization of the different monomers (Swi4, Swi6, Whi5). Export and reimport of Whi5P, although not shown explicitly, follows the same steps as phosphorylated Whi5 in the cartoon. Step 1 shows the possible states of monomers after complex export and dissociation. Step 2 corresponds to immediate reimport of unphosphorylated monomers to nucleus. In step 3, Swi4 and the P-form of Swi6 (all phosphorylation sites except S160) get dephosphorylated by PP2A and moved to the nucleus. Finally, in

step 4, the phosphatase Cdc14 that accumulates at mitotic exit dephosphorylates Whi5 and Swi6 Q-form at residue S160, following which Whi5 and Swi6 get reimported to the nucleus resetting the localization state for the G1-phase of the next cell cycle.

Whi5 localization

Single-cell experiments from Cross's group (Di Talia et al, 2007) reveal that Whi5 is nuclear only in G1 and is rendered cytoplasmic with the onset of the START transition until the beginning of the next cycle. We have encoded this behavior in the model by allowing phosphorylation of all forms of Whi5 (SBF-bound and free forms of Whi5) in the nucleus by G1 and G1/S cyclins, Cln3, Cln2 (in the model, Cln2 represents Cln1,2) and Clb5 (represents Clb5,6). These phosphorylation events allow certain eligible forms to be exported to the cytoplasm in late G1 by the transport protein, Msn5 (free form of Whi5P and any Whi5 that binds with SBF, with either Swi6 being phosphorylated on the Q-form by Clb kinase or Whi5 being phosphorylated by Cln kinase) in late G1 (Figure 21). Phosphorylated and cytoplasmic Whi5 is then dephosphorylated by Cdc14, which gets activated at mitotic exit (Figure 21, Step 4).

Swi6 localization

Swi6 localization is known to depend on a particular serine residue, S160, which when phosphorylated in late S-phase by S-phase cyclin Clb6 enables Swi6 to be transported to the cytoplasm (Sidorova et al, 1995). Sidorova et al, showed that Swi6 S160A (serine mutated to Alanine) mutant, Swi6 remained in the nucleus throughout the cell cycle. In our model, this residue and hence the phosphorylated form is designated as the 'Q-form' (black phosphorylation site in Figure 21) to distinguish it from the other

activatory phosphorylations that happen on Swi6 (P-forms) by Cln kinases (white phosphorylation site in Figure 21). Those responsible for the Q-form are Clb5 (Geymonat et al, 2004) and Clb2 (represents Clb1,2). The presence of the Q-forms is to ensure cytoplasmic localization of Swi6 from late-S phase through end of the cycle. Queralt and Igual (2003) showed that the export of phosphorylated Swi6 depends on the transport protein, Msn5, as well as the presence of Swi4. In our model, the phosphatase, PP2A dephosphorylates the P-form (Figure 21, step 3). Similar to Whi5, we assume that the final dephosphorylation (on Q-form) and re-import of Swi6 happens at mitotic exit by Cdc14 (Geymonat et al, 2004) (Figure 21, step 4).

Swi4 localization

Unlike Whi5 and Swi6, Swi4 is known to show nuclear localization at all times (Baetz & Andrews, 1999). For this reason, we assume that phosphorylated Swi4 (irrespective of the compartment) is dephosphorylated by an unspecified active phosphatase (Ppase in our case) instead of waiting for Cdc14 to accumulate. This explains the predominant nuclear localization of Swi4 in our model (Figure 21, step 3).

Simulation of localization and export of monomers

We have captured the picture of the localization of monomers through numerical simulations (Figure 22). To compare with experimental localization data, we look at the profiles of phosphorylated and cytoplasmic monomeric components and the timing of their nuclear export. We observe that phosphorylated Whi5 moves to the cytoplasm in late G1, while phosphorylated Swi6 moves out after START (mid-S phase) and both

monomers stay in the cytoplasm until mitotic exit. There is a negligible level (<10%) of phosphorylated Swi4 in the cytoplasm in most phases of the cell cycle. These simulations match well with previously discussed experimental results on the localization of Whi5, Swi6 and Swi4. We observe that ~70% of Swi6 goes to the cytoplasm. This is because Swi6 monomer also constitutes MBF, which is incapable of moving to the cytoplasm. Swi6 also seems to be trapped in certain phosphorylated SBF forms, which too cannot be localized to the cytoplasm.

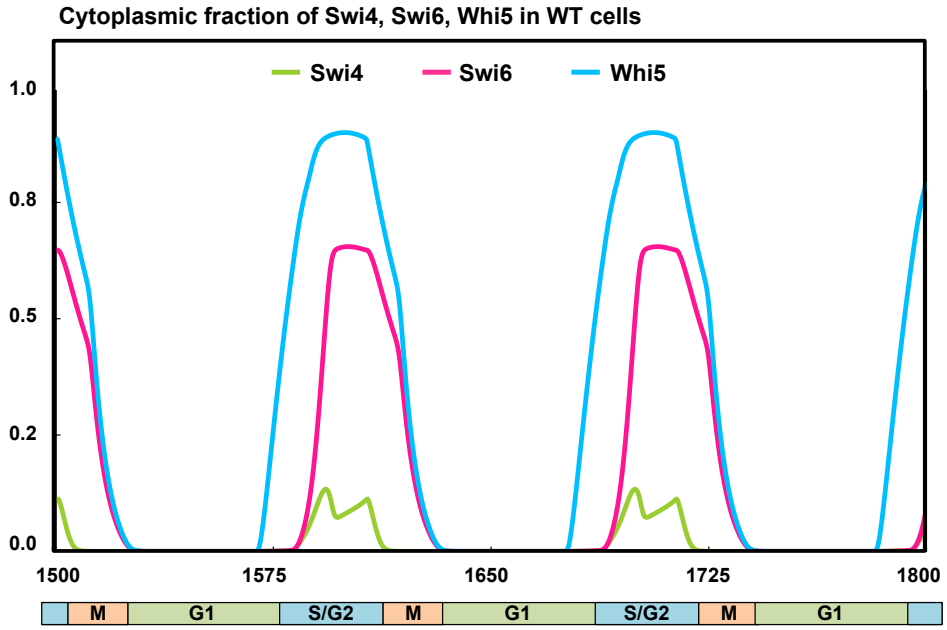

Figure 22. Simulation of the timing of localization (export) of different monomers.

Cytoplasmic fraction of monomers Swi4, Swi6 and Whi5 are plotted against time. The bar at the bottom of the graph shows the timing w.r.t. different phases of the cell cycle. In the model, the onset of S and M phases correspond to DNA synthesis (ORI=1) and spindle assembly checkpoint (SPN=1), respectively. In compliance with experiments, Whi5 enters cytoplasm (exits nucleus) in late G1, followed by Swi6 in S-phase. Both Swi6 and Whi5 are cytoplasmic until mitotic exit. Swi4 is mostly nuclear at all times. Details are discussed in the main text.

We are also able to reproduce the results pertaining to the importance of the export protein, Msn5, in the cell. *msn5*Δ mutants are known to be about 40% larger than WT cells (Queralt & Igual, 2003), and our simulations show that these cells are considerably larger too, since SBF localization is upset and there is only active MBF (Figure 23). In *msn5*Δ, both Whi5 and Swi6 are nuclear at all times.

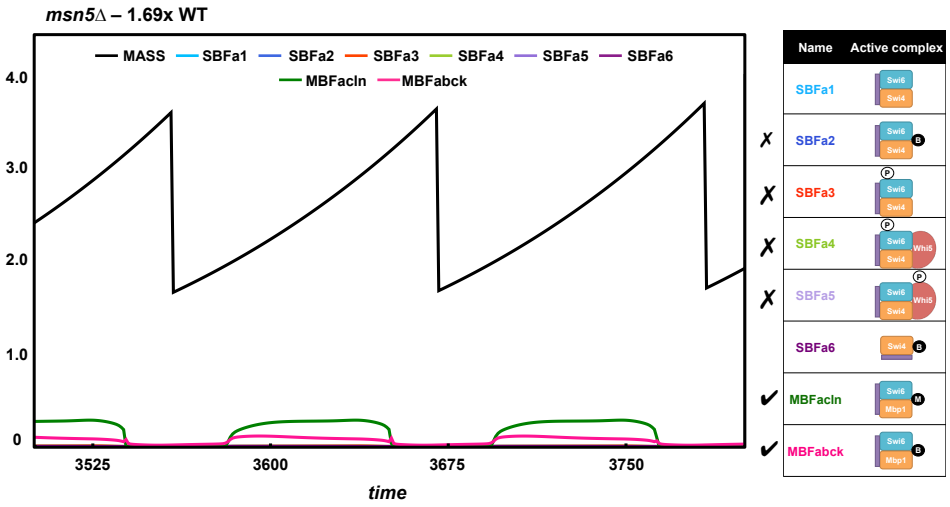

Figure 23. Importance of transport protein, Msn5.

These simulations are plotted for msn5Δ cells (MSN5=0 in our model). The cells are significantly larger than WT cells due to the absence of active SBF, and lesser amount of active MBF (MBFacln and MBFabck in plot above).

Case of the non-phosphorylable mutants

A critical gap in our previous understanding of START is the complex role of phosphorylation in regulating the transition. Recent studies have uncovered the regulatory details of SBF activation using non-phosphorylable single mutants *WHI5-12A*, *SWI6-SA4*, and the double mutant *WHI5-12A SWI6-SA4* (Sidorova et al, 1995; Wagner et

al, 2009). In each of these mutants, specific CDK sites have been mutated to alanine, so as to mimic a non-phosphorylated residue. Surprisingly, the two single mutants grow to wild type size (blue and pink curves in Figure 6 in comparison to red curve of WT), while only the double mutant shows an increase in cell size: double mutant cells are ~40% larger than wild type cells (Cyan curve in Figure 6) (Wagner et al, 2009). The larger cell size indicates that there is a delay in the START transition only in the case of the double mutant when neither Whi5 nor Swi6 can be phosphorylated (Figure 6; (Wagner et al, 2009). This is contrary to previous belief that Whi5 phosphorylation is absolutely essential for relieving the inhibition of SBF (Costanzo et al, 2004; de Bruin et al, 2004).

We have encoded this information in the current model by considering all possible phosphorylation states and intermediate complexes (Figure 24). For example, in the mutant *WHI5-12A*, Whi5 cannot be phosphorylated, but the phosphorylation sites on Swi6 are intact. Therefore, SBF as well as SBF-Whi5 complexes can get phosphorylated on Swi6 to yield active transcription factor (Figure 24A). We assume these complexes to be fully active (same activity as the complexes present in wild type cells) so that there is no difference in size. Similarly, in the case of *SWI6-SA4* mutants where the phosphorylation sites on Swi6 have been mutated to alanine, Whi5 phosphorylation sites are intact. Therefore, though SBF cannot be phosphorylated by Clns, the SBF-Whi5 complex can be phosphorylated on Whi5 (Figure 24B). In this scenario, therefore, this phosphorylated complex is assumed to be fully active like the wild type forms ensuring a cell size similar to WT cells. In the case of the double mutants (*WHI5-12A SWI6-SA4*), however, neither Swi6 nor Whi5 can be phosphorylated (Figure 24C). Consequently, the SBF-Whi5 complex would remain unphosphorylated and inactive. Even though

promoter-bound SBF, by itself, has some residual activity and Bck2 is still present, because Whi5 is present in excess, most SBF is bound by Whi5, very little Whi5-free promoter-bound SBF is present. So in the double mutant, SBF is completely off. Despite the absence of active SBF, these double mutant cells are larger in size, but still viable. Their viability can be explained by the presence of intact MBF that can transcribe Clb5,6 and Cln1,2 (through functional overlap with SBF).

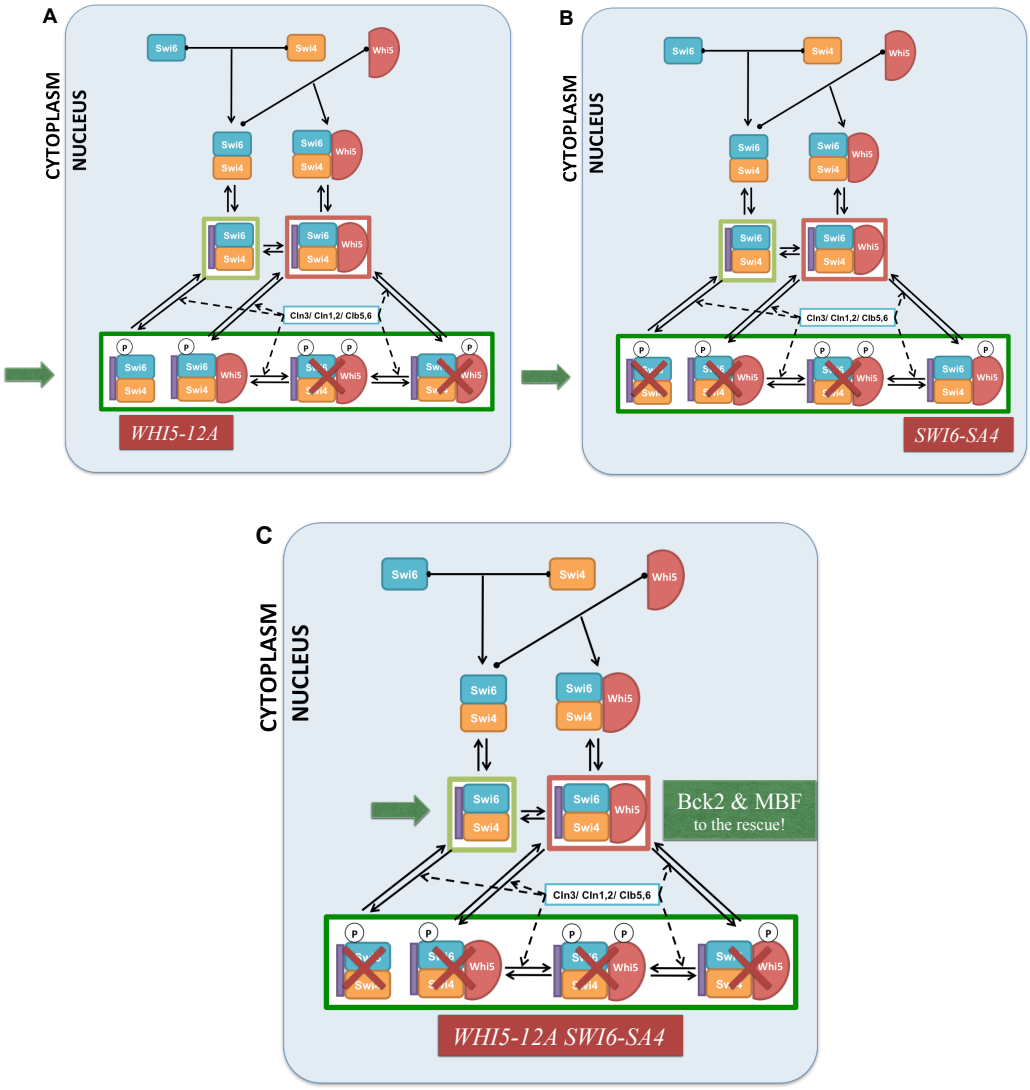

Figure 24. Non-phosphorylable mutants.

Active complexes in (A) *WHI5-12A* (This mutant will have size similar to that of WT due to the Swi6 P-forms), (B) *SWI6-SA4* (WT size due to phosphorylation of Whi5), (C) *WHI5-12A SWI6-SA4* (Viable, yet large, due to inactive SBF-Whi5 complex and support from Bck2 activation and MBF).

Simulating these three mutant genotypes by applying the corresponding constraints on phosphorylation states of SBF-Whi5 results in phenotypes similar to our expectations (Figure 25).

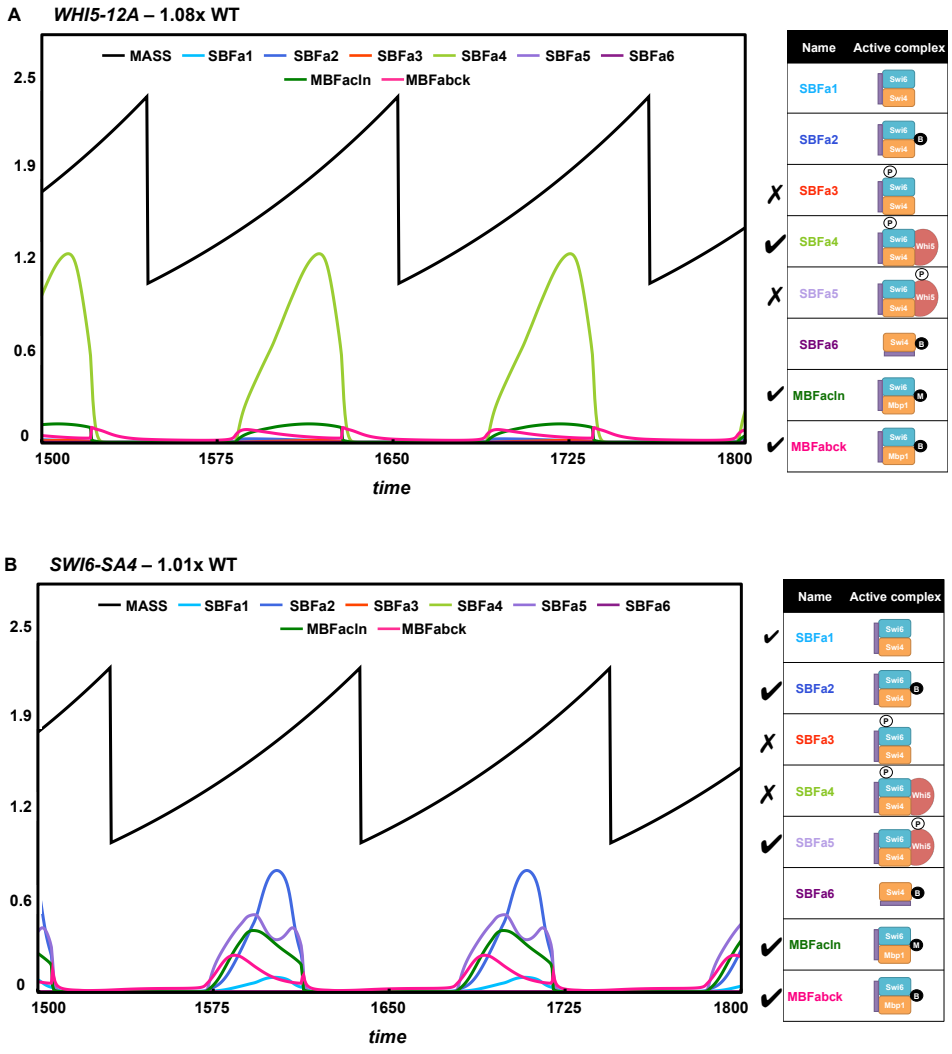

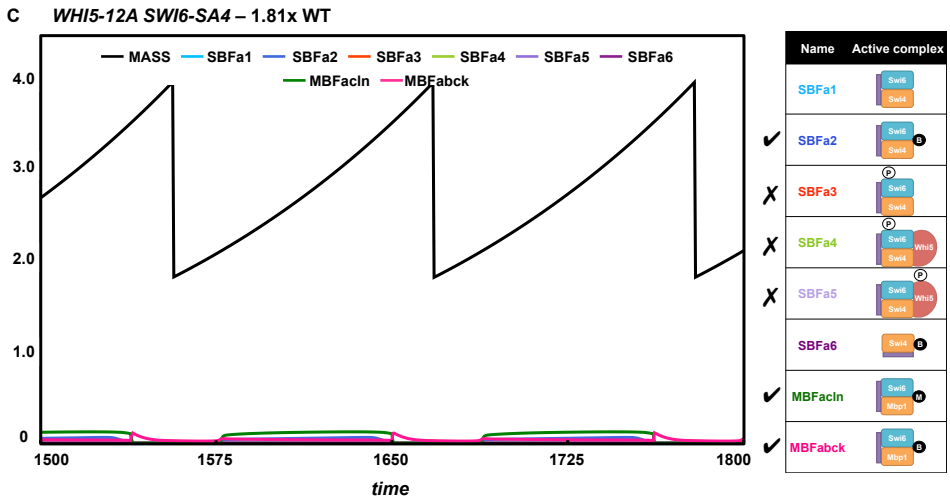

Figure 25. Simulation of non-phosphorylable mutants.

(**A**) *WHI5-12A* (SBF-Whi5 complex phosphorylated on Swi6 and MBF are the primary active forms – SBFa4, MBFacln, MBFabck; cells are ~WT size), (**B**) *SWI6-SA4* (SBF activated by Bck2, SBF-Whi5 complex phosphorylated on Whi5, and MBF are the primary active forms – SBFa2, SBFa5, MBFacln, MBFabck; cells are ~WT size), (**C**) *WHI5-12A SWI6-SA4* (only very little of Bck2 activated SBF and MBF forms are present – SBFa2, MBFacln and MBFabck; cells are larger than WT)

Mutants pertaining to regulation of Bck2

Another important, yet less understood, regulator of the START transition is Bck2. To explain the previously described mechanism of activation of SBF by Bck2, we consider mutants pertaining to Cln3 and Bck2 and analyze the role played by Bck2.

According to our model, in *cln3*Δ mutants, most of the SBF complexes would be bound to Whi5 and be in their inactive state (WSB form), with very little scope for activation by Bck2 (there is some SBFa2 but very little SBFa1 and SBFa6). The only active MBF form is the Bck2 activated form, and most of MBF is in the inactive form. So, *cln3*Δ mutants have to grow to a very large size to accumulate enough Bck2 to trigger START.

On the other hand, in *bck2*Δ mutant, most of the active SBF complexes are intact, and only the minor forms BSB and Swi4B (SBFa2 and SBFa6) are lost. So, the size is slightly larger but still quite close to wild type cell size. The active SBF/MBF complexes responsible for START in *cln3*Δ and *bck2*Δ mutants complement each other. If we want *bck2*Δ to show significant increase in size, that would mean the contribution from Bck2-activated forms is significant in wild type cells. This would automatically result in a smaller size for *cln3*Δ mutants. Since, *cln3*Δ is much larger than wild type cells (>2x), *bck2*Δ cells are close to wild type size.

We also assume that Bck2 plays a role in the activation of a residual form of SBF (Swi4B) that remains in the absence of Swi6. This assumption has been made to be consistent with the following mutant phenotypes: *swi6*Δ is viable and large, whereas *swi6*Δ *swi4*Δ is inviable (Nasmyth & Dirick, 1991) (Figure 26D). This means that in *swi6*Δ cells, Swi4 has some residual transcriptional activity (due to Swi4B, SBFa6 in the model). This also explains why further deletion of Cln3 has no deleterious effect on the viability (Nasmyth & Dirick, 1991), since the activity of Swi4B does not depend on Cln3. However, *swi6*Δ *bck2*Δ is inviable (Wijnen et al, 2002) (Figure 26E), suggesting that the only remaining component of SBF/MBF, Swi4B, depends on Bck2 for its activation.

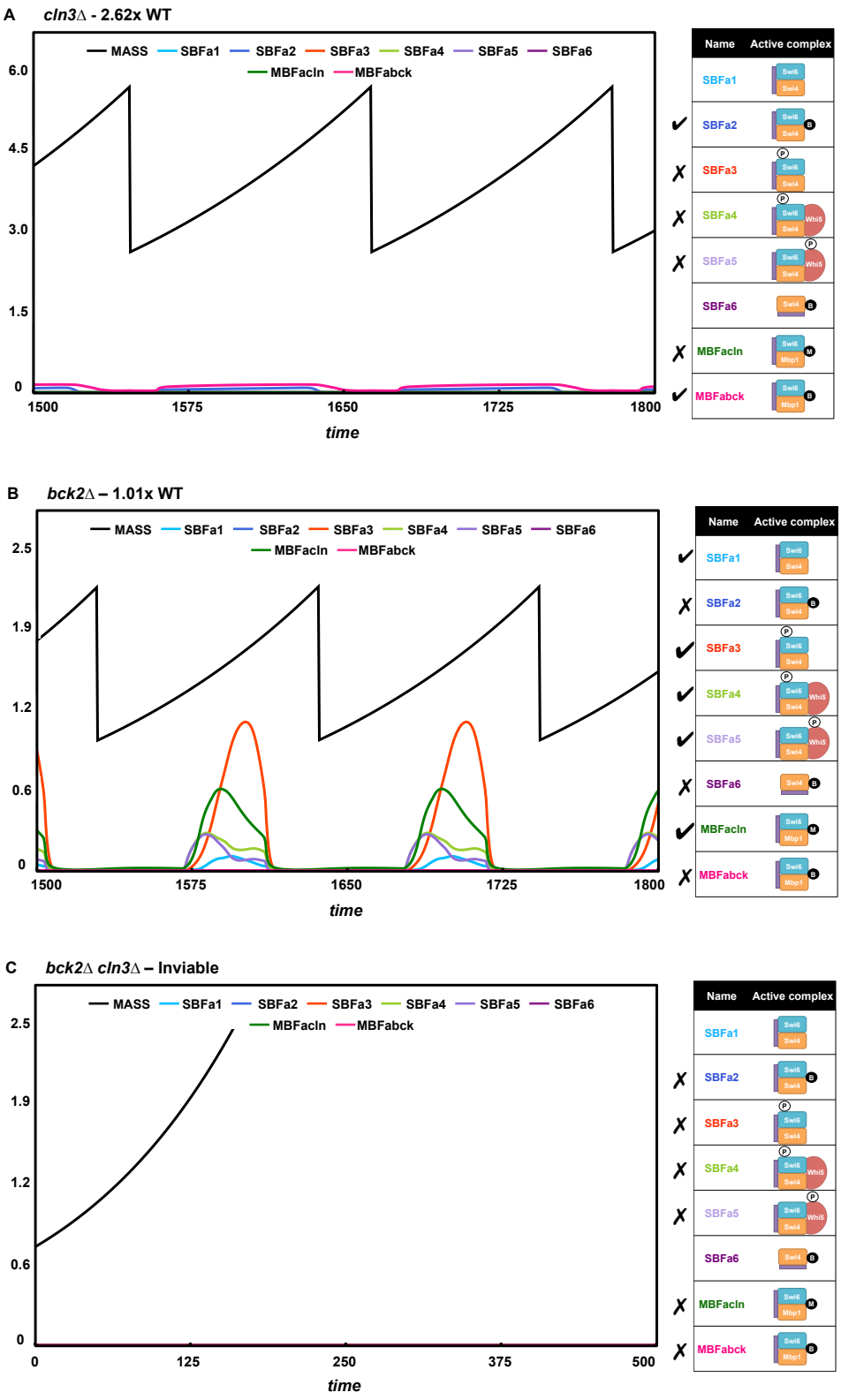
A
cln3Δ - 2.62x WT
MASS
SBFa1
SBFa2
SBFa3
SBFa4
SBFa5
SBFa6
MBFacln
MBFabck
6.0
4.5
3.0
1.5
0
1500
1575
1650
1725
1800
time
Name
Active complex
SBFa1
SBFa2
SBFa3
SBFa4
SBFa5
SBFa6
MBFacln
MBFabck
Swi6
Swi4
Whi5
Mbp1
B
M
P
✔
✗
B
bck2Δ – 1.01x WT
2.5
1.9
1.2
0.6
0
1500
1575
1650
1725
1800
time
C
bck2Δ cln3Δ – Inviable
2.5
1.9
1.2
0.6
0
0
125
250
375
500
time

D1 *swi6*Δ – 2.31x WT

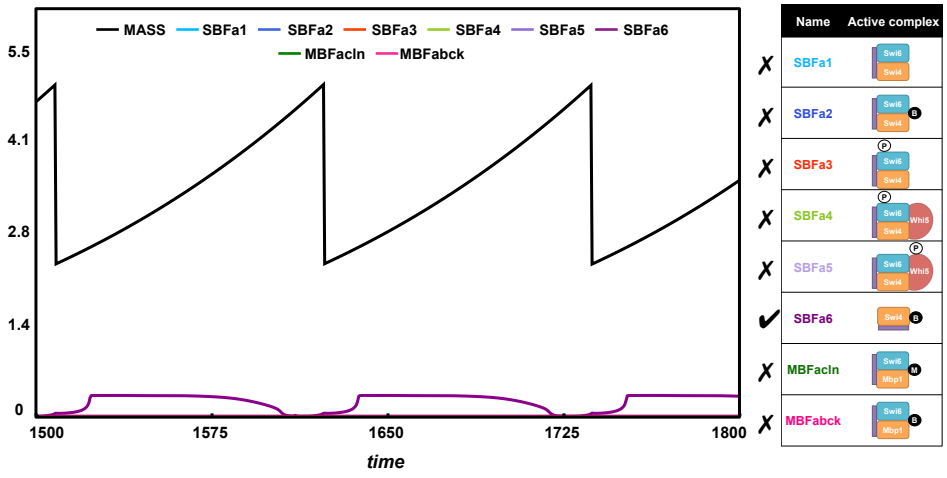

D2 *swi4*Δ *swi6*Δ – Inviable

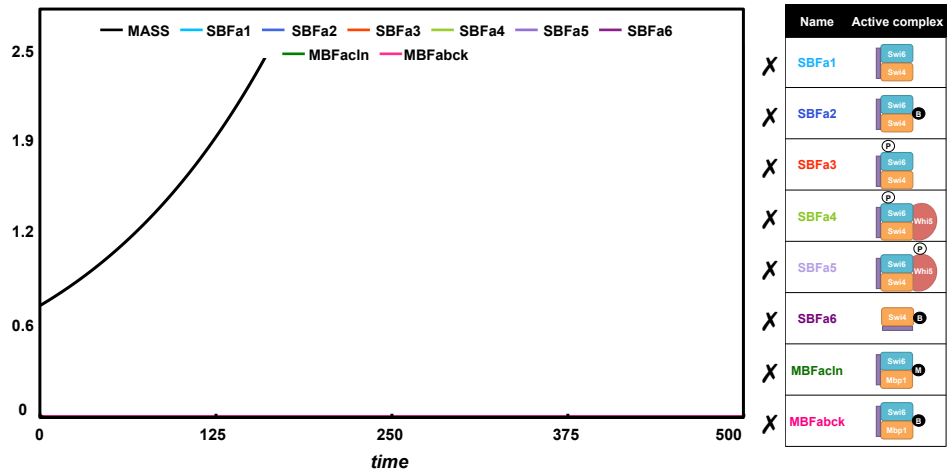

E1 *cln3*Δ *swi6*Δ – 2.34x WT

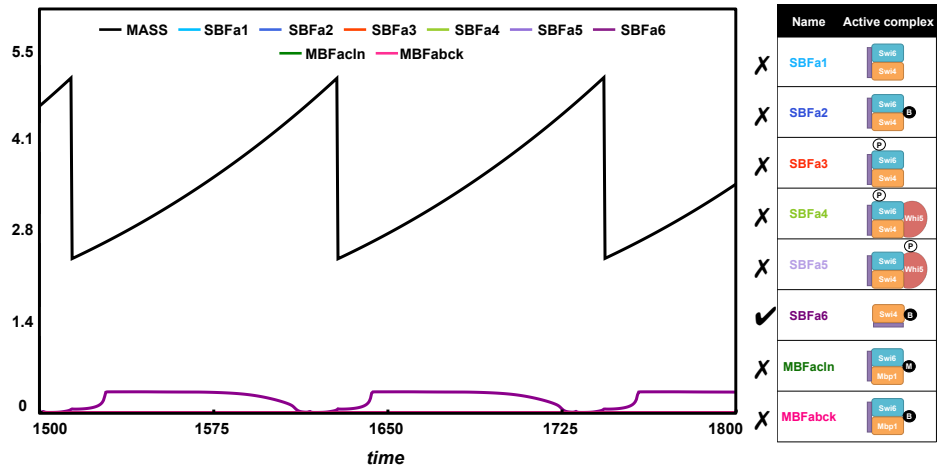

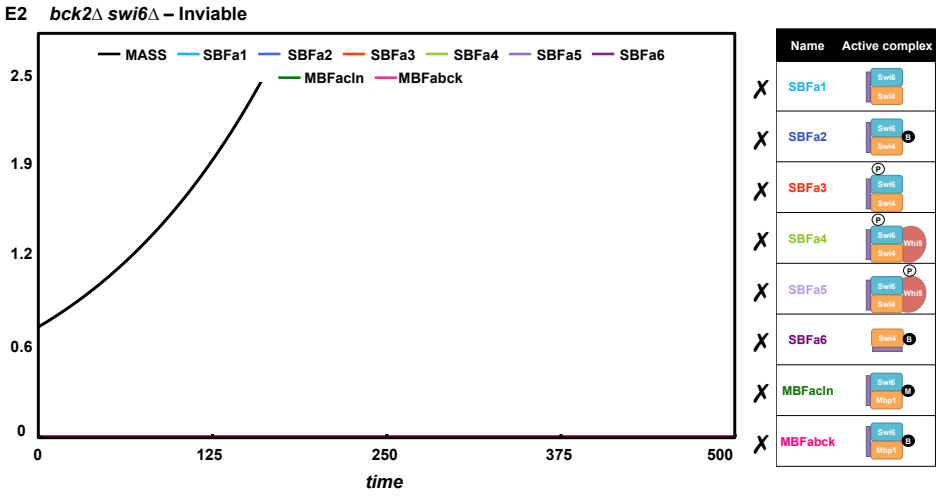

Figure 26. Importance of Bck2 in the model.

Simulations of the following mutants and their steady state sizes (viability/inviability) and the active SBF/MBF complexes present are shown: (**A**) *cln3*Δ (only Bck2 activated forms are present; cells are very large), (**B**) *bck2*Δ (only Cln-activated forms are present; cells are slightly larger than WT), (**C**) *bck2*Δ *cln3*Δ (no active SBF/MBF; cells are inviable), (**D**) D1: *swi6*Δ (only Swi4dimers (SBFa6) present; cells are viable yet large), D2: *swi4*Δ *swi6*Δ (no SBF/MBF; cells are inviable), and (**E**) *swi6*Δ *cln3*Δ (only Swi4dimers (SBFa6) present; cells are viable yet large).

Mutants pertaining to regulation of MBF

The relative importance of SBF and MBF, and their functional overlap are calibrated in the model based on the relative sizes of several known single and double deletion mutants of Mbp1, Swi4 and Swi6 (Table 3). For instance, *swi4*Δ cells (absence of SBF, presence of MBF) are about 1.3-1.5x WT size, whereas *mbp1*Δ cells (absence of MBF, presence of SBF) are 1.2-1.3x WT size (Koch et al, 1993) (Figure 27A,B). The double mutant is inviable signifying that either SBF or MBF should be present for the activation of START and viability of cells (Figure 27C).

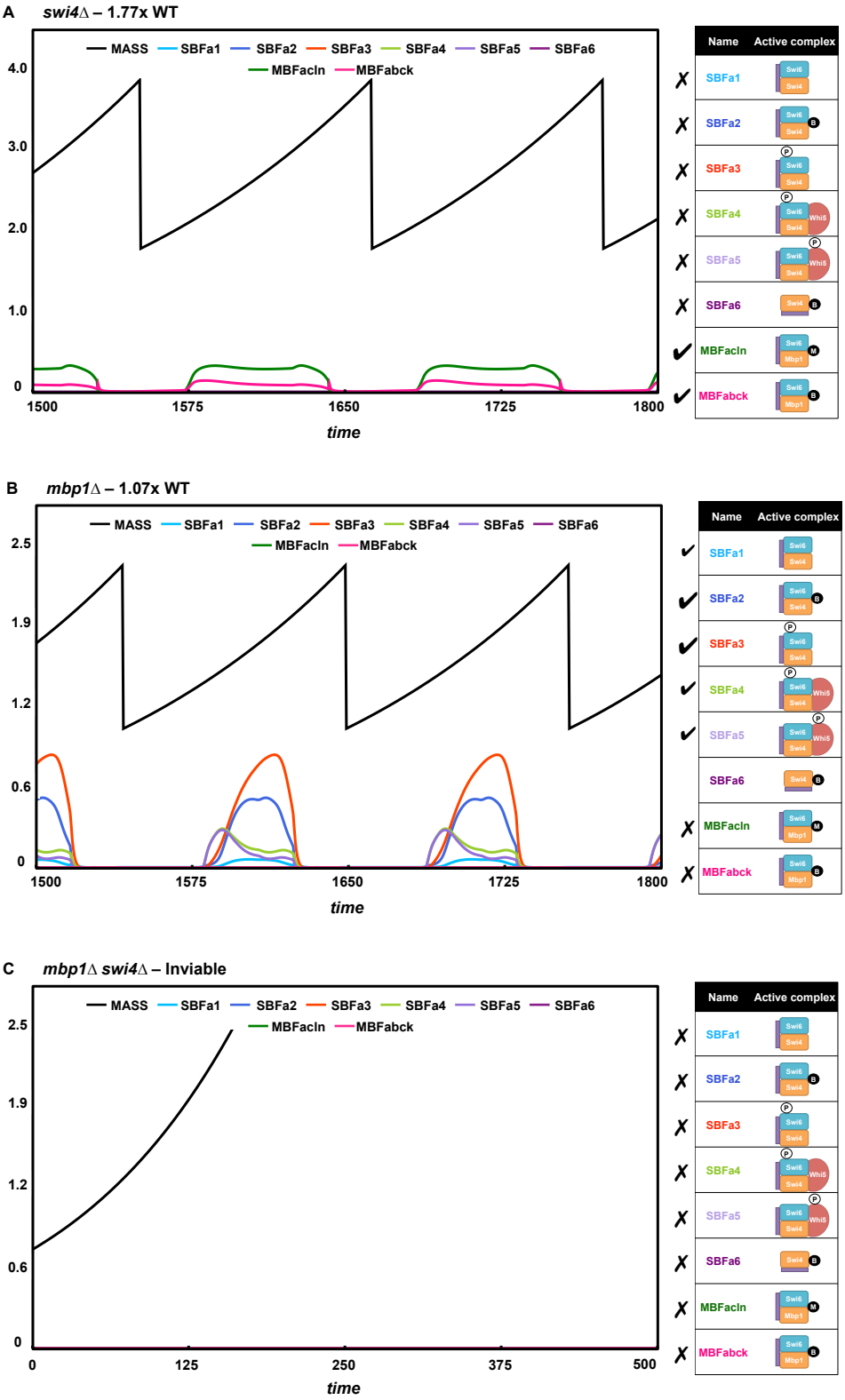
A swi4Δ – 1.77x WT
MASS SBFa1 SBFa2 SBFa3 SBFa4 SBFa5 SBFa6
MBFacIn MBFabck
4.0
3.0
2.0
1.0
0
1500
1575
1650
1725
1800
time
Name
Active complex
SBFa1
SBFa2
SBFa3
SBFa4
SBFa5
SBFa6
MBFacIn
MBFabck
B mbp1Δ – 1.07x WT
MASS SBFa1 SBFa2 SBFa3 SBFa4 SBFa5 SBFa6
MBFacIn MBFabck
2.5
1.9
1.2
0.6
0
1500
1575
1650
1725
1800
time
Name
Active complex
SBFa1
SBFa2
SBFa3
SBFa4
SBFa5
SBFa6
MBFacIn
MBFabck
C mbp1Δ swi4Δ – Inviable
MASS SBFa1 SBFa2 SBFa3 SBFa4 SBFa5 SBFa6
MBFacIn MBFabck
2.5
1.9
1.2
0.6
0
0
125
250
375
500
time
Name
Active complex
SBFa1
SBFa2
SBFa3
SBFa4
SBFa5
SBFa6
MBFacIn
MBFabck

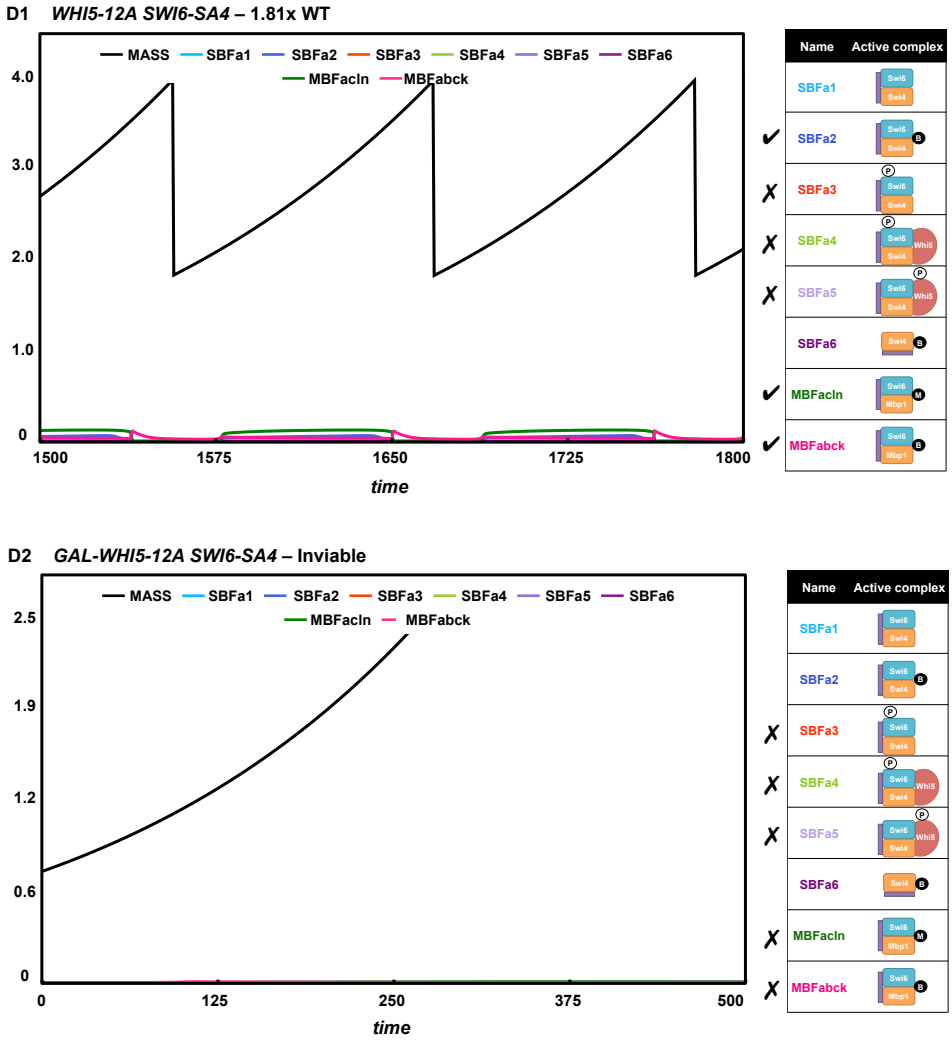

Figure 27. Importance of MBF in the model.

The figure includes simulations of the following mutants: (**A**) *swi4*Δ (only MBF present; cells are very large), (**B**) *mbp1*Δ (only SBF present; cells are slightly larger than WT), (**C**) *swi4*Δ *mbp1*Δ (no SBF or MBF; cells are inviable), (**D**) D1: *WHI5-12A SWI6-SA4* (cells depend on MBF forms for viability); D2: *GAL-WHI5-12A SWI6-SA4* (excess non-phosphorylable Whi5 inhibits MBF; cells are inviable).

In our model, we consider Whi5 inhibition of MBF to play a role primarily in *GAL-WHI5* mutants, where there is an excess of Whi5. Excess Whi5 could potentially have non-specific binding to MBF resulting in inhibition. For example, consideration of

this inhibition is needed to explain the lethality of the mutant *GAL-WHI5-12A SWI6-SA4* (Wagner et al, 2009). The double mutant *WHI5-12A SWI6-SA4* is viable and large solely due to the presence of MBF (MBFacln and MBFabck) and SBF activated by Bck2 to a lesser extent (SBFa2) (Figure 27D). If Whi5 only binds to SBF and inhibits it, it would be difficult to explain why *GAL-WHI5-12A SWI6-SA4* is inviable. Assuming that Whi5, when in excess, can bind to and inhibit MBF as well (similar to the in vitro studies presented by (Costanzo et al, 2004)) helps in resolving the problem; since MBF is the primary active complex in the double mutant, it would also be inhibited in the *GAL-WHI5-12A SWI6-SA4* mutant making the mutant inviable (Figure 27D).

Mutant simulations

We have simulated several mutants pertaining to START and other phases of the cell cycle with our current model. We have summarized our results in Table 3 where we list the mutants, their observed phenotypes, and the results from our simulations. We have described the START mutants with iconic representations of the major active SBF and MBF complexes that could exist in the different mutants alongside our simulation plots.

Table 3. START mutants

(In blue: Predictions; In red: Contradictions; *GAL* mutants are scaled w.r.t *GAL*-WT)

Genotype	Experimental Phenotype [scaled w.r.t WT]	Simulation Phenotype [scaled w.r.t WT in Glu or Gal (G)]	References
Cln3 mutants			
cln3Δ	1.8-2.7	2.62	Dirick 95; Costanzo 04
CLN3-1	0.85	0.73	Costanzo 04
GAL-CLN3	0.44	0.59G	Tyers 92
bck2Δ cln3Δ	Inviable	Inviable	Wijnen 99
bck2Δ cln3Δ GAL-CLN2 cln1Δ cln2Δ	Viable	2.65G	Di Como 95
bck2Δ cln3Δ multicopy *CLN2*	G_1 arrest	Inviable	Wijnen 99
bck2Δ cln3Δ sic1Δ	G_1 arrest	Inviable	Wijnen 99
bck2Δ cln3Δ whi5Δ	1.4	1.4	Costanzo 04; de Bruin 04
cln1Δ cln2Δ cln3Δ sic1Δ	Viable, large	2.07	Schneider 96
CLN3-1 swi6Δ	2.4	2.14	Wijnen 02
CLN3-1 whi5Δ	Viable, small; size~*whi5Δ*< *CLN3-1*	0.68	Costanzo 04
cln3Δ GAL-WHI5	Inviable	Inviable	Costanzo 04
cln3Δ GAL-WHI5-12A	Inviable	Inviable	Wagner 09
cln3Δ mbp1Δ	-	Inviable	–
cln3Δ mbp1Δ swi6Δ	2.4	2.34	Koch 93
cln3Δ swi4Δ	Inviable	Inviable	Ferrezuelo 09
cln3Δ swi4Δ whi5Δ	-	Inviable	–
cln3Δ swi6Δ	2.4	2.34	Wijnen 02
cln3Δ whi5Δ	0.7-0.9	0.85	Costanzo 04; de Bruin 04
Bck2 mutants			
bck2Δ	1.3	1.01	Wijnen 99
GAL-BCK2	0.5	0.98G	Costanzo 04
Multicopy *BCK2*	0.8	0.97	Di Como 95
bck2Δ cln1Δ cln2Δ	Viable, large	2.67	Epstein 94
bck2Δ cln3Δ	Inviable	Inviable	Wijnen 99
bck2Δ cln3Δ GAL-CLN2 cln1Δ cln2Δ	Viable	2.65G	Di Como 95
bck2Δ cln3Δ multicopy *CLN2*	G_1 arrest	Inviable	Wijnen 99
bck2Δ cln3Δ sic1Δ	G_1 arrest	Inviable	Wijnen 99
bck2Δ cln3Δ whi5Δ	1.4	1.4	Costanzo 04; de Bruin 04
bck2Δ GAL-WHI5	Viable, large	1.07G	Costanzo 04
bck2Δ GAL-WHI5-12A	-	1.17G	–
bck2Δ mbp1Δ	-	1.1	–
bck2Δ mbp1Δ GAL-WHI5	-	1.1G	–
bck2Δ swi4Δ	1.55	2.34	Wijnen 99
bck2Δ swi6Δ	Inviable	Inviable	Wijnen 02
bck2Δ swi6Δ whi5Δ	Inviable	Inviable	de Bruin 04
bck2Δ whi5Δ	0.85	0.86	Costanzo 04; de Bruin 04
cln1Δ cln2Δ cln3Δ multicopy *BCK2*	Viable	1.91	Epstein 94
GAL-BCK2 whi5Δ	0.5	0.34G	Costanzo 04
SBF/MBF mutants			
mbp1Δ	1.3	1.07	Ferrezuelo 09
swi4Δ	1.3-1.5	1.77	Wijnen 99; Wijnen 02
swi6Δ	2.4	2.31	Wijnen 02
SWI6-SA4	1	1.01	Wagner 09
bck2Δ mbp1Δ	-	1.1	–
bck2Δ mbp1Δ GAL-WHI5	-	1.1G	–
bck2Δ swi4Δ	1.55; bck2Δ<swi4Δ<size	2.34	Wijnen 99
bck2Δ swi6Δ	Inviable	Inviable	Wijnen 02
bck2Δ swi6Δ whi5Δ	Inviable	Inviable	de Bruin 04
CLN3-1 swi6Δ	2.4	2.14	Wijnen 02
cln3Δ mbp1Δ	-	Inviable	–
cln3Δ mbp1Δ swi6Δ	2.4	2.34	Koch 93
cln3Δ swi4Δ	Inviable	Inviable	Ferrezuelo 09
cln3Δ swi4Δ whi5Δ	-	Inviable	–
cln3Δ swi6Δ	2.4	2.34	Wijnen 02
mbp1Δ GAL-WHI5	-	1.08G	–
mbp1Δ GAL-WHI5-12A	-	1.17G	–
mbp1Δ swi4Δ	Inviable	Inviable	Koch 93

mbp1Δ swi6Δ	2.4	2.31	Ferrezuelo 09
mbp1Δ whi5Δ	Viable, smaller than WT	0.92	de Bruin 04
swi4Δ GAL-WHI5	Viable; size ~swi4Δ	1.69G	Costanzo 04
swi4Δ swi6Δ	Inviable	Inviable	Dirick 91
swi4Δ swi6Δ whi5Δ	-	Inviable	–
swi4Δ whi5Δ	1.3-1.5	1.63	Jorgensen 02
SWI6-SA4 GAL-WHI5-12A	Inviable	Inviable	Wagner 09
SWI6-SA4 WHI5-12A	1.4	1.81	Wagner 09
swi6Δ GAL-WHI5	Inviable	Viable; 1.27G	Costanzo 04
swi6Δ whi5Δ	2.4	2.31	Costanzo 04
Whi5 mutants			
whi5Δ	0.6-0.7	0.83	Costanzo 04; de Bruin 04
WHI5-12A	1	1.08	Wagner 09
GAL-WHI5	WT<size<cln3Δ	1.08G	Costanzo 04; de Bruin 04
GAL-WHI5-12A	Viable, large	1.17G	Wagner 09
bck2Δ cln3Δ whi5Δ	1.4	1.4	Costanzo 04; de Bruin 04
bck2Δ GAL-WHI5	Viable, large	1.07G	Costanzo 04
bck2Δ GAL-WHI5-12A	-	1.17G	--
bck2Δ mbp1Δ GAL-WHI5	-	1.1G	–
bck2Δ swi6Δ whi5Δ	Inviable	Inviable	de Bruin 04
bck2Δ whi5Δ	0.85	0.86	Costanzo 04; de Bruin 04
CLN3-1 whi5Δ	Viable, small; size~*whi5Δ*< *CLN3-1*	0.68	Costanzo 04
cln3Δ GAL-WHI5	Inviable	Inviable	Costanzo 04
cln3Δ GAL-WHI5-12A	Inviable	Inviable	Wagner 09
cln3Δ swi4Δ whi5Δ	-	Inviable	–
cln3Δ whi5Δ	0.7-0.9	0.85	Costanzo 04; de Bruin 04
GAL-BCK2 whi5Δ	0.5	0.34G	Costanzo 04
mbp1Δ GAL-WHI5	-	1.08G	–
mbp1Δ GAL-WHI5-12A	-	1.17G	–
mbp1Δ whi5Δ	Viable, smaller than WT	0.92	de Bruin 04
msn5Δ swi4Δ	Inviable	Viable; 2.02	Queralt 03
msn5Δ swi6Δ	Inviable	Viable; 2.3	Queralt 03
swi4Δ GAL-WHI5	Viable. ~swi4Δ	1.69G	Costanzo 04
swi4Δ swi6Δ whi5Δ	-	Inviable	–
swi4Δ whi5Δ	1.3-1.5	1.63	Jorgensen 02
SWI6-SA4 GAL- WHI5-12A	Inviable	Inviable	Wagner 09
SWI6-SA4 WHI5-12A	1.4	1.81	Wagner 09
swi6Δ GAL-WHI5	Inviable	Viable; 1.27G	Costanzo 04
swi6Δ whi5Δ	2.4	2.31	Costanzo 04
Non-phosphorylable mutants			
SWI6-SA4	1	1.01	Wagner 09
WHI5-12A	1	1.08	Wagner 09
WHI5-12A SWI6-SA4	1.4	1.81	Wagner 09
GAL-WHI5-12A	Viable, large	1.17G	Wagner 09
GAL- WHI5-12A SWI6-SA4	Inviable	Inviable	Wagner 09
bck2Δ GAL-WHI5-12A	-	1.17G	–
cln3Δ GAL-WHI5-12A	Inviable	Inviable	Wagner 09
mbp1Δ GAL-WHI5-12A	-	1.17G	–
Export prtotein Msn5			
msn5Δ	1.4	1.69	Queralt 03
msn5Δ swi4Δ	Inviable	Viable; 2.02	Queralt 03
msn5Δ swi6Δ	Inviable	Viable; 2.3	Queralt 03
Cln1, 2; Clb5,6 mutants pertaining to START			
clb5Δ clb6Δ	~1.2-1.3 (~mbp1Δ)	1.18	Schwob 93
GAL-CLB5	Viable	0.95G	Schwob 93
CLB5-dbΔ	Viable	1.01	Wasch 02
GAL-CLB5-dbΔ	Inviable	Inviable	Schwob 94; Jacobson 00
cln1Δ cln2Δ	3.2	2	Dirick 95
bck2Δ cln1Δ cln2Δ	Viable, large; size~1.7	2.67	Epstein 94
bck2Δ cln3Δ GAL-CLN2 cln1Δ cln2Δ	Viable	2.64G	Di Como 95
bck2Δ cln3Δ multicopy *CLN2*	G_1 arrest	Inviable	Wijnen 99
CLB5-dbΔ pds1Δ	Viable	0.92	Wasch 02
CLB5-dbΔ pds1Δ cdc20Δ	T arrest	Inviable	Wasch 02
CLB5-dbΔ sic1Δ	Inviable	Inviable	Jacobson 00; Wasch 02
cln1,2Δ clb5,6Δ	G_1 arrest	Inviable	Schwob 93

cln1Δ cln2Δ cdh1Δ	Viable	Inviable	Cross 02
cln1Δ cln2Δ cdh1Δ GAL-CLN2	Viable	Inviable	Cross 02
cln1Δ cln2Δ cdh1Δ GAL-SIC1	Inviable	Inviable	Cross 02
cln1Δ cln2Δ GAL-CLN2	Viable, small; size~0.5	~0.82G	Dirick 95
cln1Δ cln2Δ GAL-CLN2 cdh1Δ GAL-SIC1	Viable	0.88G	Cross 02
cln1Δ cln2Δ GAL-CLN2 GAL-SIC1	Viable	1.07G	Cross 02
cln1Δ cln2Δ GAL-SIC1	G1 arrest	Inviable	Cross 02
cln1Δ cln2Δ sic1Δ	1.1	1.11	Dirick 95
GAL-CLB5 cdh1Δ	Viable*	0.82G	Chen 04; Cross (personal communication)
GAL-CLB5 sic1Δ	Inviable	Inviable	Jacobson 00
Triple cln mutants			
cln1Δ cln2Δ cln3Δ	Inviable	Inviable	Richardson 89
bck2Δ cln3Δ GAL-CLN2 cln1Δ cln2Δ	Viable	2.64G	Di Como 95
cln1Δ cln2Δ cln3Δ apc-ts	M arrest	Inviable	Irniger 97
cln1Δ cln2Δ cln3Δ cdh1Δ	Inviable	Inviable	Schwab 97
cln1Δ cln2Δ cln3Δ GAL-CLB2	G1 arrest	Inviable	Amon 94
cln1Δ cln2Δ cln3Δ GAL-CLB5	Viable	1.29G	Schwob 93
cln1Δ cln2Δ cln3Δ GAL-CLN2	Viable	~0.8G	Cross 91
cln1Δ cln2Δ cln3Δ GAL-CLN3	Viable	0.75G	Cross 90; Schwob 93
cln1Δ cln2Δ cln3Δ multicopy *BCK2*	Viable	1.91	Epstein 94
cln1Δ cln2Δ cln3Δ multicopy *CLB5*	Viable	2.89	Epstein 92
cln1Δ cln2Δ cln3Δ sic1Δ	Viable, large	2.07	Schneider 96
Important CKI-Cdh1 and related mutants			
cdc6Δ	Viable; size~cdc6Δ2-49	1	Calzada 01; Nguyen 01
cdh1Δ	Viable, smaller than WT	0.89	Schwab 97; Jorgensen 02; Wasch 02
CDH1 constitutively active	G2 arrest	Inviable	Zachariae 98
sic1Δ	Viable	0.97	Schneider 96
GAL-SIC1	Viable, larger than WT	1.1G	Nugroho 94; Verma 97
GAL-SIC1-dbΔ	G1 arrest	Inviable	Verma 97
swi5Δ	Viable	0.7	Toyn 97; Giaever 02
bck2Δ cln3Δ sic1Δ	G_1 arrest	Inviable	Wijnen 99
cdc6Δ sic1Δ	Viable	0.98	Calzada 01; Wasch 02
cdh1Δ cdc6Δ	Viable, larger than WT	Inviable	
cdh1Δ cdc6Δ sic1Δ	Inviable	Inviable	Archambault 03
cdh1Δ cdc6Δ sic1Δ GALL-CDC20	Viable	1.02G	Cross 03
cdh1Δ sic1Δ	Inviable	Inviable	Schwab 97; Visintin 97; Wasch 03; Archambault 03
cdh1Δ sic1Δ GALL-CDC20	Viable, larger than WT	1.02G	Cross 03
cdh1Δ swi5Δ	Inviable	Inviable	Archambault 03
cdh1Δ swi5Δ GAL-SIC1	Viable	0.93G	Archambault 03
CLB5-dbΔ pds1Δ	Viable	0.92	Wasch 02
CLB5-dbΔ pds1Δ cdc20Δ	T arrest	Inviable	Wasch 02
CLB5-dbΔ sic1Δ	Inviable	Inviable	Jacobson 00; Wasch 02
cln1Δ cln2Δ cdh1Δ	Viable	Inviable	Cross 02
cln1Δ cln2Δ cdh1Δ GAL-CLN2	Viable	Inviable	Cross 02
cln1Δ cln2Δ cdh1Δ GAL-SIC1	Inviable	Inviable	Cross 02
cln1Δ cln2Δ cln3Δ apc-ts	M arrest	Inviable	Irniger 97
cln1Δ cln2Δ cln3Δ cdh1Δ	G_1 or S arrest	Inviable	Schwab 97
cln1Δ cln2Δ cln3Δ GAL-CLB2	G1 arrest	Inviable	Amon 94
cln1Δ cln2Δ cln3Δ sic1Δ	Viable, large	2.07	Schneider 96
cln1Δ cln2Δ GAL-CLN2 cdh1Δ GAL-SIC1	Viable	0.88G	Cross 02
cln1Δ cln2Δ GAL-CLN2 GAL-SIC1	Viable	1.07G	Cross 02
cln1Δ cln2Δ GAL-SIC1	G1 arrest	Inviable	Cross 02
cln1Δ cln2Δ sic1Δ	1.1	1.11	Dirick 95
GAL-CLB5 cdh1Δ	Viable*	0.82G	Chen 04; Cross (personal communication)
GAL-CLB5 sic1Δ	Inviable	Inviable	Jacobson 00

* Cross: Although *GAL-CLB5 cdh1Δ* is ultimately inviable or extremely slow-growing on galactose, these mutants are not associated with any obvious problems in a short-term experiment. These cells go through several doublings, probably without much difficulty, on galactose medium, and they remain reasonably

viable when returned to glucose, like *GAL-CLB5* cells. So, it is not reasonable to expect the mathematical model to predict inviability of *GAL-CLB5 cdh1*Δ mutants. They should probably look viable.

The iconic tables beside the simulations list the major complexes that are responsible for SBF and MBF activity. In wild type, we would expect to see SBF and MBF activated by Cln3 and Bck2 (to different extents), and the complex resulting from the dissociation of the doubly phosphorylated Whi5-SBF complex to be the primary Cln activated SBF form (SBF phosphorylated on Swi6, P-form; Figure 12E). In contrast, in *WHI5-12A* and *SWI6-SA4*, we would only see Whi5-SBF complexes phosphorylated at either Swi6 or Whi5, respectively (Figure 24A, B, 25A, B). Since, we assume these to have the same activity as the phosphorylated SBF complex in wild type cells, we expect these two non-phosphorylable mutants to show no delay in START. In the double mutant *WHI5-12A SWI6-SA4*, the predominant SBF form would the inactive trimer with Whi5, making these cells larger than WT (Figure 24C, 25C). However, the reason for the viability of these mutants is the intact functioning of MBF activation by Cln3 and Bck2 (Figure 25C). The simulations shown in Figure 25 confirm our intuition about the working of the non-phosphorylable mutants, wherein the sizes of *WHI5-12A* and *SWI6-SA4* are comparable to WT, but the double mutant is significantly larger (Figure 25).

Similarly, the reason why *whi5*Δ is small (Costanzo et al, 2004; de Bruin et al, 2004) is because in the absence of Whi5, the SBF complex starts in G1 in its uninhibited form, which still carries some residual activity. Thus, START gets advanced because the cells don't need to wait for the accumulation of Cln3 or Bck2 to activate SBF (Figure 28A).

Likewise, the large size of *cln3*Δ can be explained by the absence of Cln3-activated SBF and MBF (Dirick et al, 1995), and dependence on Bck2-activated forms (SBFa2, SBFa6 and MBFabck). Although SBF (unmodified; SBFa1) and Swi4dimers (SBFa6) could contribute, since Whi5 is present, most of SBF is in a Whi5-bound inhibited complex. Therefore, if Whi5 is deleted, the *cln3*Δ *whi5*Δ could be much smaller in size, since now SBF and Swi4dimers (to a lesser extent) would now be present.

*bck2*Δ is larger than WT according to experimental observations (1.3x WT). However, in our simulations, it is only slightly larger than wild type cells (1.01x WT). This is because the contribution of Bck2 activated forms is minor in wild type cells (SBF is mostly Whi5-bound and hence inactive), and these forms are also less active when compared to Cln-activated forms. If we make the contribution of Bck2 larger (sit gat *bck2*Δ cells are larger than WT), then *cln3*Δ cells would not be as large as they are now (2.62x WT), and *cln3*Δ *swi4*Δ would not be viable. Therefore, the large size of *bck2*Δ (Wijnen & Futcher, 1999) mutants can be explained by the absence of Bck2-activated SBF, MBF forms.

The double mutant *cln3*Δ *bck2*Δ is inviable (Wijnen & Futcher, 1999) since both Cln3 and Bck2 activated forms of SBF and MBF are absent and the inhibitor is still present to inhibit any available SBF (Figure 26 A, B, C). The double mutant can however be rescued by additionally deleting Whi5 (*cln3*Δ *bck2*Δ *whi5*Δ) (Costanzo et al, 2004; de Bruin et al, 2004), because there are now SBF forms (SBFa1) available that would be free of inhibition and ready to transcribe. These mutants are, however, larger than WT cells because they only depend on a less active form of SBF for transcription (due to lack of activators and resultant modifications; Figure 28B). Our model is parameterized and

the activity/contribution of different complexes are adjusted in such a way that the simulations match the known experimental phenotypes as much as possible.

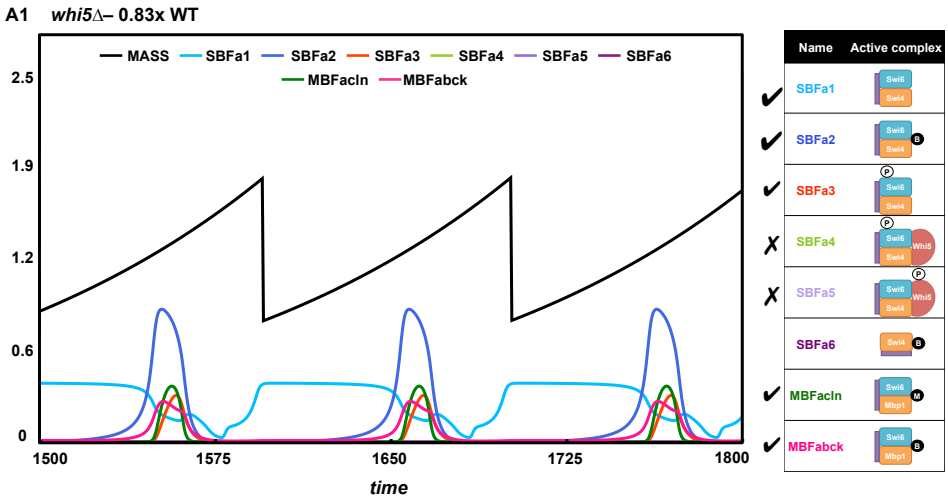

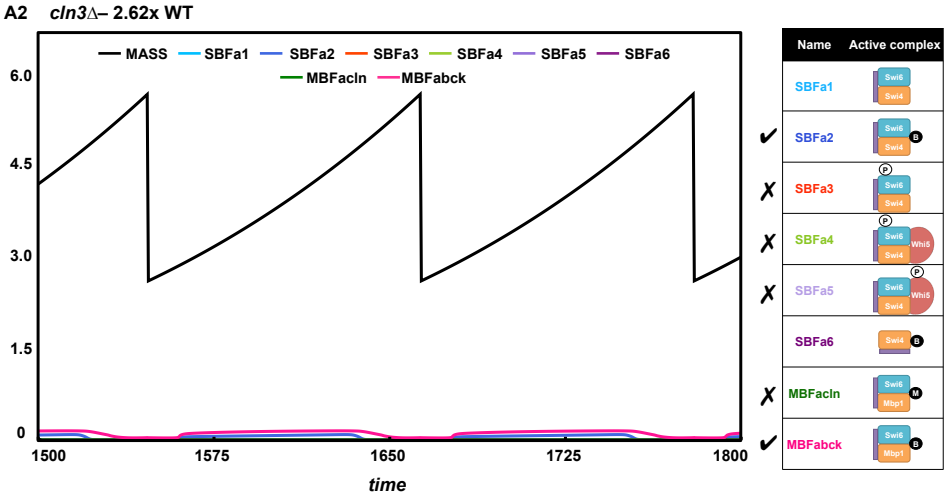

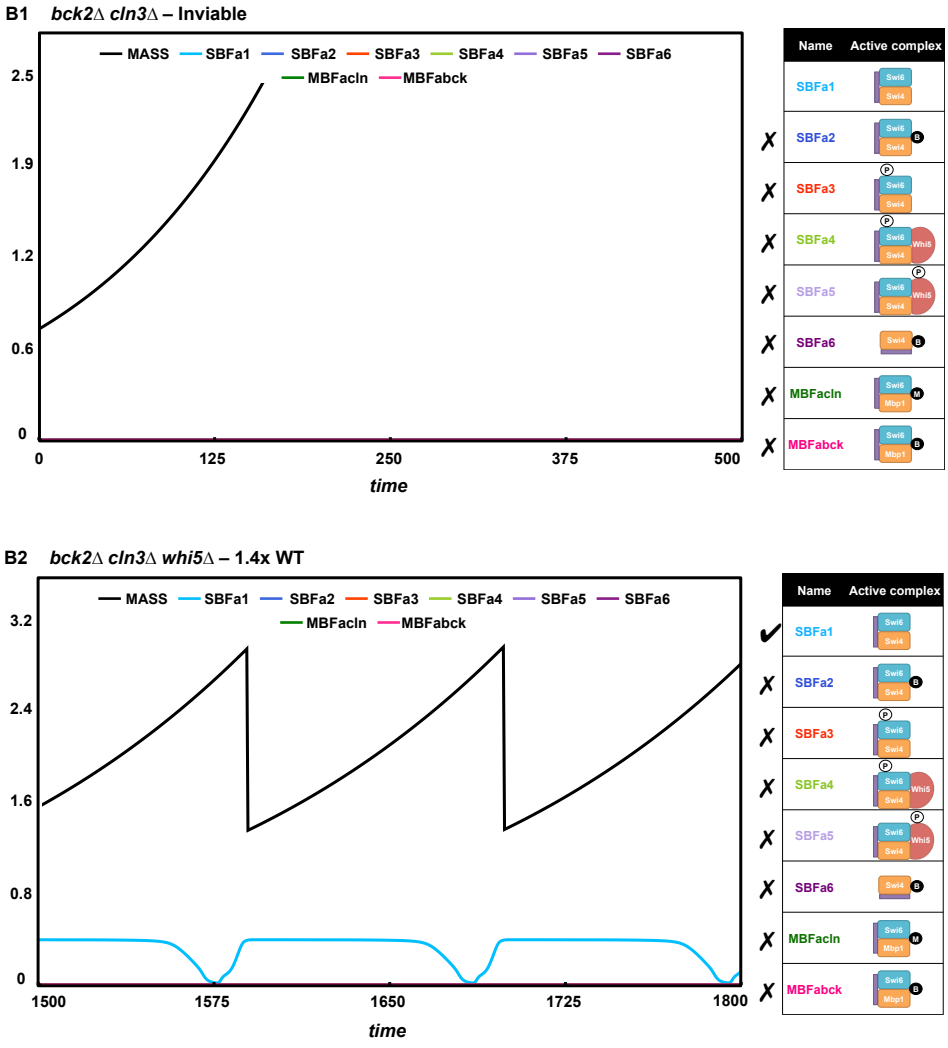

Figure 28. START Mutants I. Interplay between Whi5, Cln3 and Bck2.

The figure includes simulations of the following mutants: (**A**) A1: *whi5*Δ (cells begin the cycle with less active SBF (SBFa1) instead of Whi5-bound inactive SBF, and get converted into more active forms by Bck2 (SBFa2) and Clns (SBFa3). Active MBF is also present. Hence, cells are smaller than WT.), A2: *cln3*Δ (only Bck2 activated forms are present; cells are very large), (**B**) B1: *cln3*Δ *bck2*Δ (no active SBF/MBF; cells are inviable), B2: *cln3*Δ *bck2*Δ *whi5*Δ (deletion of Whi5 relieves SBF and the unmodified form of SBF (SBFa1) is consistently present and cells become viable).

Another set of mutants, *swi6*Δ, *cln3*Δ and *swi6*Δ *cln3*Δ, can be understood with the help of the iconic tables used in Figure 29, and the simulations showing the

redistribution of SBF and MBF forms. We note from the simulations that the reason behind viability of *swi6*Δ (2.31x) and *cln3*Δ (2.62x) are very different, even though they are both viable and large START mutants (Figure 26A, 29). *swi6*Δ is viable due to the presence of Swi4 (or Swi4 dimers) that can be activated by Bck2, it yields an extremely large (2.31x WT) cells due to the low activity of Swi4. In contrast, the viability of *cln3*Δ is due to MBF activated by Bck2 (Figure 28A2). Both depend on Bck2 for their survival. Supporting evidence for our observation comes from the fact that both these mutants are lethal in a *bck2*Δ background (Wijnen & Futcher, 1999; Wijnen et al, 2002). Furthermore, this explanation can account for the observation that *swi6*Δ and *swi6*Δ *cln3*Δ cells are about the same size (Wijnen et al, 2002). However the observation that *swi6*Δ *CLN3-1* also have similar size and their conclusion that Cln3 activation of SBF and MBF is entirely through its action on Swi6 (i.e. if Swi6 is deleted, whether there is Cln3 or not (*cln3*Δ or *CLN3-1*), START is activated at the same time) does not come naturally from the model.

As shown in Figure 29, the only active complex in *swi6*Δ is the Swi4dimer form (SBFa6) activated by Bck2, and it appears as though deletion or over-expression of Cln3 would have no additional effect. However, to pass the START transition, Cln kinases (resulting from SBF transcription) are needed to inactivate Sic1, such that Clb5 kinase (transcribed by MBF genes) can be active to trigger DNA synthesis; and to inactive Cdh1 to allow Clb2 accumulate in preparation for mitosis. In order to make the three mutants swi6Δ, swi6Δ cln3Δ, swi6Δ CLN3-1 of similar size, we have to turn the effect of Cln3 on CKI and Cdh1 inactivation very low. But, if we turn the efficiency of Cln3 on Sic1 phosphorylation very low, then *cln1*Δ *cln2*Δ mutant (which depends on Cln3 and Bck2 to

inactivate Sic1 for Clb5 to start DNA synthesis) would have difficulty in timely execution of DNA synthesis and would be 'G1 arrested'. The compromise we reach for the basal parameter set (listed in Materials and Methods section) is that we choose the efficiency of Cln3 on Sic1 to be small enough so that *cln1*Δ *cln2*Δ is big and viable (~2x WT) and swi6Δ CLN3-1 to be big as well (~2.14x WT), even if it is not as big as swi6Δ.

Here, again, we benefit from looking at the complexes present in each of these single, double or triple mutants using the corresponding iconic tables and the time-course simulations for different complexes.

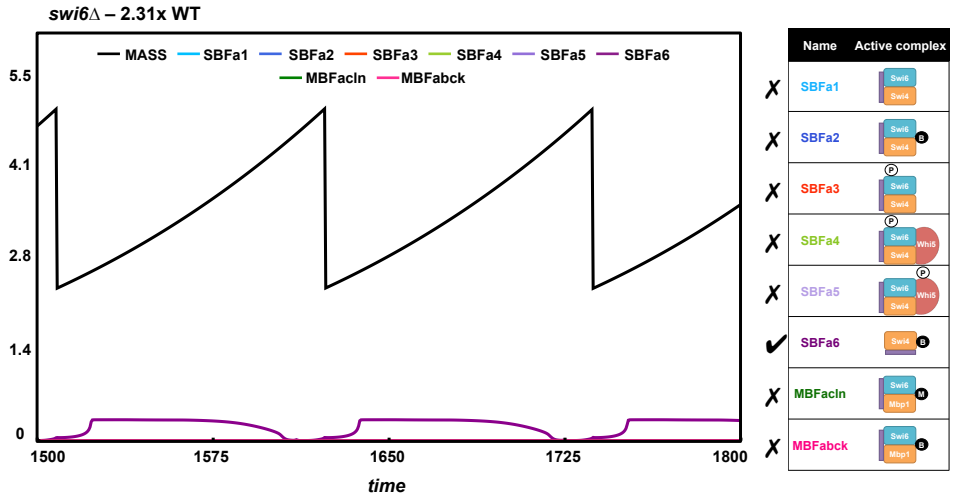

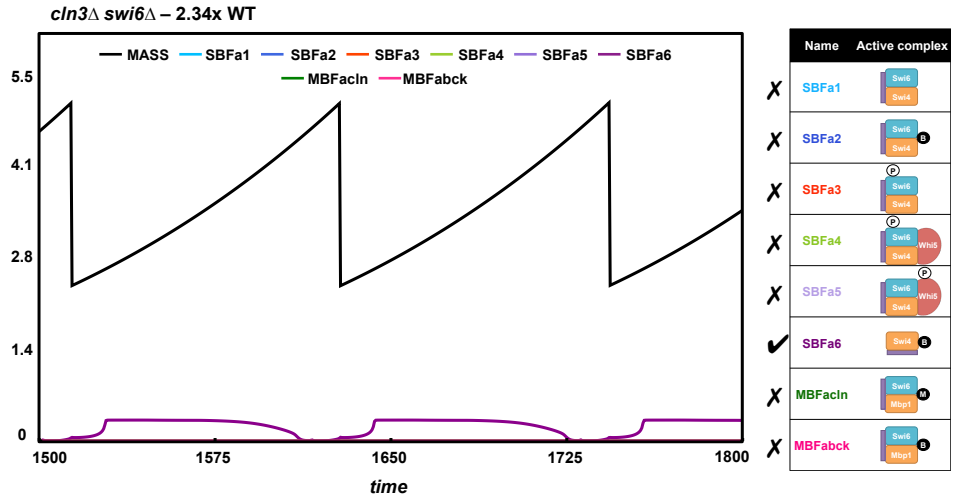

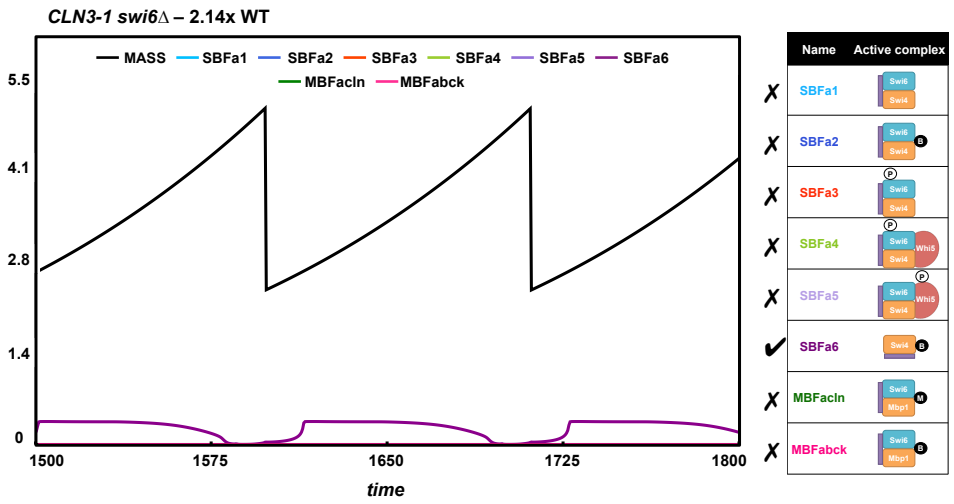

Figure 29. START mutants II. Epistasis of Swi6 to Cln3.

The figure includes a comparison between complexes available in the following mutants: *swi6*Δ (only Swi4dimers (SBFa6) present; cells are viable yet large), *swi6*Δ *cln3*Δ (only Swi4dimers (SBFa6) present; cells are viable yet large), and *swi6*Δ *CLN3-1* (only Swi4dimers (SBFa6) present; cells are viable yet large).

Model predictions

Developing this mathematical model not only helps in understanding the molecular mechanisms behind known mutant phenotypes; it summarizes and organizes the knowledge about the cell cycle regulation in these mutants. Furthermore, it makes testable predictions. In this section, we list some of the predictions (Table 4; Figure 30).

Table 4. Model predictions

Mutants	Expected Phenotypes
***bck2*Δ *mbp1*Δ**	Viable
bck2*Δ *mbp1*Δ *GAL-WHI5	Viable
***cln3*Δ *mbp1*Δ**	Inviable

***cln3*Δ *mbp1*Δ *swi6*Δ**	Viable (rescues *cln3*Δ *mbp1*Δ)
***cln3*Δ *mbp1*Δ *whi5*Δ**	Viable (rescues *cln3*Δ *mbp1*Δ)
mbp1*Δ *GAL-WHI5	Viable
mbp1*Δ *GAL-WHI5-12A	Viable
***cln3*Δ *swi4*Δ *whi5*Δ**	Still inviable (~*cln3*Δ *swi4*Δ)
cln3*Δ *swi4*Δ *GAL-BCK2	Viable (rescues *cln3*Δ *swi4*Δ)
cln3*Δ *swi4*Δ *whi5*Δ *GAL-BCK2	Viable (rescues *cln3*Δ *swi4*Δ *whi5*Δ)
***cln3*Δ *swi4*Δ *whi5*Δ *sic1*Δ**	Viable (rescues *cln3*Δ *swi4*Δ *whi5*Δ)
***swi4*Δ *swi6*Δ *whi5*Δ**	Still inviable (~*swi4*Δ *swi6*Δ)
swi4*Δ *swi6*Δ *GAL-CLN2 or GAL-CLN3	Still inviable (~*swi4*Δ *swi6*Δ)
swi4*Δ *swi6*Δ *GAL-CLB5	Viable (rescues *swi4*Δ *swi6*Δ)

Let us consider the following cases: deletion of Bck2 and Cln3 in *mbp1*Δ background. Based on the sizes of *cln3*Δ and *bck2*Δ (*cln3*Δ >> *bck2*Δ), we infer that Cln3 is a more efficient activator of SBF and MBF when compared to Bck2. Similarly, based on the sizes of *swi4*Δ and *mbp1*Δ, we know that SBF is more active than MBF. We, therefore, expect the mutant, *bck2*Δ *mbp1*Δ to be viable since the major activator of SBF, Cln3, is still present (Figure 30A). In the simulation, we observe that the Cln-activated SBF forms are present (SBFa3>>SBFa4, SBFa5, SBFa1), and that they contribute to the viability of the cell in the absence of MBF and Bck2.

Even though Whi5 is an inhibitor of SBF, *GAL-WHI5* need not always be highly detrimental to the cell. This is because we expect that the G1 cyclin (Cln3) and the

downstream cyclins that engage in a positive feedback loop (Cln1,2 and Clb5,6), would be efficient in phosphorylating the additional amount of Whi5-bound SBF that is added to the system. We, therefore, expect the mutant *bck2*Δ *mbp1*Δ *GAL-WHI5*, to have the Cln-activated forms (SBFa3>SBFa4, SBFa5) to contribute to cell viability (Figure 30B). Since we give full activity to Whi5-bound SBF that is phosphorylated on Swi6 by Cln kinases, SBFa4 and SBFa5 will contribute to overall SBF activity, and the triple mutant will also be viable.

In our model, we would expect the double mutant *cln3*Δ *mbp1*Δ to be inviable. This is because most of SBF is Whi5-bound and there is very little free SBF to be activated by Bck2 (low amount of the SBF form, SBFa2, is insufficient to rescue the cell as seen in Figure 30C). (i) One strategy to rescue the double mutant (that works in the model) would be to delete Swi6. Although counter-intuitive due to the usual adverse effects of deleting Swi6 in the cell (removal of SBF, MBF complexes), this triple deletion mutant (*cln3*Δ *mbp1*Δ *swi6*Δ) is viable. This is because the cells are left with only Swi4, and the Swi4 form that is activated by Bck2 (that exist as monomers or homodimers). The Swi4 dimers are active and do not need phosphorylation by Cln kinases or Mbp1 for their activity. Swi4dimers (SBFa6) are sufficient to rescue the double mutant as seen in Figure 30D. (ii) An alternate strategy to rescue *cln3*Δ *mbp1*Δ is the additional deletion of Whi5. The rescue is because, as expected, SBF is now free from Whi5 inhibition and it is assessable to be activated by Bck2 (cells start with unmodified less active SBF form (SBFa1) that gets activated by Bck2 (SBFa2) as seen in Figure 30E).

Similar to the mutant *bck2*Δ *mbp1*Δ *GAL-WHI5* (Figure 30B), the double mutants *mbp1*Δ *GAL-WHI5* and *mbp1*Δ *GAL-WHI5-12A* are viable even though there is excessive

Whi5 in the system, because as we expect that they get converted to active Whi5-bound SBF forms (SBFa3, SBFa4, SBFa5 in the former case and SBFa4in the latter non-phosphorylable case). These forms are present in sufficiently high levels to ensure viability. It is possible that very high doses of Whi5 might saturate the kinases in the system resulting in inviability of cells. For other moderate increase in Whi5 or Whi5-12A levels, we expect the afore-mentioned response in the background of *mbp1*Δ cells.

The double mutant *swi4*Δ *cln3*Δ is inviable, because the only active form present is MBF activated by Bck2 (MBFacln) (Ferrezuelo et al, 2009). Consequently, we do not expect an additional deletion of Whi5 to rescue the phenotype (there seems to be an initial rescue-like phenotype in Figure 30F probably because part of MBF gets relieved in the absence of Whi5, but this is still not sufficient to rescue the double mutant). Overexpression of Bck2, however, rescues the double mutant, because now there is enough of Bck2-activated MBF (MBFabck forms in Figure 30G) to drive forward the cell cycle. Alternatively, deletion of Sic1 in the triple mutant (*cln3*Δ *swi4*Δ *whi5*Δ) makes the cells viable (*cln3*Δ *swi4*Δ *whi5*Δ *sic1*Δ has a size ~ WT; simulation not shown).

Another simple prediction from the model is the triple deletion *swi4*Δ *swi6*Δ *whi5*Δ. These cells do not have any SBF or MBF, and hence Whi5 does not have any stoichiometric partner to bind with and inhibit. However, swi4Δ swi6Δ can be rescued by GAL-CLB5 (but not by GAL-CLN2 or GAL-CLN3, since in these cases, no CLB5 kinase is made to trigger DNA synthesis (simulations not shown).

Similar to rescue by multi-copy Swi6 (Wijnen & Futcher, 1999), we also expect the lethal mutants *swi4*Δ *swi6*Δ and *bck2*Δ *swi6*Δ to be rescued by *SWI6-SA4*, since there would MBF available again in the former case, and both SBF (although non-

phosphorylable at Swi6) and MBF available in the latter case to rescue the lethal phenotype (simulations not shown).

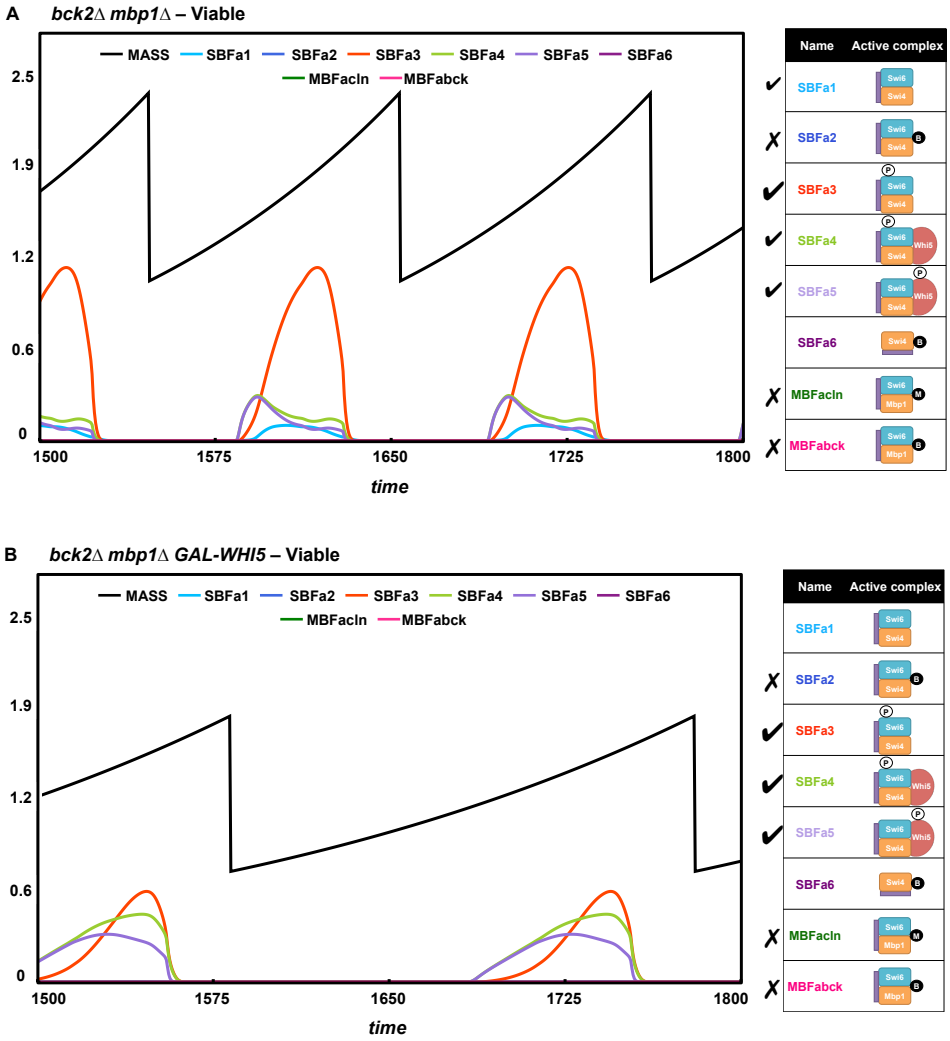

C *cln3*Δ *mbp1*Δ – Inviable

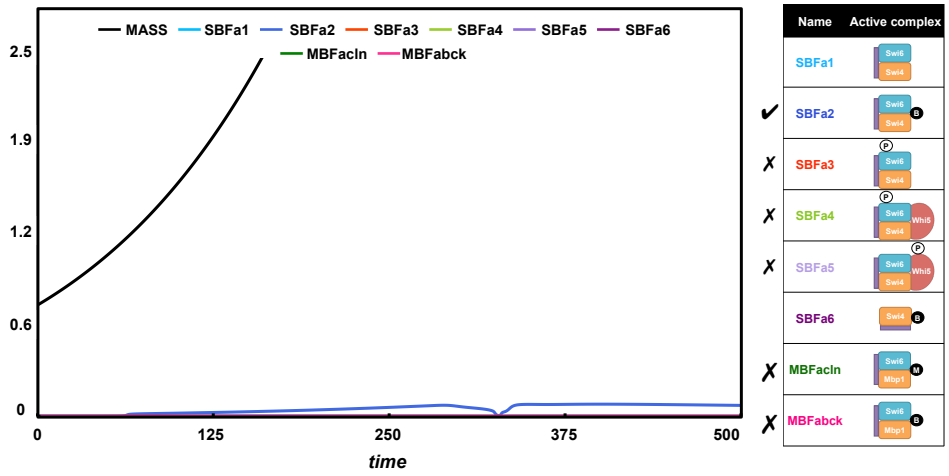

D *cln3*Δ *mbp1*Δ *swi6*Δ – Viable

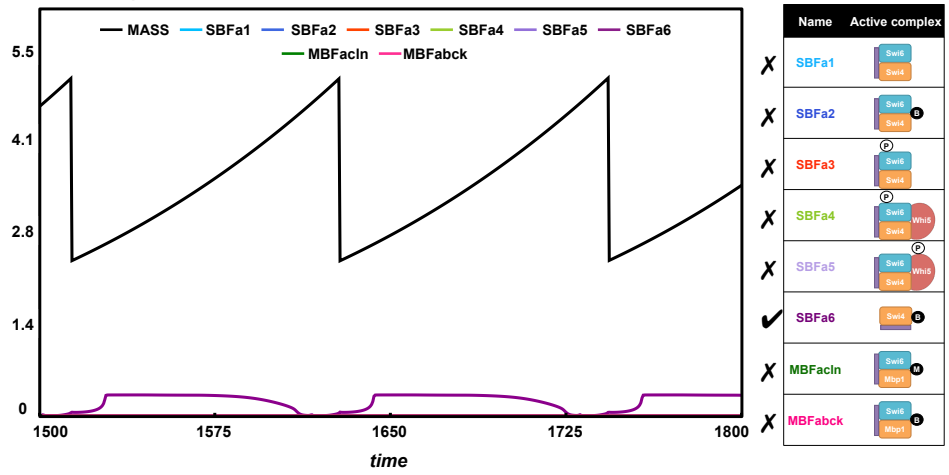

E *cln3*Δ *mbp1*Δ *whi5*Δ – Viable

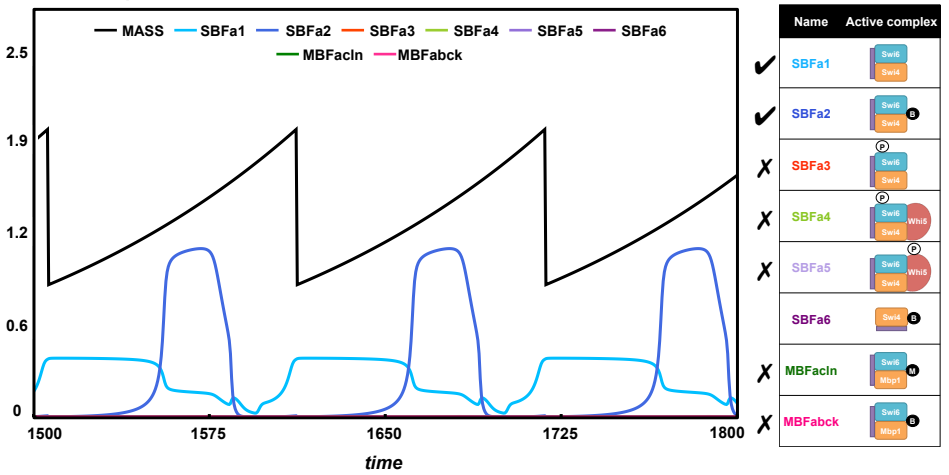

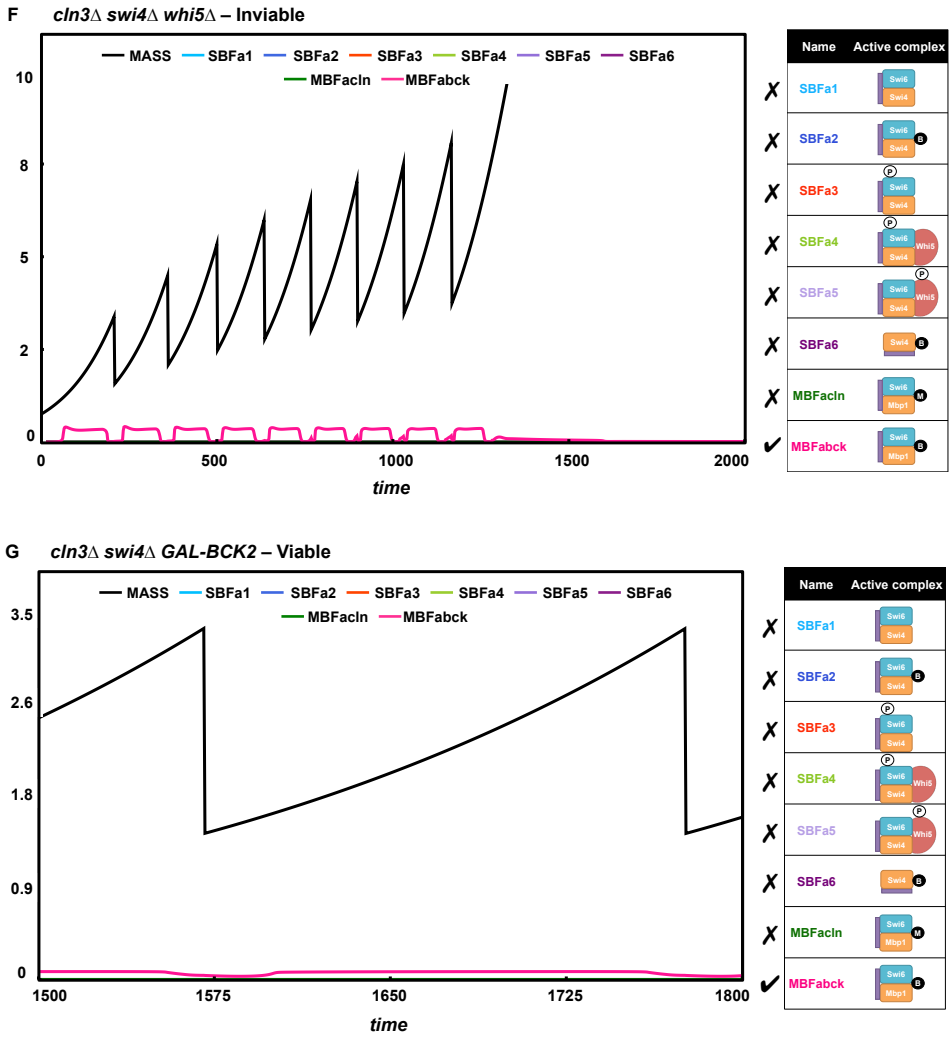

Figure 30. Few model predictions.

(**A**) *bck2*Δ *mbp1*Δ (Cln-activated forms of SBF are present in varying fractions (SBFa3>SBFa4, SBFa5> SBFa1); cells are viable), (**B**) *bck2*Δ *mbp1*Δ *GAL-WHI5* (Cln-activated forms of SBF are present (SBFa3, SBFa4, SBFa5) even if they are lesser than in **A**; cells are still viable), (**C**) *cln3*Δ *mbp1*Δ (Very little Bck2-activated SBF (SBFa2) is present, and no Cln-activated SBF or MBF is present; cells are inviable), (**D**) *cln3*Δ *mbp1*Δ *swi6*Δ (Swi4dimers (SBFa6) are present sufficiently enough to rescue cells; cells are viable), (**E**) *cln3*Δ *mbp1*Δ *whi5*Δ (Inhibition on SBF is relieved and Bck2-activated form of SBF is present (SBFa2>SBFa1); cells are rescued), (**F**) *cln3*Δ *swi4*Δ *whi5*Δ (Only Bck2-activated MBF is present (MBFabck), there's no SBF; cells are inviable), (**G**) *cln3*Δ *swi4*Δ *GAL-BCK2* (There's sufficient amount of Bck2-activated MBF (MBFabck); cells are rescued).

Model contradictions

In addition to making predictions, we discuss important aspects of our model that are in contradiction with the yeast cell cycle literature. For instance, de Bruin *et al*. (2004) show that Whi5 only binds to intact SBF complex and not either Swi4 or Swi6 in isolation. Following this, we do not allow Whi5 to bind to and inhibit the only available active form in *swi6*Δ, the Swi4 complex activated by Bck2. Therefore, contrary to experimental findings (Costanzo et al, 2004), we expect *swi6*Δ *GAL-WHI5* cells to be similar in size to *swi6*Δ cells. If we allow such inhibition, then in *swi6*Δ cells, there are free Whi5 molecules in the nucleus, and its inhibition on Swi4 would make it hard for swi6Δ to trigger START, the single mutant would be too big to fit the experimental data.

We expect the double mutants *msn5*Δ *swi4*Δ and *msn5*Δ *swi6*Δ to be the same size as *swi4*Δ and *swi6*Δ cells, respectively (Figures 31B, C). This is because the only direct effect of Msn5 in our model is through the export of Whi5 and Swi6, which predominantly affects the localization of SBF and MBF to a much lesser extent. In both these double mutants, there is no SBF is to begin with. Therefore, an additional deletion of Msn5 does not have any significant effect on either of these single mutants Swi4 and Swi6. There is, however, a minor difference in size between *swi4*Δ and *msn5*Δ *swi4*Δ. The single deletion mutant depends only on MBF for its viability, and further deletion of Msn5 results in retaining phosphorylated Whi5 and Swi6 in the nucleus. Although dephosphorylation of these forms occurs in the nucleus, there is substantial amount of phosphorylated Swi6 that cannot form MBF. The decrease in the amount of net MBF could explain the slightly larger size of *msn5*Δ *swi4*Δ as compared to the single deletion mutant of *swi4*Δ (Figure 31B). On the other hand, *swi6*Δ only depends on Swi4 for its

viability. Therefore, the double mutant *msn5*Δ *swi6*Δ has the same size *swi6*Δ cells (Figure 31C). This is in contrast to the experimental observation that these double mutants are inviable (Queralt & Igual, 2003). Clearly our model cannot explain this scenario because we do not consider the other diverse effects of Msn5 on the cell such as transport of other phosphoproteins like Cdh1 (Jaquenoud et al, 2002). Addition of these interactions to the model could help in explaining these mutants.

Two other important mutants that our model currently fails to explain are the *cln1*Δ *cln2*Δ *cdh1*Δ and *cln1*Δ *cln2*Δ *cdh1*Δ *GAL-CLN2* mutants. Contrary to experimental findings (Cross et al, 2002) and simulations from Chen2004, these mutants are inviable in our simulations (Figures 31D). We suspect that this is due to abnormally high Sic1 inhibition by Clb2, which is an artifact of re-parameterizing the model to fit several other START mutants. We tested that lowering the efficiency of Clb2 on Sic1 indeed rescues the phenotypes, but results in other problems such as viability of the lethal phenotype *swi4*Δ *swi6*Δ. The latter mutant does not have Cln1,2 or Clb5,6 and relies on Clb2 to keep CKIs levels low. Therefore, alteration of these parameters results in cycling of *swi4*Δ *swi6*Δ cells. These two Cdh1 mutants remain to be analyzed further and fixed.

Another problem among START mutants in our model is the *cdc6*Δ *cdh1*Δ mutant. These colonies are supposed to viable experimentally (Calzada et al, 2001), but are inviable in our model according to our current parameter set (Figure 31E). Again, this mutant can be made viable by changing the same parameter as with the previous two Cdh1 mutants, and would result in similar counter-effects. We are yet to fix this mutant as well.

A ***swi6*Δ *GAL-WHI5*** **– Viable**

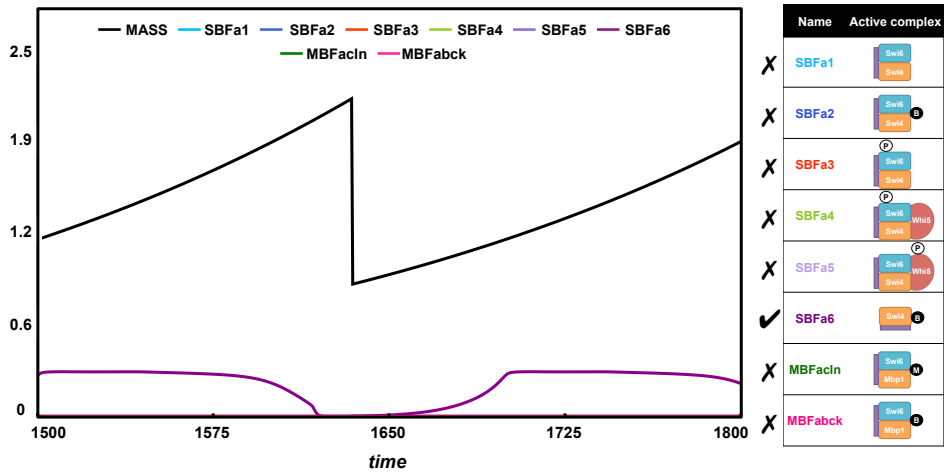

B1 ***swi4*Δ – Viable (1.77x WT)**

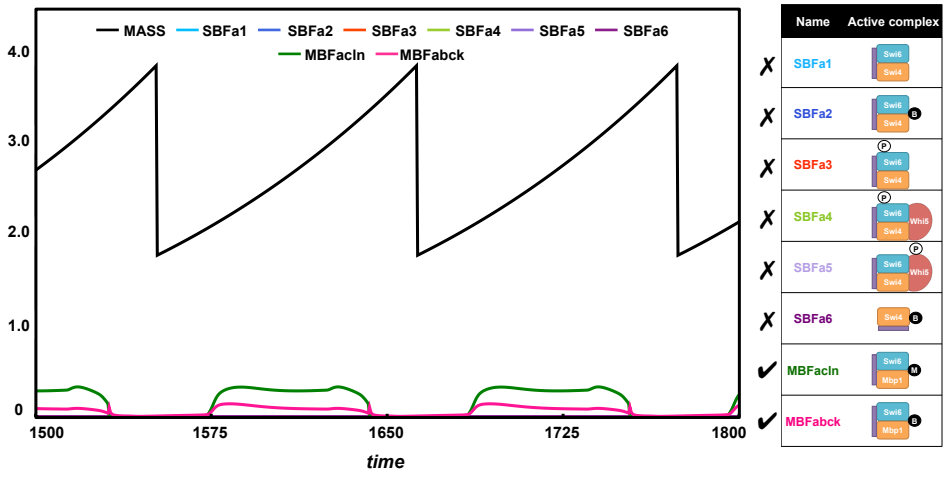

B2 ***msn5*Δ *swi4*Δ – Viable (2.02x WT)**

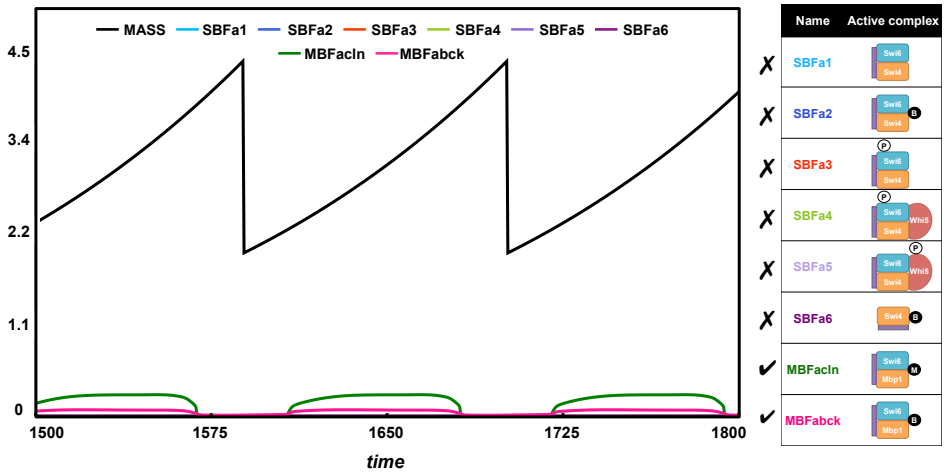

C1 *swi6*Δ – Viable (2.31x WT)

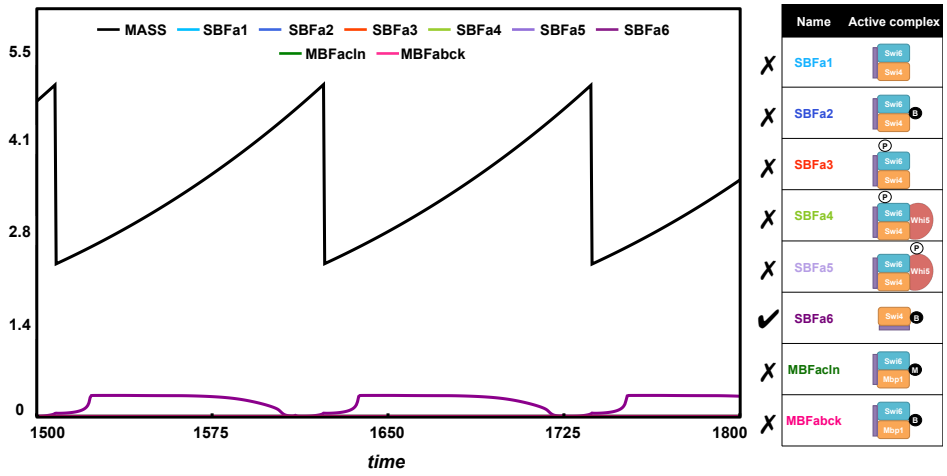

C2 *msn5*Δ *swi6*Δ – Viable (2.31x WT)

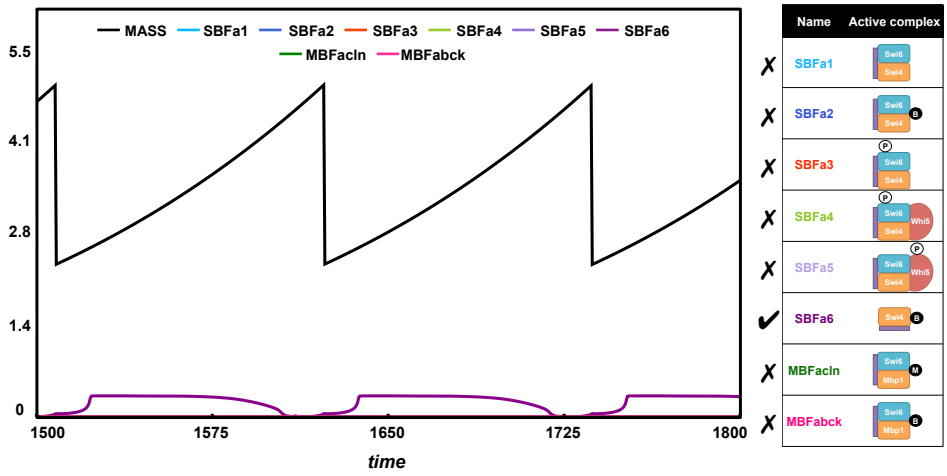

D1 *cln1*Δ *cln2*Δ *cdh1*Δ – Inviable

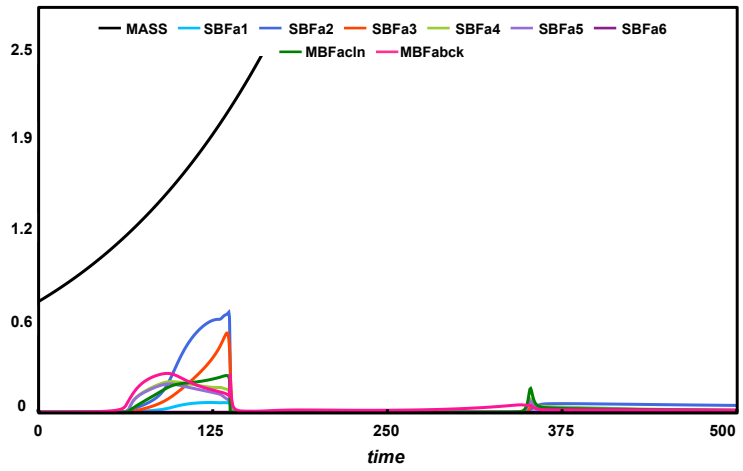

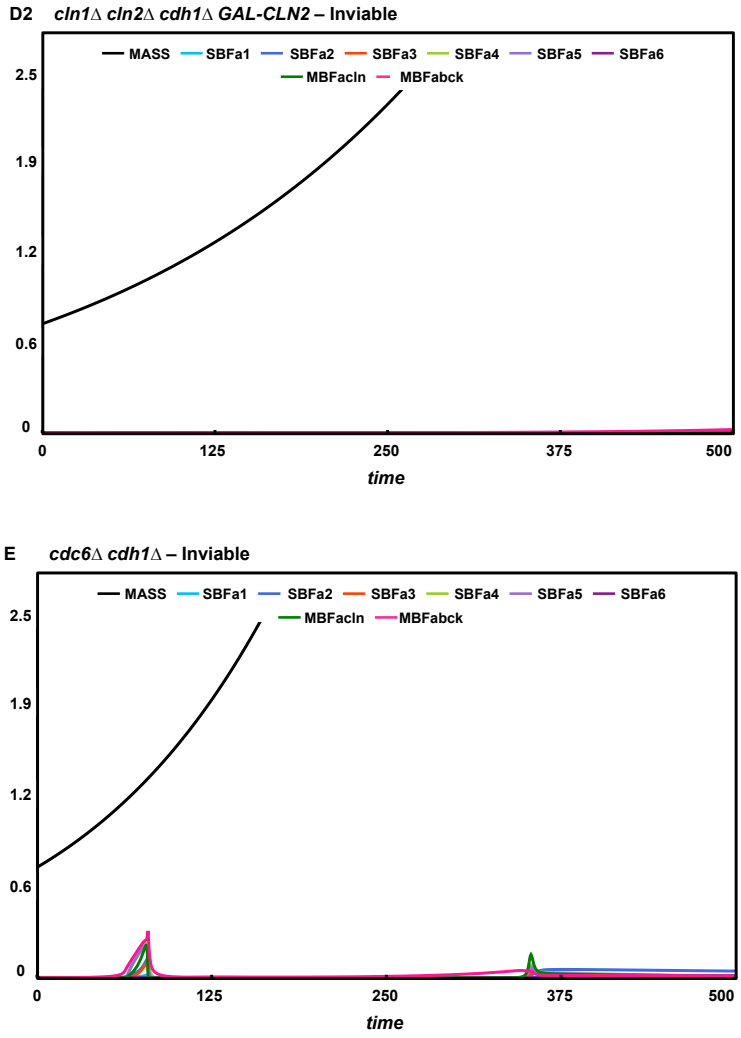

Figure 31. Model contradictions.

The figure shows simulations of the following mutants: (**A**) A1: *swi6*Δ *GAL-WHI5* (only Swi4dimers present (SBFa6); cells are viable yet large), (**B**) B1: *swi4*Δ (only MBF present; cells are viable yet large), B2: *msn5*Δ *swi4*Δ (only MBF present; cells are viable and large), (**C**) C1: *swi6*Δ (only Swi4dimers (SBFa6) present; cells are viable yet large), C2: *msn5*Δ *swi6*Δ (only Swi4dimers (SBFa6) present; cells are viable yet large), (**D**) D1: *cln1*Δ *cln2*Δ *cdh1*Δ (cells are inviable), D2: *cln1*Δ *cln2*Δ *cdh1*Δ *GAL-CLN2* (cells are inviable), (**E**) *cdc6*Δ *cdh1*Δ (cells are inviable).

Conclusions and Future directions

The cell cycle circuit is the central machinery of the cell that drives its controlled growth and division. The START transition in the budding yeast cell cycle serves as an important checkpoint that ensures proper absence of inhibitory signals, and growth of the cell to a critical size before commitment to cell division. In this study, we have developed a very detailed mathematical model of the START transition, incorporating many molecular details of this process including information about signaling/regulatory interactions, phosphorylation states and subcellular localization of key START proteins. The model explains the experimentally observed phenotypes of over 100 START mutants and the subcellular localization and translocation of transcription factor, SBF. The model also provides a mechanism for size control.

First and foremost, the in-depth analysis presented in this chapter enables generation of novel hypotheses and precise predictions on the mechanism of START transition for experimental verification. Secondly, as introduced earlier, the nutritional conditions of a cell greatly influence its size control mechanism, with several molecular players that mediate this effect being discovered recently. These interactions can be dovetailed into our model to generalize the existing mechanism for size control. Thirdly, our group has been developing detailed models for the other phases and events of the budding yeast cell cycle including DNA damage response, spindle assembly checkpoint and mitotic exit. The model for START presented here is therefore in its course to becoming a part of an integrated model for the entire budding yeast cell cycle, a 'queriable', navigable, 'tweakable' and executable cellular model system for cell biologists. And, finally, this detailed model for budding yeast offers a path towards

dealing with the enormous complexity of the cell cycle mechanism in high eukaryotes, including humans. The evolutionary conservation of the molecular circuitry underlying the START transition in the yeast cell cycle and R-point in mammalian counterpart supports this view. Modeling the R-point not only offers an understanding of the working of a healthy cell cycle but also tenders insights into its characteristic deregulation in diseases like cancer.

Materials and Methods

Current model

A wiring diagram with considerable amount of detail was drawn for the START transition (Figures 8, 13, 17) in conjunction with the Chen2004 model for the budding yeast cell cycle. Several aspects of the regulation of START have been revealed since 2004 including the action of a protein Whi5, which is a stoichiometric inhibitor of the transcription factor SBF. The START module of the model has been described in detail under Results section. The remaining cell cycle model (from START to mitotic exit) has been used almost as is from the Chen2004 model (except for changes in equations of START proteins like Cln3, Bck2, Cln2 and Clb5).

The wiring diagram was then converted to chemical reactions (mass-action), and algebraic relations that were then translated to ordinary differential equations and algebraic equations.

Modifications from Chen2004 model

We have used a previously published and well-established mathematical model for the budding yeast cell cycle from (Chen et al, 2004). The major modifications are

associated with the START transition of the cell cycle. The simplified Goldbeter-Koshland switch that was previously used to describe the activation of SBF, MBF leading to START (Figure 8) has been changed to with a much more detailed model (Figures 8, 13, 17) delineating several important phosphorylation and transportation events occurring at START. For this purpose, we have considered two compartments: nucleus and cytoplasm, to exist within the cell, but the compartments are assumed to have constant volume ratio (1:4) throughout the cell cycle. The species that move across compartments are scaled with the corresponding volumes to make the concentrations in the equations consistent.

Additionally, in the current version of the model, we have removed mass dependence from cyclins such as Cln1,2 and Clb5,6, represented by Cln2 and Clb5, since they are not concentrated in the nucleus and are distributed roughly throughout the cell. We have retained mass dependence only on Cln3 (through Ydj1 as the size sensor, and on Cln3 level in the nucleus), Bck2 and Clb2 in order to explain the complicated contributions to size control by these species. We also use a Hill function to model Cln activation at START (equation of Vpcln in table) due to the existence of cooperativity (Charvin et al, 2010), and to avoid the complexity and additional intermediates that would stem from considering multi-site phosphorylation of Whi5, Swi6 and Swi4. We do compare simpler versions of the START module modeled with either Hill function or multi-site phosphorylation, and show that the behavior is similar (data not shown). The comparison shows that Hill function is a reasonable approximation and phenomenological abstraction of multi-site phosphorylation in our case (data not shown).

Equations and Parameters

The equations and parameters used for our simulations are listed below and the files in the following formats will be provided upon request: ODE, SBML, PET and Matlab including the parameter set used and simulation settings for all the mutants. We have also listed all changes that have been made to the initial conditions and parameters in simulating specific mutants (Table 5).

Functions

$$BB(A1, A2, A3, A4) = A2 - A1 + A3 * A2 + A4 * A1$$

$$GK(A1, A2, A3, A4) = \frac{2 * A4 * A1}{\sqrt{(BB(A1, A2, A3, A4) + (BB(A1, A2, A3, A4)^2 - 4.0 * (A2 - A1) * A4 * A1))}}$$

Variables

$$IET = 1.0 * IEP + 1.0 * IE$$

$$TEM1T = 1.0 * TEM1GDP + 1.0 * TEM1GTP$$

$$CDC15T = 1.0 * CDC15 + 1.0 * CDC15i$$

$$ESP1T = 1.0 * ESP1 + 1.0 * PE$$

$$\begin{aligned} PROM2T = {} & 1.0 * BSB + 1.0 * PROM2 + 1.0 * SBFB6PQ + 1.0 * SBFB6P + 1.0 * SBFB \\ & + 1.0 * SWI4B + 1.0 * W4B + 1.0 * WSB56P + 1.0 * WSB5P + 1.0 * WSB6PQ \\ & + 1.0 * WSB6P + 1.0 * WSB \end{aligned}$$

$$\begin{aligned} SWI4T = {} & 1.0 * BSB + 1.0 * BSF + 1.0 * SBFB6PQ + 1.0 * SBFB6P + 1.0 * SBFB \\ & + 1.0 * SBFF46PQ + 1.0 * SBFF46P + 1.0 * SBFF4P + 1.0 * SBFF6PQ \\ & + 1.0 * SBFF6P + 1.0 * SBFF + 1.0 * SWI4B + 4.0 * SWI4C + 1.0 * SWI4F \\ & + 4.0 * SWI4PC + 1.0 * SWI4P + 1.0 * SWI4 + 1.0 * W4B + 1.0 * WSB56P \\ & + 1.0 * WSB5P + 1.0 * WSB6PQ + 1.0 * WSB6P + 1.0 * WSB + 1.0 * WSF45P \\ & + 1.0 * WSF46PQ + 1.0 * WSF46P + 1.0 * WSF4P + 1.0 * WSF56P + 1.0 * WSF5P \\ & + 1.0 * WSF6PQ + 1.0 * WSF6P + 1.0 * WSF \end{aligned}$$

$$\begin{aligned} WHI5T = {} & 1.0 * W4B + 4.0 * WHI5C + 4.0 * WHI5PC + 1.0 * WHI5PN + 1.0 * WHI5 \\ & + 1.0 * WMB + 1.0 * WSB56P + 1.0 * WSB5P + 1.0 * WSB6PQ + 1.0 * WSB6P \\ & + 1.0 * WSB + 1.0 * WSF45P + 1.0 * WSF46PQ + 1.0 * WSF46P + 1.0 * WSF4P \\ & + 1.0 * WSF56P + 1.0 * WSF5P + 1.0 * WSF6PQ + 1.0 * WSF6P + 1.0 * WSF \end{aligned}$$

$$PROM5T = 1.0 * MBFa + 1.0 * MBFi + 1.0 * MBFo + 1.0 * MBFp + 1.0 * MBFpo + 1.0 * PROM5 + 1.0 * WMB$$

$$MBP1T = 1.0 * MBFF + 1.0 * MBFa + 1.0 * MBFi + 1.0 * MBFo + 1.0 * MBFp + 1.0 * MBFpo + 1.0 * MBP1 + 1.0 * WMB$$

$$SWI6T = 1.0 * BSB + 1.0 * BSF + 1.0 * MBFF + 1.0 * MBFa + 1.0 * MBFi + 1.0 * MBFo + 1.0 * MBFp + 1.0 * MBFpo + 1.0 * SBFB6PQ + 1.0 * SBFB6P + 1.0 * SBFB + 1.0 * SBFF46PQ + 1.0 * SBFF46P + 1.0 * SBFF4P + 1.0 * SBFF6PQ + 1.0 * SBFF6P + 1.0 * SBFF + 4.0 * SWI6C + 4.0 * SWI6PQC + 1.0 * SWI6PQ + 1.0 * SWI6P + 4.0 * SWI6QC + 1.0 * SWI6 + 1.0 * WMB + 1.0 * WSB56P + 1.0 * WSB5P + 1.0 * WSB6PQ + 1.0 * WSB6P + 1.0 * WSB + 1.0 * WSF45P + 1.0 * WSF46PQ + 1.0 * WSF46P + 1.0 * WSF4P + 1.0 * WSF56P + 1.0 * WSF5P + 1.0 * WSF6PQ + 1.0 * WSF6P + 1.0 * WSF$$

$$D = \frac{1.026}{mu - 32.0}$$

$$F = \exp(-mu) * D$$

$$YDJ1 = kydj0 + kydj1 * MASS$$

$$SSA1 = kssa0 + kssab2 * CLB2 + kssaw5 * SWI5$$

$$Vacln3 = kgkcln3 * YDJ1$$

$$CLN3 = \text{if}(CLN3T == 0)\ \text{then}(0)\ \text{else}(CLN3T * MASS * GK(Vacln3, SSA1, Jacln3 * CLN3T, Jicln3 * CLN3T))$$

$$BCK2 = \text{if}(BCK2T == 0)\ \text{then}(0)\ \text{else}(BCK2T * MASS * GK(Vacln3, SSA1, Jabck2 * BCK2T, Jibck2 * BCK2T))$$

$$MCM1 = GK(kamcm * CLB2, kimcm, Jamcm, Jimcm)$$

$$Vdb2 = kdb2_p + kdb2_{pp} * CDH1 + kdb2_{ppp} * CDC20$$

$$Vdb5 = kdb5_p + kdb5_{pp} * CDC20$$

$$Vd2c1 = kd2c1 * (ec1n3 * CLN3 + ec1k2 * BCK2 + ec1n2 * CLN2 + ec1b5 * CLB5 + ec1b2 * CLB2)$$

$$Vd2f6 = kd2f6 * (ef6n3 * CLN3 + ef6k2 * BCK2 + ef6n2 * CLN2 + ef6b5 * CLB5 + ef6b2 * CLB2)$$

$$Vppc1 = kppc1 * CDC14$$

$$Vppf6 = kppf6 * CDC14$$

$$Vkpc1 = kd1c1 + \frac{Vd2c1}{(Jd2c1 + SIC1 + C2 + C5)}$$

$$Vkpf6 = kd1f6 + \frac{Vd2f6}{(Jd2f6 + CDC6 + F2 + F5)}$$

$$Vaiep = kaiep * CLB2$$

$$Vacdh = kacdh_p + kacdh_{pp} * CDC14$$

$$Vicdh = kicdh_p + kicdh_{pp} * (eicdhn3 * CLN3 + eicdhn2 * CLN2 + eicdhb5 * CLB5 + eicdhb2 * CLB2)$$

$$Vkpnet = kpnet_p + kpnet_{pp} * CDC15$$

$$Vppnet = kppnet_p + kppnet_{pp} * PPX$$

$$Vdpds = kdpds_{p} + kdpds_{pp} * CDC20 + kdpds_{ppp} * CDH1$$

$$Vdppx = kdppx_{p} + kdppx_{pp} * (J20ppx + CDC20) * \frac{Jdpds}{(Jdpds + PDS1)}$$

$$Vpn = epn3 * CLN3 + epn2 * CLN2 + epb5 * CLB5$$

$$Vpcln = kp + Vpnmax * \frac{Vpn^{N}}{(Jpn^{N} + Vpn^{N})}$$

$$Vpclb = kp_{p} + kp_{pp} * CLB2$$

$$Vpclb26 = kp_{p} + kp_{pp} * CLB2 + epb5q * CLB5$$

$$Vppase = kppase * PPase$$

$$Vpp14 = kpp14 * CDC14$$

$$CLB2T = CLB2 + C2 + F2 + C2P + F2P$$

$$CLB5T = CLB5 + C5 + F5 + C5P + F5P$$

$$CDC14T = CDC14 + RENT + RENTP$$

$$NET1T = NET1 + NET1P + RENT + RENTP$$

$$SIC1T = SIC1 + C2 + C5 + SIC1P + C2P + C5P$$

$$CDC6T = CDC6 + F2 + F5 + CDC6P + F2P + F5P$$

$$CKIT = SIC1T + CDC6T$$

$$SBFact = kasbf + kasbf1 * SBFB + kasbf2 * BSB + kasbf3 * (SBFB6P + SBFB6PQ) + kasbf4 * (WSB6P + WSB6PQ) + kasbf5 * WSB5P + kasbf6 * SWI4B$$

$$MBFact = kambf * MBFa$$

$$SBFa1 = kasbf1 * SBFB$$

$$SBFa2 = kasbf2 * BSB$$

$$SBFa3 = kasbf3 * (SBFB6P + SBFB6PQ)$$

$$SBFa4 = kasbf4 * (WSB6P + WSB6PQ)$$

$$SBFa5 = kasbf5 * WSB5P$$

$$SBFa6 = kasbf6 * SWI4B$$

$$MBFacln = MBFact * \frac{(kambfns * Vpcln)}{(kambfns * Vpcln + kambfk2 * BCK2)}$$

$$MBFabck = MBFact * \frac{(kambfk2 * BCK2)}{(kambfns * Vpcln + kambfk2 * BCK2)}$$

$$SWI4nuc = SWI4T - 4.0 * (SWI4C + SWI4PC)$$

$$WHI5nuc = WHI5T - 4.0 * (WHI5C + WHI5PC)$$

$$SWI6nuc = SWI6T - 4.0 * (SWI6C + SWI6PQC + SWI6QC)$$

$$SWI4CTOT = 4.0 * (SWI4C + SWI4PC)$$

$$SWI6CTOT = 4.0 * (SWI6C + SWI6QC + SWI6PQC)$$

$$WHI5CTOT = 4.0 * (WHI5C + WHI5PC)$$

Parameter Equations

$$mu = \frac{log(2)}{mdt}$$

Variable Equations

$$\frac{dMASS}{dt} = mu * MASS * \left(1 - \frac{MASS}{MAXMASS}\right)$$

$$\frac{dCLN2}{dt} = (ksn2_p + ksn2_{pp} * SBFact + ksn2_{ppp} * SBFnull * MBFact) - (kdn2 * CLN2)$$

$$\begin{aligned}\frac{dCLB5}{dt} &= (ksb5_p + ksb5_{pp} * MBFnull * SBFact + ksb5_{ppp} * MBFact) \\ &- (Vdb5 * CLB5) - (kasb5 * CLB5 * SIC1) + (kdib5 * C5) + (kd3c1 * C5P) \\ &- (kasf5 * CLB5 * CDC6) + (kdif5 * F5) + (kd3f6 * F5P)\end{aligned}$$

$$\begin{aligned}\frac{dCLB2}{dt} &= ((ksb2_p + ksb2_{pp} * MCM1) * MASS) - (Vdb2 * CLB2) \\ &- (kasb2 * CLB2 * SIC1) + (kdib2 * C2) + (kd3c1 * C2P) - (kasf2 * CLB2 * CDC6) \\ &+ (kdif2 * F2) + (kd3f6 * F2P)\end{aligned}$$

$$\begin{aligned}\frac{dSIC1}{dt} &= (ksc1_p + ksc1_{pp} * SWI5) - (kdc1 * SIC1) - (Vkpc1 * SIC1) \\ &+ (Vppc1 * SIC1P) - (kasb2 * CLB2 * SIC1) + (kdib2 * C2) - (kasb5 * CLB5 * SIC1) \\ &+ (kdib5 * C5) + (Vdb2 * C2) + (Vdb5 * C5)\end{aligned}$$

$$\frac{dSIC1P}{dt} = (Vkpc1 * SIC1) - (Vppc1 * SIC1P) - (kd3c1 * SIC1P) + (Vdb2 * C2P) + (Vdb5 * C5P)$$

$$\frac{dC2}{dt} = (kasb2 * CLB2 * SIC1) - (kdib2 * C2) - (Vkpc1 * C2) + (Vppc1 * C2P) - (Vdb2 * C2)$$

$$\frac{dC5}{dt} = (kasb5 * CLB5 * SIC1) - (kdib5 * C5) - (Vkpc1 * C5) + (Vppc1 * C5P) - (Vdb5 * C5)$$

$$\frac{dC2P}{dt} = (Vkpc1 * C2) - (Vppc1 * C2P) - (kd3c1 * C2P) - (Vdb2 * C2P)$$

$$\frac{dC5P}{dt} = (Vkpc1 * C5) - (Vppc1 * C5P) - (kd3c1 * C5P) - (Vdb5 * C5P)$$

$$\frac{dCDC6}{dt} = (ksf6_{p} + ksf6_{pp} * SWI5 + ksf6_{ppp} * SBFact) - (kdf6 * CDC6) - (Vkpf6 * CDC6) + (Vppf6 * CDC6P) - (kasf2 * CLB2 * CDC6) + (kdif2 * F2) - (kasf5 * CLB5 * CDC6) + (kdif5 * F5) + (Vdb2 * F2) + (Vdb5 * F5)$$

$$\frac{dCDC6P}{dt} = (Vkpf6 * CDC6) - (Vppf6 * CDC6P) - (kd3f6 * CDC6P) + (Vdb2 * F2P) + (Vdb5 * F5P)$$

$$\frac{dF2}{dt} = (kasf2 * CLB2 * CDC6) - (kdif2 * F2) - (Vkpf6 * F2) + (Vppf6 * F2P) - (Vdb2 * F2)$$

$$\frac{dF5}{dt} = (kasf5 * CLB5 * CDC6) - (kdif5 * F5) - (Vkpf6 * F5) + (Vppf6 * F5P) - (Vdb5 * F5)$$

$$\frac{dF2P}{dt} = (Vkpf6 * F2) - (Vppf6 * F2P) - (kd3f6 * F2P) - (Vdb2 * F2P)$$

$$\frac{dF5P}{dt} = (Vkpf6 * F5) - (Vppf6 * F5P) - (kd3f6 * F5P) - (Vdb5 * F5P)$$

$$\frac{dSWI5}{dt} = (ksswi_p + ksswi_{pp} * MCM1) - (kdswi * SWI5) - ((kiswi * CLB2) * SWI5) + (kaswi * CDC14) * SWI5P$$

$$\frac{dSWI5P}{dt} = (kiswi * CLB2) * SWI5 - ((kaswi * CDC14) * SWI5P) - (kdswi * SWI5P)$$

$$\frac{dIE}{dt} = -\left(Vaiep * IE * \frac{1}{(Jaiep + IE)}\right) + \left(kiiep * IEP * \frac{1}{(Jiiep + IEP)}\right)$$

$$\frac{dIEP}{dt} = \left(Vaiep * IE * \frac{1}{(Jaiep + IE)}\right) - \left(kiiep * IEP * \frac{1}{(Jiiep + IEP)}\right)$$

$$\frac{dCDC20i}{dt} = (ks20_p + ks20_{pp} * MCM1) - (kd20 * CDC20i) - ((ka20_p + ka20_{pp} * IEP) * CDC20i) + (MAD2 * CDC20)$$

$$\frac{dCDC20}{dt} = (ka20_p + ka20_{pp} * IEP) * CDC20i - (MAD2 * CDC20) - (kd20 * CDC20)$$

$$\frac{dCDH1}{dt} = (kscdh) - (kdcdh * CDH1) - \left(Vicdh * CDH1 * \frac{1}{(Jicdh + CDH1)}\right) + \left(Vacdh * CDH1i * \frac{1}{(Jacdh + CDH1i)}\right)$$

$$\frac{dCDH1i}{dt} = \left(Vicdh * CDH1 * \frac{1}{(Jicdh + CDH1)}\right) - \left(Vacdh * CDH1i * \frac{1}{(Jacdh + CDH1i)}\right) - (kdcdh * CDH1i)$$

$$\frac{dCDC14}{dt} = (ks14) - (kd14 * CDC14) - (kasrent * CDC14 * NET1) + (kdirent * RENT) - (kasrentp * CDC14 * NET1P) + (kdirentp * RENTP) + (kdnet * RENT) + (kdnet * RENTP)$$

$$\frac{dNET1}{dt} = (ksnet) - (kdnet * NET1) - (Vkpnet * NET1) + (Vppnet * NET1P) - (kasrent * CDC14 * NET1) + (kdirent * RENT) + (kd14 * RENT)$$

$$\frac{dRENT}{dt} = (kasrent * CDC14 * NET1) - (kdirent * RENT) - (Vkpnet * RENT) + (Vppnet * RENTP) - (kdnet * RENT) - (kd14 * RENT)$$

$$\frac{dNET1P}{dt} = (Vkpnet * NET1) - (Vppnet * NET1P) - (kdnet * NET1P) - (kasrentp * CDC14 * NET1P) + (kdirentp * RENTP) + (kd14 * RENTP)$$

$$\frac{dRENTP}{dt} = (kasrentp * CDC14 * NET1P) - (kdirentp * RENTP) + (Vkpnet * RENT) - (Vppnet * RENTP) - (kdnet * RENTP) - (kd14 * RENTP)$$

$$\frac{dTEM1GDP}{dt} = -\left(LTE1 * TEM1GDP * \frac{1}{(Jatem + TEM1GDP)}\right) + \left(BUB2 * TEM1GTP * \frac{1}{(Jitem + TEM1GTP)}\right)$$

$$\frac{dTEM1GTP}{dt} = \left(LTE1 * TEM1GDP * \frac{1}{(Jatem + TEM1GDP)}\right) - \left(BUB2 * TEM1GTP * \frac{1}{(Jitem + TEM1GTP)}\right)$$

$$\frac{dCDC15i}{dt} = -((ka15_{p} * TEM1GDP + ka15_{pp} * TEM1GTP + ka15_{ppp} * CDC14) * CDC15i)$$

$$+ (ki15 * CDC15)$$

$$\frac{dCDC15}{dt} = (ka15_{p} * TEM1GDP + ka15_{pp} * TEM1GTP + ka15_{ppp} * CDC14) * CDC15i - (ki15 * CDC15)$$

$$\frac{dPPX}{dt} = (ksppx) - (Vdppx * PPX)$$

$$\frac{dPDS1}{dt} = (kspds_{p} + kspds_{pp} * SBFact + kpds_{ppp} * MCM1) - (Vdpds * PDS1) - (kasesp * PDS1 * ESP1) + (kdiesp * PE)$$

$$\frac{dESP1}{dt} = -(kasesp * PDS1 * ESP1) + (kdiesp * PE) + (Vdpds * PE)$$

$$\frac{dPE}{dt} = (kasesp * PDS1 * ESP1) - (kdiesp * PE) - (Vdpds * PE)$$

$$\frac{dORI}{dt} = (ksori * (eorib5 * CLB5 + eorib2 * CLB2)) - (kdori * ORI)$$

$$\frac{dBUD}{dt} = (ksbud * (ebudn2 * CLN2 + ebudn3 * CLN3 + ebudb5 * CLB5)) - (kdbud * BUD)$$

$$\frac{dSPN}{dt} = ksspn * \frac{CLB2}{(Jspn + CLB2)} - (kdspn * SPN)$$

$$\frac{dMAD2}{dt} = 0$$

$$\frac{dLTE1}{dt} = 0$$

$$\frac{dBUB2}{dt} = 0$$

$$\begin{aligned}\frac{dSWI4}{dt} &= -(kas46 * SWI4 * SWI6) + (kdi46 * SBFF) - ((ksbs4 * BCK2) * SWI4) \\ &+ (kdbs4 * SWI4F) - ((ef4p * Vpclb) * SWI4) + (Vpp14 * SWI4P) \\ &- (kas46 * SWI6P * SWI4) - (kas46 * SWI6PQ * SWI4) + (kdi46 * SBFF6P) \\ &+ (kdi46 * SBFF6PQ) + (kimp * SWI4C) * \frac{cytoplasm}{nucleus}\end{aligned}$$

$$\begin{aligned}\frac{dSWI6}{dt} &= -(kas46 * SWI4 * SWI6) + (kdi46 * SBFF) - ((ef6p * Vpcln) * SWI6) \\ &+ (kppcln * SWI6P) + (kimp * SWI6C) * \frac{cytoplasm}{nucleus} \\ &- (kasmbf * MBP1 * SWI6) + (kdimbf * MBFF)\end{aligned}$$

$$\begin{aligned}\frac{dWHI5}{dt} &= -(kasws * WHI5 * SBFF) + (kdiws * WSF) - (kasws * WHI5 * SBFB) \\ &+ (kdiws * WSB) - (kasw4 * SWI4B * WHI5) + (kdiw4 * W4B) - ((ef5p * Vpcln) * WHI5) \\ &+ (kppcln * WHI5PN) + (kimp * WHI5C) * \frac{cytoplasm}{nucleus} \\ &- (kaswm * MBFa * WHI5) + (kdiwm * WMB)\end{aligned}$$

$$\frac{dMBP1}{dt} = -(kasmbf * MBP1 * SWI6) + (kdimbf * MBFF)$$

$$\begin{aligned}\frac{dPROM2}{dt} &= -(kasprom * SBFF * PROM2) + (kdiprom * SBFB) - (kasprom * WSF * PROM2) \\ &+ (kdiprom * WSB) - (kasprom * BSF * PROM2) + (kdiprom * BSB) \\ &- (kasprom * SWI4F * PROM2) + (kdiprom * SWI4B) + (ef4p * Vpclb) * SBFB \\ &+ (ef4p * Vpclb) * SBFB6P + (ef4p * Vpclb) * SBFB6PQ + (ef4p * Vpclb) * WSB \\ &+ (ef4p * Vpclb) * WSB5P + (ef4p * Vpclb) * WSB6P + (ef4p * Vpclb) * WSB6PQ \\ &+ (Vpclb * SWI4B) + (Vpclb * BSB)\end{aligned}$$

$$\frac{dPROM5}{dt} = -(kasprom * MBFF * PROM5) + (kdiprom * MBFi)$$

$$\frac{dNRM1}{dt} = (ksnrm1 + ksnrm1_p * MBFact) - (kdnrm1 * NRM1)$$

$$\begin{aligned}\frac{dSWI4C}{dt} &= (kexp * MSN5) * SBFF6PQ * \frac{nucleus}{cytoplasm} \\ &+ (kexp * MSN5) * WSF6PQ * \frac{nucleus}{cytoplasm} + (Vppase * SWI4PC) - (kimp * SWI4C)\end{aligned}$$

$$\begin{aligned}\frac{dSWI4PC}{dt} &= (kexp * MSN5) * SBFF46PQ * \frac{nucleus}{cytoplasm} \\ &+ (kexp * MSN5) * WSF46PQ * \frac{nucleus}{cytoplasm} \\ &+ (kexp * MSN5) * WSF45P * \frac{nucleus}{cytoplasm} - (Vppase * SWI4PC)\end{aligned}$$

$$\begin{aligned}\frac{dSWI4P}{dt} &= (ef4p * Vpclb) * SWI4 - (Vpp14 * SWI4P) - (kas46 * SWI6P * SWI4P) \\ &- (kas46 * SWI6PQ * SWI4P) + (kdi46 * SBFF46P) + (kdi46 * SBFF46PQ) \\ &+ (Vpclb * SWI4B)\end{aligned}$$

$$\begin{aligned}\frac{dSWI4B}{dt} &= (kasprom * SWI4F * PROM2) - (kdiprom * SWI4B) - (kasw4 * SWI4B * WHI5) \\ &+ (kdiw4 * W4B) + (ef5p * Vpcln) * W4B - (Vpclb * SWI4B)\end{aligned}$$

$$\begin{aligned}\frac{dSWI4F}{dt} &= (ksbs4 * BCK2) * SWI4 - (kdbs4 * SWI4F) - (kasprom * SWI4F * PROM2) \\ &+ (kdiprom * SWI4B)\end{aligned}$$

$$\frac{dW4B}{dt} = (kasw4 * SWI4B * WHI5) - (kdiw4 * W4B) - ((ef5p * Vpcln) * W4B)$$

$$\frac{dBSF}{dt} = (ksbs * BCK2) * SBFF - (kdbs * BSF) - (kasprom * BSF * PROM2) + (kdiprom * BSB)$$

$$\frac{dBSB}{dt} = (ksbs * BCK2) * SBFB - (kdbs * BSB) + (kasprom * BSF * PROM2) - (kdiprom * BSB) - (Vpclb * BSB)$$

$$\frac{dSBFF}{dt} = (kas46 * SWI4 * SWI6) - (kdi46 * SBFF) - (kasws * WHI5 * SBFF) + (kdiws * WSF) - (kasprom * SBFF * PROM2) + (kdiprom * SBFB) - ((ksbs * BCK2) * SBFF) + (kdbs * BSF) - ((ef6p * Vpcln) * SBFF) + (kppcln * SBFF6P) + (kdiwp * WSF5P) - ((ef4p * Vpclb) * SBFF) +$$

$$\frac{dSBFF4P}{dt} = (ef4p * Vpclb) * SBFF - (Vpp14 * SBFF4P) + (kppcln * SBFF46P) + (ef4p * Vpclb) * SBFB + (Vpclb * BSB)$$

$$\frac{dSBFF6P}{dt} = (ef6p * Vpcln) * SBFF - (kppcln * SBFF6P) + (kdiwp * WSF56P) + (kas46 * SWI6P * SWI4) - (kdi46 * SBFF6P) - ((ef4p * Vpclb) * SBFF6P) + (Vpp14 * SBFF46P) - ((ef6q * Vpclb26) * SBFF6P) + (Vpp14 * SBFF6PQ)$$

$$\frac{dSBFF6PQ}{dt} = (kas46 * SWI6PQ * SWI4) - (kdi46 * SBFF6PQ) + (ef6q * Vpclb26) * SBFF6P - (Vpp14 * SBFF6PQ) - ((ef4p * Vpclb) * SBFF6PQ) + (Vpp14 * SBFF46PQ) - ((kexp * MSN5) * SBFF6PQ)$$

$$\frac{dSBFF46P}{dt} = (kas46 * SWI6P * SWI4P) - (kdi46 * SBFF46P) + (ef4p * Vpclb) * SBFF6P - (Vpp14 * SBFF46P) - (kppcln * SBFF46P) - ((ef6q * Vpclb26) * SBFF46P) + (Vpp14 * SBFF46PQ) + (ef4p * Vpclb) * SBFB6P$$

$$\frac{dSBFF46PQ}{dt} = (kas46 * SWI6PQ * SWI4P) + (ef4p * Vpclb) * SBFF6PQ$$
$$- (Vpp14 * SBFF46PQ) + (ef6q * Vpclb26) * SBFF46P - (kdi46 * SBFF46PQ)$$
$$- (Vpp14 * SBFF46PQ) + (ef4p * Vpclb) * SBFB6PQ - ((kexp * MSN5) * SBFF46PQ)$$

$$\frac{dSBFB}{dt} = (kasprom * SBFF * PROM2) - (kdiprom * SBFB) - (kasws * WHI5 * SBFB)$$
$$+ (kdiws * WSB) - ((ksbs * BCK2) * SBFB) + (kdbs * BSB) - ((ef6p * Vpcln) * SBFB)$$
$$+ (kppcln * SBFB6P) - ((ef4p * Vpclb) * SBFB)$$

$$\frac{dSBFB6P}{dt} = (ef6p * Vpcln) * SBFB - (kppcln * SBFB6P) + (kdiwp * WSB56P)$$
$$- ((ef6q * Vpclb26) * SBFB6P) + (Vpp14 * SBFB6PQ) - ((ef4p * Vpclb) * SBFB6P)$$

$$\frac{dSBFB6PQ}{dt} = (ef6q * Vpclb26) * SBFB6P - (Vpp14 * SBFB6PQ) - ((ef4p * Vpclb) * SBFB6PQ)$$

$$\frac{dWSF}{dt} = (kasws * WHI5 * SBFF) - (kdiws * WSF) - (kasprom * WSF * PROM2)$$
$$+ (kdiprom * WSB) - ((ef5p * Vpcln) * WSF) + (kppcln * WSF5P)$$
$$- ((ef6p * Vpcln) * WSF) + (kppcln * WSF6P) - ((ef4p * Vpclb) * WSF)$$
$$+ (Vpp14 * WSF4P)$$

$$\frac{dWSF4P}{dt} = (ef4p * Vpclb) * WSF - (Vpp14 * WSF4P) + (kppcln * WSF46P)$$
$$+ (ef4p * Vpclb) * WSB$$

$$\frac{dWSF5P}{dt} = (ef5p * Vpcln) * WSF - (kppcln * WSF5P) - (kdiwp * WSF5P)$$

$$\frac{dWSF6P}{dt} = (ef6p * Vpcln) * WSF - (kppcln * WSF6P) - ((ef5p * Vpcln) * WSF6P)$$
$$- ((ef4p * Vpclb) * WSF6P) + (Vpp14 * WSF46P) - ((ef6q * Vpclb26) * WSF6P)$$
$$+ (Vpp14 * WSF6PQ)$$

$$\frac{dWSF6PQ}{dt} = (ef6q * Vpclb26) * WSF6P - (Vpp14 * WSF6PQ) - ((ef4p * Vpclb) * WSF6PQ) + (Vpp14 * WSF46PQ) - ((kexp * MSN5) * WSF6PQ)$$

$$\frac{dWSF45P}{dt} = (ef4p * Vpclb) * WSB5P - ((kexp * MSN5) * WSF45P)$$

$$\frac{dWSF46P}{dt} = (ef4p * Vpclb) * WSF6P - (Vpp14 * WSF46P) - (kppcln * WSF46P) + (Vpp14 * WSF46PQ) - ((ef6q * Vpclb26) * WSF46P) + (ef4p * Vpclb) * WSB6P$$

$$\frac{dWSF46PQ}{dt} = (ef4p * Vpclb) * WSF6PQ - (Vpp14 * WSF46PQ) - (Vpp14 * WSF46PQ) + (ef6q * Vpclb26) * WSF46P + (ef4p * Vpclb) * WSB6PQ - ((kexp * MSN5) * WSF46PQ)$$

$$\frac{dWSF56P}{dt} = (ef5p * Vpcln) * WSF6P - (kdiwp * WSF56P)$$

$$\frac{dWSB}{dt} = (kasprom * WSF * PROM2) - (kdiprom * WSB) + (kasws * WHI5 * SBFB) - (kdiws * WSB) - ((ef5p * Vpcln) * WSB) + (kppcln * WSB5P) - ((ef6p * Vpcln) * WSB) + (kppcln * WSB6P) - ((ef4p * Vpclb) * WSB)$$

$$\frac{dWSB5P}{dt} = (ef5p * Vpcln) * WSB - (kppcln * WSB5P) - ((ef6p * Vpcln) * WSB5P) + (kppcln * WSB56P) - ((ef4p * Vpclb) * WSB5P)$$

$$\frac{dWSB6P}{dt} = (ef6p * Vpcln) * WSB - (kppcln * WSB6P) - ((ef5p * Vpcln) * WSB6P) + (kppcln * WSB56P) - ((ef6q * Vpclb26) * WSB6P) + (Vpp14 * WSB6PQ) - ((ef4p * Vpclb) * WSB6P)$$

$$\frac{dWSB6PQ}{dt} = (ef6q * Vpclb26) * WSB6P - (Vpp14 * WSB6PQ) - ((ef4p * Vpclb) * WSB6PQ)$$

$$\frac{dWSB56P}{dt} = (ef6p * Vpcln) * WSB5P - (kppcln * WSB56P) + (ef5p * Vpcln) * WSB6P - (kppcln * WSB56P) - (kdiwp * WSB56P)$$

$$\frac{dSWI6C}{dt} = (kexp * MSN5) * WSF45P * \frac{nucleus}{cytoplasm} + (Vpp14 * SWI6QC) - (kimp * SWI6C)$$

$$\frac{dSWI6QC}{dt} = (Vppase * SWI6PQC) - (Vpp14 * SWI6QC)$$

$$\frac{dSWI6PQC}{dt} = (kexp * MSN5) * SBFF6PQ * \frac{nucleus}{cytoplasm} + (kexp * MSN5) * SBFF46PQ * \frac{nucleus}{cytoplasm} + (kexp * MSN5) * WSF6PQ * \frac{nucleus}{cytoplasm} + (kexp * MSN5) * WSF46PQ * \frac{nucleus}{cytoplasm} - (Vppase * SWI6PQC)$$

$$\frac{dSWI6P}{dt} = (ef6p * Vpcln) * SWI6 - (kppcln * SWI6P) - ((ef6q * Vpclb26) * SWI6P) + (Vpp14 * SWI6PQ) - (kas46 * SWI6P * SWI4) - (kas46 * SWI6P * SWI4P) + (kdi46 * SBFF6P) + (kdi46 * SBFF46P)$$

$$\frac{dSWI6PQ}{dt} = (ef6q * Vpclb26) * SWI6P - (Vpp14 * SWI6PQ) - (kas46 * SWI6PQ * SWI4) - (kas46 * SWI6PQ * SWI4P) + (kdi46 * SBFF6PQ) + (kdi46 * SBFF46PQ)$$

$$\frac{dMBFF}{dt} = (kasmbf * MBP1 * SWI6) - (kdimbf * MBFF) - (kasprom * MBFF * PROM5) + (kdiprom * MBFi)$$

$$\frac{dMBFi}{dt} = (kasprom * MBFF * PROM5) - (kdiprom * MBFi) - ((kambfns * Vpcln + kambfk2 * BCK2) * MBFi) + (kimbf * kppcln) * MBFa$$

$$\frac{dMBFa}{dt} = (kambfns * Vpcln + kambfk2 * BCK2) * MBFi - ((kimbf * kppcln) * MBFa) - (kaswm * MBFa * WHI5) + (kdiwm * WMB) + (ef5p * (kambfns * Vpcln)) * WMB - ((kimbf01 * CLB2) * MBFa) + (kmbf10 * MBFp) - ((kimbf02 * NRM1) * MBFa) + (kmbf20 * MBFo)$$

$$\frac{dMBFp}{dt} = (kimbf01 * CLB2) * MBFa - (kmbf10 * MBFp) - ((kimbf13 * NRM1) * MBFp) + (kmbf31 * MBFpo)$$

$$\frac{dMBFo}{dt} = (kimbf02 * NRM1) * MBFa - (kmbf20 * MBFo) - ((kimbf23 * CLB2) * MBFo) + (kmbf32 * MBFpo)$$

$$\frac{dMBFpo}{dt} = (kimbf13 * NRM1) * MBFp - (kmbf31 * MBFpo) + (kimbf23 * CLB2) * MBFo - (kmbf32 * MBFpo)$$

$$\frac{dWMB}{dt} = (kaswm * MBFa * WHI5) - (kdiwm * WMB) - ((ef5p * (kambfns * Vpcln)) * WMB)$$

$$\frac{dWHI5PC}{dt} = (kexp * MSN5) * WHI5PN * \frac{nucleus}{cytoplasm} + (kexp * MSN5) * WSF45P * \frac{nucleus}{cytoplasm} - (Vpp14 * WHI5PC)$$

$$\frac{dWHI5C}{dt} = (kexp * MSN5) * WSF6PQ * \frac{nucleus}{cytoplasm} + (kexp * MSN5) * WSF46PQ * \frac{nucleus}{cytoplasm} + (Vpp14 * WHI5PC) - (kimp * WHI5C)$$

$$\frac{dWHI5PN}{dt} = (ef5p * Vpcln) * W4B + (ef5p * Vpcln) * WHI5 - (kppcln * WHI5PN) + (kdiwp * WSF5P) + (kdiwp * WSF56P) + (kdiwp * WSB56P) - ((kexp * MSN5) * WHI5PN) + (ef5p * (kambfns * Vpcln)) * WMB$$

$$\frac{dTCYCLE}{dt} = 1$$

$$\frac{dORIFLAG}{dt} = 0$$

$$\frac{dTORI}{dt} = 0$$

$$\frac{dUDNA}{dt} = 0$$

$$\frac{dREPDNA}{dt} = 0$$

$$\frac{dTSPN}{dt} = 0$$

$$\frac{dSPNALIGN}{dt} = 0$$

$$\frac{dSACOFF}{dt} = 0$$

Globals

global $-1\ CLB2 + CLB5 - KEZ2 - 0.0\ ORI = 0.0; ORIFLAG = 1.0$

global $1\ ORI - 1.0 - 0.0\ TORI = TCYCLE * ORIFLAG;\ UDNA = 1.0 * ORIFLAG;\ MAD2 = mad2h * ORIFLAG + mad2l * (1.0 - ORIFLAG);\ BUB2 = bub2h * ORIFLAG + bub2l * (1.0 - ORIFLAG)$

global $1\ TCYCLE - TORI - DNATIMER - 0.0\ REPDNA = UDNA;\ SACOFF = SPNALIGN * ORIFLAG;\ UDNA = 0.0;\ ORIFLAG = 0.0$

global $1\ TCYCLE - TORI - DNATIMER - 0.0\ MAD2 = mad2l * SACOFF + mad2h * (1.0 - SACOFF);\ BUB2 = bub2l * SACOFF + bub2h * (1.0 - SACOFF);\ LTE1 = lte1h * SACOFF + lte1l * (1.0 - SACOFF)$

global $1\ SPN - 1.0 - 0.0\ SPNALIGN = 1.0; TSPN = TCYCLE;\ SACOFF = REPDNA$

global $1\ SPN - 1.0 - 0.0\ MAD2 = mad2l * SACOFF + mad2h * (1.0 - SACOFF);\ BUB2 = bub2l * SACOFF + bub2h * (1.0 - SACOFF);\ LTE1 = lte1h * SACOFF + lte1l * (1.0 - SACOFF)$

global $-1\ CLB2 - KEZ - 0.0\ MASS = F * MASS * REPDNA + MASS * (1.0 - REPDNA);\ LTE1 = lte1l * REPDNA + LTE1 * (1.0 - REPDNA);\ BUD = 0.0 + BUD * (1.0 - REPDNA);\ SPN = 0.0 + SPN * (1.0 - REPDNA);\ TCYCLE = 0.0 + TCYCLE * (1.0 - REPDNA);\ TORI = 1000.0 + TORI * (1.0 - REPDNA);\ TSPN = 0.0 + TSPN * (1.0 - REPDNA);\ SPNALIGN = 0.0; SACOFF = 0.0;\ REPDNA = 0.0$

Initial Conditions

$BSB = 0.0$; $BSF = 0.0$; $BUB2 = 0.2$
$BUD = 0.013865$; $C2 = 0.060189$; $C2P = 0.056408$
$C5 = 0.015792$; $C5P = 0.014685$; $CDC14 = 0.714825$
$CDC15 = 0.660294$; $CDC15i = 0.339705$; $CDC20 = 0.492649$
$CDC20i = 0.955920$; $CDC6 = 0.051241$; $CDC6P = 0.061135$
$CDH1 = 0.987313$; $CDH1i = 0.012686$; $CLB2 = 0.0$
$CLB5 = 0.0$; $CLN2 = 0.676243$; $ESP1 = 0.6$
$F2 = 0.075175$; $F2P = 0.072911$; $F5 = 4.650913$
$F5P = 4.400947$; $IE = 0.781375$; $IEP = 0.218624$
$LTE1 = 0.1$; $MAD2 = 0.01$; $MASS = 0.75$
$MBFa = 0.0$; $MBFF = 0.0$; $MBFi = 0.0$
$MBFo = 0.0$; $MBFp = 0.0$; $MBFpo = 0.0$
$MBP1 = 5.5$; $NET1 = 0.015608$; $NET1P = 1.499216$
$NRM1 = 0.0$; $ORI = 0.0$; $ORIFLAG = 1.0$
$PDS1 = 0.010232$; $PE = 0.4$; $PPX = 0.083887$
$PROM2 = 2.0$; $PROM5 = 2.0$; $RENT = 0.545970$
$RENTP = 0.739204$; $REPDNA = 0.0$; $SACOFF = 0.0$
$SBFB6P = 0.0$; $SBFB6PQ = 0.0$; $SBFB = 0.0$
$SBFF46P = 0.0$; $SBFF46PQ = 0.0$; $SBFF4P = 0.0$
$SBFF6P = 0.0$; $SBFF6PQ = 0.0$; $SBFF = 0.0$
$SIC1 = 0.009344$; $SIC1P = 0.016561$; $SPN = 0.016799$
$SPNALIGN = 0.0$; $SWI4 = 5.5$; $SWI4B = 0.0$
$SWI4C = 0.0$; $SWI4F = 0.0$; $SWI4P = 0.0$
$SWI4PC = 0.0$; $SWI5 = 0.746522$; $SWI5P = 0.020545$
$SWI6 = 30.0$; $SWI6C = 0.0$; $SWI6P = 0.0$
$SWI6PQ = 0.0$; $SWI6PQC = 0.0$; $SWI6QC = 0.0$
$TCYCLE = 0.0$; $TEM1GDP = 0.061371$; $TEM1GTP = 0.938628$
$TORI = 1000.0$; $TSPN = 0.0$; $UDNA = 0.0$
$W4B = 0.0$; $WHI5 = 10.0$; $WHI5C = 0.0$
$WHI5PC = 0.0$; $WHI5PN = 0.0$; $WMB = 0.0$
$WSB56P = 0.0$; $WSB5P = 0.0$; $WSB6P = 0.0$
$WSB6PQ = 0.0$; $WSB = 0.0$; $WSF45P = 0.0$
$WSF46P = 0.0$; $WSF46PQ = 0.0$; $WSF4P = 0.0$
$WSF56P = 0.0$; $WSF5P = 0.0$; $WSF6P = 0.0$
$WSF6PQ = 0.0$; $WSF = 0.0$

Parameters

$BCK2T = 0.1$; $bub2h = 1.0$; $bub2l = 0.2$ $cell = 1.0$; $CLN3T = 0.1$;
$cytoplasm = 0.8$ $DNATIMER = 20.0$; $ebudb5 = 0.5$; $ebudn2 = 0.15$ $ebudn3 = 0.25$;
$ec1b2 = 0.5$; $ec1b5 = 0.25$ $ec1k2 = 0.075$; $ec1n2 = 0.3$; $ec1n3 = 0.125$
$ef4p = 1.0$; $ef5p = 1.0$; $ef6b2 = 1.0$ $ef6b5 = 0.4$; $ef6k2 = 0.075$;
$ef6n2 = 0.35$ $ef6n3 = 0.125$; $ef6p = 1.0$; $ef6q = 1.0$ $eicdhb2 = 1.0$;
$eicdhb5 = 4.0$; $eicdhn2 = 0.3$ $eicdhn3 = 0.0$; $eorib2 = 0.45$; $eorib5 = 0.5$
$epb5 = 0.05$; $epb5q = 0.125$; $epn2 = 0.1$ $epn3 = 5.0$; $J20ppx = 0.15$;
$Jabck2 = 0.05$ $Jacdh = 0.03$; $Jacln3 = 0.05$; $Jaiep = 0.1$ $Jamcm = 0.1$;
$Jatem = 0.1$; $Jd2c1 = 0.05$ $Jd2f6 = 0.05$; $Jdpds = 0.04$; $Jibck2 = 0.05$
$Jicdh = 0.03$; $Jicln3 = 0.05$; $Jiiep = 0.1$ $Jimcm = 0.1$; $Jitem = 0.1$;
$Jpn = 1.25$ $Jspn = 0.14$; $ka15_{p} = 0.0020$; $ka15_{pp} = 1.0$ $ka15_{ppp} = 0.0010$;
$ka20_{p} = 0.06$; $ka20_{pp} = 0.2$ $kacdh_{p} = 0.01$; $kacdh_{pp} = 0.5$; $kaiep = 0.1$
$kambf = 1.0$; $kambfk2 = 2.5$; $kambfns = 1.2$ $kamcm = 1.0$; $kas46 = 30.0$;
$kasb2 = 50.0$ $kasb5 = 25.0$; $kasbf1 = 0.2$; $kasbf2 = 1.0$ $kasbf3 = 1.0$;
$kasbf4 = 1.0$; $kasbf5 = 1.0$ $kasbf6 = 0.16$; $kasbf = 0.0$; $kasesp = 50.0$
$kasf2 = 15.0$; $kasf5 = 0.015$; $kasmbf = 30.0$ $kasprom = 50.0$; $kasrent = 100.0$;
$kasrentp = 1.0$ $kasw4 = 0.0$; $kaswi = 2.0$; $kaswm = 3.0$ $kasws = 30.0$;
$kd14 = 0.1$; $kd1c1 = 0.01$ $kd1f6 = 0.01$; $kd20 = 0.3$; $kd2c1 = 1.0$
$kd2f6 = 1.0$; $kd3c1 = 1.0$; $kd3f6 = 1.0$ $kdb2_{p} = 0.0030$; $kdb2_{pp} = 0.4$;
$kdb2_{ppp} = 0.2$ $kdb5_{p} = 0.011$; $kdb5_{pp} = 0.16$; $kdbs4 = 5.0$ $kdbs = 5.0$;
$kdbud = 0.06$; $kdc1 = 0.0010$ $kdcdh = 0.01$; $kdf6 = 0.0010$; $kdi46 = 0.5$
$kdib2 = 0.05$; $kdib5 = 0.06$; $kdiesp = 0.5$ $kdif2 = 0.5$; $kdif5 = 0.03$;
$kdimbf = 1.0$ $kdiprom = 1.0$; $kdirent = 1.0$; $kdirentp = 2.0$ $kdiw4 = 1.0$;
$kdiwm = 1.0$; $kdiwp = 15.0$ $kdiws = 1.0$; $kdn2 = 0.2$; $kdnet = 0.03$
$kdnrm1 = 0.08$; $kdori = 0.06$; $kdpds_{ppp} = 0.04$ $kdpds_{p} = 0.01$; $kdpds_{pp} = 0.2$;
$kdppx_{p} = 0.17$ $kdppx_{pp} = 2.0$; $kdspn = 0.06$; $kdswi = 0.08$ $kexp = 5.0$;
$KEZ2 = 0.15$; $KEZ = 0.2$ $kgkcln3 = 1.0$; $ki15 = 0.5$; $kicdh_{p} = 0.0050$
$kicdh_{pp} = 0.08$; $kiiep = 0.15$; $kimbf01 = 0.2$ $kimbf02 = 0.4$; $kimbf13 = 0.4$;
$kimbf23 = 0.2$ $kimbf = 1.0$; $kimcm = 0.48$; $kimp = 2.0$ $kiswi = 0.1$;
$kmbf10 = 0.04$ $kmbf20 = 0.04$; $kmbf31 = 0.04$; $kmbf32 = 0.04$
$kp = 0.0$; $kp_{p} = 0.01$; $kp_{pp} = 1.0$ $kpnet_{p} = 0.01$; $kpnet_{pp} = 2.0$;
$kpp14 = 1.0$ $kppase = 1.0$; $kppc1 = 4.0$; $kppcln = 1.0$ $kppf6 = 4.0$;
$kppnet_{pp} = 3.0$; $kppnet_{p} = 0.05$ $ks14 = 0.22$; $ks20_{p} = 0.0060$; $ks20_{pp} = 0.6$
$ksb2_{p} = 0.0060$; $ksb2_{pp} = 0.12$; $ksb5_{p} = 2.0E-4$ $ksb5_{pp} = 0.0044$; $ksb5_{ppp} = 0.04$;
$ksbs4 = 5.0$ $ksbs = 50.0$; $ksbud = 0.2$; $ksc1_{p} = 0.0132$ $ksc1_{pp} = 0.132$;

$kscdh = 0.01$; $ksf6_{p} = 0.02$ $ksf6_{pp} = 0.2$; $ksf6_{ppp} = 0.0040$; $ksn2_{p} = 0.0$
$ksn2_{pp} = 0.5$; $ksn2_{ppp} = 0.05$; $ksnet = 0.084$ $ksnrm1 = 0.0$; $ksnrm1_{p} = 0.08$;
$ksori = 2.0$ $kpds_{ppp} = 0.055$; $kspds_{p} = 0.0$; $kspds_{pp} = 0.1$ $ksppx = 0.1$;
$kssa0 = 0.8$; $kssab2 = 0.5$ $kssaw5 = 6.0$; $ksspn = 0.1$; $ksswi_{p} = 0.0050$
$ksswi_{pp} = 0.08$; $kydj0 = 0.0$; $kydj1 = 1.0$ $lte1h = 1.0$; $lte1l = 0.1$;
$mad2h = 8.0$ $mad2l = 0.01$; $MAXMASS = 30.0$; $MBFnull = 1.0$ $mdt = 90.0$;
$MSN5 = 2.0$; $N = 5.0$ $nucleus = 0.2$; $PPase = 1.0$; $SBFnull = 1.0$
$Vpnmax = 3.0$;

Table 5. Modifications in parameter & initial conditions corresponding to mutants.

(Mutants exclusive to this model are emphasized in bold.)

Mutants	Parameters changed in model
Loss of function mutants G1, S	
*cln3*Δ	CLN3T=0
*bck2*Δ	BCK2T=0
whi5Δ	init WHI5=0
WHI5-12A	ef5p=0
swi4Δ	SBFnull=1; init SWI4=0
swi6Δ	SBFnull=1, MBFnull=1; init SWI6=0
SWI6-SA4	ef6p=ef6q=0
mbp1Δ	MBFnull=1; init MBP1=0
msn5Δ	MSN5=0
*cln2*Δ	ksn2'=0, ksn2"=0, ksn2'"=0; init CLN2=0
*clb5*Δ	ksb5'=ksb5"=ksb5'"=0; init CLB5=0
*CLB5-db*Δ	kdb5"=0
Cyclin Antagonists	
*sic1*Δ	ksc1'=ksc1"=0; init SIC1=SIC1P=C2=C2P=C5=C5P=0
*cdc6*Δ *(cdc6 2-49*Δ*)*	ksf6'=ksf6"=ksf6'"=0; init CDC61=CDC6P=F2=F2P=F5=F5P=0
*cki*Δ	ksc1'=ksc1"=0, ksf6'=ksf6"=ksf6'"=0; init SIC1=SIC1P=C2=C2P=C5=C5P=0, CDC61=CDC6P=F2=F2P=F5=F5P=0
*cdh1*Δ	kscdh=0, init CDH1T=CDH1=0
M-phase	
*swi5*Δ	ksswi'= ksswi"=0
*clb2*Δ	ksb2'=ksb2"=0
*CLB2-db*Δ	kdb2'"=0, kdb2"=0.075x (=7.5% activity left due to KEN box)
*CLB1 clb2*Δ	ksb2'=0.25*ksb2', ksb2"=0.25*ksb2" (changed to 25% from 33% WT)
*cdc20*Δ	ks20'=ks20"=0
cdc20-ts	ks20'=ks20"=0
apc-ts	ks20=ks20"=0, kscdh=0, init CDH1T=CDH1=0
APC-A	ka20"=0
*pds1*Δ	kspds'=kspds"=kspds'"=0; init PDS1=0, PE=0, ESP1=1
*PDS1-db*Δ	kdpds"=kdpds'"=0 (name change)
esp1-ts	kasesp=0.002x, kdiesp=0.002x (=1/500 X WT)
*ppx*Δ	ksppx=0; init PPX=0
tem1-ts	ka15"=0.002x (=ka15')
net1-ts	kasrent=0.025*kasrent, kasrentp=0.025*kasrentp (changed to 2.5% from 2% WT)
*cdc15*Δ	kpnet'"=0 (name change)
TAB6-1	2x net1-ts (compared to 10x net1-ts in Chen2004)
cdc14-ts	ks14=0; init CDC14=0
*mad2*Δ	mad2h=0.01; MAD2=0.01
*bub2*Δ	bub2h=bub2l=0, BUB2=0
Cells in nocodazole	ksspn=0
Over-expression (gain of function) mutants	
Cells in galactose	mdt=150 (Applicable for all *GAL* mutants below)
GAL-CLN3	CLN3T=20x
GAL-BCK2	BCK2T=5x
GAL-WHI5	init WHI5=10x
GAL-WHI5-12A	e5p=ef5p=0; init WHI5=10x

GAL-CLN2	ksn2'=0.3 (ksn2"=1 here, ksn2' changed from 0.12 in Chen2004)
GAL-CLB5	ksb5'=100x (instead of 15 fold from Chen2004)
GAL-SIC1	ksc1'=20x (=2*ksc1"; instead of 10 fold in Chen2004)
GAL-CDC6	ksf6'=5x (5 fold in Chen2004)
GAL-CLB2	ksb2'=60x (60 fold in Chen2004; 3x w.r.t ksb2")
GAL-CDC20	ks20'=12 (=20*ks20"; 2000fold otherwise)
GALL-CDC20	ks20'=4 (33% of GAL-CDC20)
GAL-ESP1	init ESP1=PE=20x (20 copies)
GAL-PDS1	kspds'=0.2 (0.1 in Chen2004)
GAL-PPX	ksppx=5x (5 fold)
GAL-CDC15	init CDC15=CDC15i=20x (20 copies)
GAL-NET1	ksnet=3x (3 fold)
GAL-CDC14	ks14=3x (3 fold)
GAL-TEM1	TEM1GDP=TEM1GTP=20x (20 copies)
CLN3-1	CLN3T=15*CLN3T
CDH1 constitutively active	kicdh"=0, kscdh=3x (3 fold as in Chen2004), MDT=150
*GAL-SIC-db*Δ	ksc1'=20x (same as GAL-SIC1), kd3c1=0
*GAL-CLB5-db*Δ	ksb5'=100x (same as GAL-CLB5), kdb5"=0
*GAL-PDS1-db*Δ	kspds'=0.2, kdpds"=kdpds'"=0 (name changed)
Multi-copy (mc) mutants	
mc BCK2	BCK2T=5x
mc CLN2	ksn2"=10x
mc CLB5	ksb5'=7x, ksb5"=7x (=7 copies compared to 2copies in Chen2004)
mc GAL-CLB2	ksb2'=400x (=6.66*GAL-CLB2, similar to Chen2004)
mc SIC1	ksc1'=5x, ksc1"=5x (=5 copies instead of 2copies in Chen2004)
mc CDC6	ksf6'=6x, ksf6"=6x, ksf6'"=6x (compared to 3x in Chen2004)
mc CDC20	ks20"=6 (ks20"=10*ks20")
mc CDC14	ks14=4x (instead of 2x in Chen2004)
mc TEM1	init TEM1GDP=TEM1GTP=20x (20 copies)
mc CDC15	init CDC15=CDC15i=20x (20 copies)

Simulations

We used JigCell (Vass et al, 2004) to build our model by defining reactions, algebraic rules, conservation relations, events at the end of the cell cycle, and multiple compartments. All reactions, equations and conservation relations were verified manually. PET was used to run all our simulations (using LSODAR) (Zwolak et al, 2005) for wild type as well as mutants by defining the specified conditions mentioned in Table 5. The software offers the option of running simulations for different conditions (termed 'simulation runs') and for several sets of rate constants (termed 'basal sets') simultaneously. XPPAUT (Ermentrout, 2002) (http://www.math.pitt.edu/~bard/xpp/xpp.html) was also used to check our simulations numerically (for wild type cells).

References

Alberghina L, Rossi RL, Querin L, Wanke V, Vanoni M (2004) A cell sizer network involving Cln3 and Far1 controls entrance into S phase in the mitotic cycle of budding yeast. *J Cell Biol* **167:** 433-443

Alberts B, Johnson A, Lewis J, Raff M, Roberts K, Walter P (2002) *Molecular Biology of the Cell*, 4th edn.: Garland Sciene.

Amon A, Irniger S, Nasmyth K (1994) Closing the cell cycle circle in yeast: G2 cyclin proteolysis initiated at mitosis persists until the activation of G1 cyclins in the next cycle. *Cell* **77:** 1037-1050

Amon A, Tyers M, Futcher B, Nasmyth K (1993) Mechanisms that help the yeast cell cycle clock tick: G2 cyclins transcriptionally activate G2 cyclins and repress G1 cyclins. *Cell* **74:** 993-1007

Archambault V, Li CX, Tackett AJ, Wasch R, Chait BT, Rout MP, Cross FR (2003) Genetic and biochemical evaluation of the importance of Cdc6 in regulating mitotic exit. *Mol Biol Cell* **14:** 4592-4604

Baetz K, Andrews B (1999) Regulation of cell cycle transcription factor Swi4 through auto-inhibition of DNA binding. *Molecular and Cellular Biology* **19:** 6729-6741

Bean JM, Siggia ED, Cross FR (2005) High Functional Overlap Between MluI Cell-Cycle Box Binding Factor and Swi4/6 Cell-Cycle Box Binding Factor in the G1/S Transcriptional Program in Saccharomyces cerevisiae. *Genetics* **171:** 49-61

Brown VD, Phillips RA, Gallie BL (1999) Cumulative effect of phosphorylation of pRB on regulation of E2F activity. *Molecular and Cellular Biology* **19:** 3246-3256

Calzada A, Sacristan M, Sanchez E, Bueno A (2001) Cdc6 cooperates with Sic1 and Hct1 to inactivate mitotic cyclin-dependent kinases. *Nature* **412:** 355-358

Chang F, Herskowitz I (1990) Identification of a gene necessary for cell cycle arrest by a negative growth factor of yeast: FAR1 is an inhibitor of a G1 cyclin, CLN2. *Cell* **63:** 999-1011

Charvin G, Oikonomou C, Siggia ED, Cross FR (2010) Origin of irreversibility of cell cycle start in budding yeast. *PLoS Biol* **8:** e1000284

Chen KC, Calzone L, Csikasz-Nagy A, Cross FR, Novak B, Tyson JJ (2004) Integrative analysis of cell cycle control in budding yeast. *Mol Biol Cell* **15:** 3841-3862

Chen KC, Csikasz-Nagy A, Gyorffy B, Val J, Novak B, Tyson JJ (2000) Kinetic analysis of a molecular model of the budding yeast cell cycle. *Mol Biol Cell* **11:** 369-391

Conlon I, Raff M (2003) Differences in the way a mammalian cell and yeast cells coordinate cell growth and cell-cycle progression. *Journal of Biology* **2:** 7

Costanzo M, Nishikawa JL, Tang X, Millman JS, Schub O, Breitkreuz K, Dewar D, Rupes I, Andrews B, Tyers M (2004) CDK Activity Antagonizes Whi5, an Inhibitor of G1/S Transcription in Yeast. *Cell* **117:** 899-913

Cross F (1990) Cell cycle arrest caused by CLN gene deficiency in Saccharomyces cerevisiae resembles START-I arrest and is independent of the mating-pheromone signalling pathway. *Mol Cell Biol* **10:** 6482-6490

Cross FR (2003) Two redundant oscillatory mechanisms in the yeast cell cycle. *Dev Cell* **4:** 741-752

Cross FR, Archambault V, Miller M, Klovstad M (2002) Testing a mathematical model of the yeast cell cycle. *Mol Biol Cell* **13:** 52-70

Cross FR, Tinkelenberg AH (1991) A potential positive feedback loop controlling CLN1 and CLN2 gene expression at the start of the yeast cell cycle. *Cell* **65:** 875-883

Cross MEMaFR (2001) Mechanisms Controlling Subcellular Localization of the G1 Cyclins Cln2p and Cln3p in Budding Yeast. *Mol Cell Biol* **21:** 6291-6311

de Bruin RA, Kalashnikova TI, Aslanian A, Wohlschlegel J, Chahwan C, Yates JR, 3rd, Russell P, Wittenberg C (2008) DNA replication checkpoint promotes G1-S transcription by inactivating the MBF repressor Nrm1. *Proceedings of the National Academy of Sciences of the United States of America* **105:** 11230-11235

de Bruin RAM, Kalashnikova TI, Chahwan C, McDonald WH, Wohlschlegel J, Yates Iii J, Russell P, Wittenberg C (2006) Constraining G1-Specific Transcription to Late G1 Phase: The MBF-Associated Corepressor Nrm1 Acts via Negative Feedback. *Molecular Cell* **23:** 483-496

de Bruin RAM, McDonald WH, Kalashnikova TI, Yates J, Wittenberg C (2004) Cln3 Activates G1-Specific Transcription via Phosphorylation of the SBF Bound Repressor Whi5. *Cell* **117:** 887-898

Di Como CJ, Chang H, Arndt KT (1995) Activation of CLN1 and CLN2 G1 cyclin gene expression by BCK2. *Mol Cell Biol* **15:** 1835-1846

Di Talia S, Skotheim JM, Bean JM, Siggia ED, Cross FR (2007) The effects of molecular noise and size control on variability in the budding yeast cell cycle. *Nature* **448:** 947-951

Dirick L, Bohm T, Nasmyth K (1995) Roles and regulation of Cln-Cdc28 kinases at the start of the cell cycle of Saccharomyces cerevisiae. *The EMBO Journal* **14:** 4803-4813

Dirick L, Nasmyth K (1991) Positive feedback in the activation of G1 cyclins in yeast. *Nature* **351:** 754-757

Epstein CB, Cross FR (1994) Genes that can bypass the CLN requirement for Saccharomyces cerevisiae cell cycle START. *Molecular and Cellular Biology* **14:** 2041-2047

Ermentrout B (2002) *Simulating, analyzing, and animating dynamical systems: a guide to XPPAUT for researchers and students*, Vol. 14: Society for Industrial Mathematics.

Fantes PA (1977) Control of Cell Size and Cycle time in Schizosaccharomyces Pombe. *J Cell Sci* **24:** 51-67

Ferrezuelo F, Aldea M, Futcher B (2009) Bck2 is a phase-independent activator of cell cycle-regulated genes in yeast. *Cell Cycle* **8:** 239-252

Gari E, Volpe T, Wang H, Gallego C, Futcher B, Aldea M (2001) Whi3 binds the mRNA of the G1 cyclin CLN3 to modulate cell fate in budding yeast. *Genes Dev* **15:** 2803-2808

Geymonat M, Spanos A, Wells GP, Smerdon SJ, Sedgwick SG (2004) Clb6/Cdc28 and Cdc14 regulate phosphorylation status and cellular localization of Swi6. *Molecular and Cellular Biology* **24:** 2277-2285

Ghaemmaghami S, Huh WK, Bower K, Howson RW, Belle A, Dephoure N, O'Shea EK, Weissman JS (2003) Global analysis of protein expression in yeast. *Nature* **425:** 737-741

Giaever G, Chu AM, Ni L, Connelly C, Riles L, Veronneau S, Dow S, Lucau-Danila A, Anderson K, Andre B, Arkin AP, Astromoff A, El-Bakkoury M, Bangham R, Benito R, Brachat S, Campanaro S, Curtiss M, Davis K, Deutschbauer A et al (2002) Functional profiling of the Saccharomyces cerevisiae genome. *Nature* **418:** 387-391

Goldbeter A, Koshland DE, Jr. (1981) An amplified sensitivity arising from covalent modification in biological systems. *Proceedings of the National Academy of Sciences of the United States of America* **78:** 6840-6844

Hall DD, Markwardt DD, Parviz F, Heideman W (1998) Regulation of the Cln3-Cdc28 kinase by cAMP in Saccharomyces cerevisiae. *The EMBO Journal* **17:** 4370-4378

Hartwell LH (1974) Saccharomyces cerevisiae cell cycle. *Bacteriol Rev* **38:** 164-198

Hartwell LH, Culotti J, Reid B (1970) Genetic Control of the Cell-Division Cycle in Yeast, I. Detection of Mutants. *Proceedings of the National Academy of Sciences of the United States of America* **66:** 352-359

Irniger S, Nasmyth K (1997) The anaphase-promoting complex is required in G1 arrested yeast cells to inhibit B-type cyclin accumulation and to prevent uncontrolled entry into S-phase. *Journal of cell science* **110 (Pt 13):** 1523-1531

Jacobson MD, Gray S, Yuste-Rojas M, Cross FR (2000) Testing cyclin specificity in the exit from mitosis. *Molecular and Cellular Biology* **20:** 4483-4493

Jagadish MN, Carter BLA (1977) Genetic control of cell division in yeast cultured at different growth rates. *Nature* **269:** 145-147

Jaquenoud M, van Drogen F, Peter M (2002) Cell cycle-dependent nuclear export of Cdh1p may contribute to the inactivation of APC/C(Cdh1). *The EMBO Journal* **21:** 6515-6526

Johnston GC (1977) Cell size and budding during starvation of the yeast Saccharomyces cerevisiae. *Journal of Bacteriology* **132:** 738-739

Johnston GC, Ehrhardt CW, Lorincz A, Carter BL (1979) Regulation of cell size in the yeast Saccharomyces cerevisiae. *J Bacteriol* **137:** 1-5

Jorgensen P, Edgington NP, Schneider BL, Rupes I, Tyers M, Futcher B (2007) The size of the nucleus increases as yeast cells grow. *Mol Biol Cell* **18:** 3523-3532

Jorgensen P, Nishikawa JL, Breitkreutz B-J, Tyers M (2002) Systematic Identification of Pathways That Couple Cell Growth and Division in Yeast. *Science* **297:** 395-400

Jorgensen P, Tyers M (2004) How Cells Coordinate Growth and Division. *Current Biology* **14:** R1014-R1027

Koch C, Moll T, Neuberg M, Ahorn H, Nasmyth K (1993) A role for the transcription factors Mbp1 and Swi4 in progression from G1 to S phase. *Science* **261:** 1551-1557

Lodish H, Berk A, Zipursky L, Matsudaira P, Baltimore D, Darnell J (2000) *Molecular Cell Biology*, 4th edition edn.: New York: W. H. Freeman.

Lord PG, Wheals AE (1980) Asymmetrical division of Saccharomyces cerevisiae. *Journal of Bacteriology* **142:** 808-818

Mendenhall MD (1993) An inhibitor of p34CDC28 protein kinase activity from Saccharomyces cerevisiae. *Science* **259:** 216-219

Moll T, Schwob E, Koch C, Moore A, Auer H, Nasmyth K (1993) Transcription factors important for starting the cell cycle in yeast. *Philos Trans R Soc Lond B Biol Sci* **340:** 351-360

Nasmyth K, Dirick L (1991) The role of SWI4 and SWI6 in the activity of G1 cyclins in yeast. *Cell* **66:** 995-1013

Newcomb LL, Hall DD, Heideman W (2002) AZF1 Is a Glucose-Dependent Positive Regulator of CLN3 Transcription in Saccharomyces cerevisiae. *Mol Cell Biol* **22:** 1607-1614

Nguyen VQ, Co C, Li JJ (2001) Cyclin-dependent kinases prevent DNA re-replication through multiple mechanisms. *Nature* **411:** 1068-1073

Novak B, Tyson JJ (1993) Numerical analysis of a comprehensive model of M-phase control in Xenopus oocyte extracts and intact embryos. *Journal of cell science* **106 (Pt 4):** 1153-1168

Nugroho TT, Mendenhall MD (1994) An inhibitor of yeast cyclin-dependent protein kinase plays an important role in ensuring the genomic integrity of daughter cells. *Molecular and Cellular Biology* **14:** 3320-3328

Pardee AB (1974) A restriction point for control of normal animal cell proliferation. *Proceedings of the National Academy of Sciences of the United States of America* **71:** 1286-1290

Peter M, Herskowitz I (1994) Direct inhibition of the yeast cyclin-dependent kinase Cdc28-Cln by Far1. *Science* **265:** 1228-1231

Pramila T, Wu W, Miles S, Noble WS, Breeden LL (2006) The Forkhead transcription factor Hcm1 regulates chromosome segregation genes and fills the S-phase gap in the transcriptional circuitry of the cell cycle. *Genes Dev* **20:** 2266-2278

Queralt E, Igual JC (2003) Cell cycle activation of the Swi6p transcription factor is linked to nucleocytoplasmic shuttling. *Molecular and Cellular Biology* **23:** 3126-3140

Schneider BL, Yang QH, Futcher AB (1996) Linkage of replication to start by the Cdk inhibitor Sic1. *Science* **272:** 560-562

Schwab M, Lutum AS, Seufert W (1997) Yeast Hct1 is a regulator of Clb2 cyclin proteolysis. *Cell* **90:** 683-693

Schwob E, Bohm T, Mendenhall MD, Nasmyth K (1994) The B-type cyclin kinase inhibitor p40SIC1 controls the G1 to S transition in S. cerevisiae. *Cell* **79:** 233-244

Schwob E, Nasmyth K (1993) CLB5 and CLB6, a new pair of B cyclins involved in DNA replication in Saccharomyces cerevisiae. *Genes Dev* **7:** 1160-1175

Sidorova JM, Mikesell GE, Breeden LL (1995) Cell cycle-regulated phosphorylation of Swi6 controls its nuclear localization. *Mol Biol Cell* **6:** 1641-1658

Siegmund RF, Nasmyth KA (1996) The Saccharomyces cerevisiae Start-specific transcription factor Swi4 interacts through the ankyrin repeats with the mitotic Clb2/Cdc28 kinase and through its conserved carboxy terminus with Swi6. *Molecular and Cellular Biology* **16:** 2647-2655

Skotheim JM, Di Talia S, Siggia ED, Cross FR (2008) Positive feedback of G1 cyclins ensures coherent cell cycle entry. *Nature* **454:** 291-296

Sveiczer A, Novak B, Mitchison JM (2004) Size control in growing yeast and mammalian cells. *Theor Biol Med Model* **1:** 12

Taberner FJ, Quilis I, Igual JC (2009) Spatial regulation of the start repressor Whi5. *Cell Cycle* **8:** 3010-3018

Tokiwa G, Tyers M, Volpe T, Futcher B (1994) Inhibition of Gl cyclin activity by the Ras/cAMP pathway in yeast. *Nature* **371:** 342-345

Toyn JH, Johnson AL, Donovan JD, Toone WM, Johnston LH (1997) The Swi5 transcription factor of Saccharomyces cerevisiae has a role in exit from mitosis through induction of the cdk-inhibitor Sic1 in telophase. *Genetics* **145:** 85-96

Tyers M (2004) Cell cycle goes global. *Current Opinion in Cell Biology* **16:** 602-613

Tyers M, Tokiwa G, Nash R, Futcher B (1992) The Cln3-Cdc28 kinase complex of S. cerevisiae is regulated by proteolysis and phosphorylation. *The EMBO Journal* **11:** 1773-1784

Tyson J, Sachsenmaier W (1978) Is nuclear division in Physarum controlled by a continuous limit cycle oscillator? *Journal of Theoretical Biology* **73:** 723-738

Vass M, Allen N, Shaffer CA, Ramakrishnan N, Watson LT, Tyson JJ. (2004) The JigCell Model Builder and Run Manager. Oxford Univ Press, Vol. 20, pp. 3680-3681.

Verges E, Colomina N, Gari E, Gallego C, Aldea M (2007) Cyclin Cln3 is retained at the ER and released by the J chaperone Ydj1 in late G1 to trigger cell cycle entry. *Molecular Cell* **26:** 649-662

Verma R, Feldman RM, Deshaies RJ (1997) SIC1 is ubiquitinated in vitro by a pathway that requires CDC4, CDC34, and cyclin/CDK activities. *Mol Biol Cell* **8:** 1427-1437

Visintin R, Prinz S, Amon A (1997) CDC20 and CDH1: a family of substrate-specific activators of APC-dependent proteolysis. *Science* **278:** 460-463

Wagner MV, Smolka MB, de Bruin RAM, Zhou H, Wittenberg C, Dowdy SF (2009) Whi5 Regulation by Site Specific CDK-Phosphorylation in <italic>Saccharomyces cerevisiae</italic>. *PLoS ONE* **4:** e4300

Wang Y, Pierce M, Schneper L, Guldal CG, Zhang X, Tavazoie S, Broach JR (2004) Ras and Gpa2 mediate one branch of a redundant glucose signaling pathway in yeast. *PLoS Biol* **2:** E128

Wasch R, Cross FR (2002) APC-dependent proteolysis of the mitotic cyclin Clb2 is essential for mitotic exit. *Nature* **418:** 556-562

Wijnen H, Futcher B (1999) Genetic Analysis of the Shared Role of CLN3 and BCK2 at the G1-S Transition in Saccharomyces cerevisiae. *Genetics* **153:** 1131-1143

Wijnen H, Landman A, Futcher B (2002) The G(1) cyclin Cln3 promotes cell cycle entry via the transcription factor Swi6. *Molecular and Cellular Biology* **22:** 4402-4418

Wittenberg C, Reed SI (1996) Plugging it in: signaling circuits and the yeast cell cycle. *Current Opinion in Cell Biology* **8:** 223-230

Yao G, Lee TJ, Mori S, Nevins JR, You L (2008) A bistable Rb-E2F switch underlies the restriction point. *Nat Cell Biol* **10:** 476-482

Zachariae W, Schwab M, Nasmyth K, Seufert W (1998) Control of cyclin ubiquitination by CDK-regulated binding of Hct1 to the anaphase promoting complex. *Science* **282:** 1721-1724

Zwolak JW, Tyson JJ, Watson LT (2005) Parameter Estimation for a Mathematical Model of the Cell Cycle in Frog Eggs. *Journal of Computational Biology* **12:** 48-63

Modeling Bistability in the Canonical Wnt Signaling Pathway

Abstract

Control of stem cell self-renewal and differentiation are paramount to the development of multicellular organisms. The Wnt signaling system is a key regulator of these processes, playing a role in development in embryos and regeneration in adults. Naturally, deregulation in this pathway is linked to several diseases including osteoarthritis, polycystic kidney disease, cardiac hypertrophy, neurodegenerative disease, and colon cancer. Secreted by cells into their tissue microenvironment, Wnt functions as a morphogen to activate surface receptors (Frizzled), signal transduction components (Axin/GSK3β/APC destruction core) and transcription factors (β-catenin/TCF) in neighboring cells. The Wnt pathway exists in two states, OFF and ON (in the absence and presence of Wnt). Recent experimental evidence suggests the existence of 'bistability' in this pathway that ensures robust switching between the two states. Here, we propose the existence of a molecular positive feedback loop that underlies this bistability. We develop a mathematical model to explain this behavior in the pathway. Our model recapitulates experimental observations of bimodality (bistability) and hysteresis under the effects of the physiological signal (Wnt), a Wnt-mimic (LiCl), and a stabilizer of one of the key members of destruction core complex (IWR-1, which stabilizes Axin). Furthermore, we have made novel predictions about the dynamics of this pathway that are currently being verified experimentally.

Abbreviations used in this chapter:

Fz: Frizzled

Dsh: Dishevelled

APC: Adenomatous Polyposis Coli

LRP5: Low density lipoprotein receptor-related protein 5

TCF: T-Cell Factor

LEF: Lymphoid Enhancer Factor

CK1α: Casein Kinase 1α

GSK3β: Glycogen Synthase Kinase 3β

Introduction

Cellular control systems tightly regulate pivotal processes like cell growth, division, physiological function and death. Complex diseases like cancer are characterized by deregulation of one or more of these control systems. Hence, a systems-level understanding of such control systems considering their molecular circuitry and dynamics is key in exploring potential avenues for prevention and cure.

Wnt signaling is a central control system involved in the patterning of organs and organisms through regulation of cell proliferation and determination of stem cell fate [Liu et al, 1999], cell polarity, migration, and adhesion [Croce and McClay, 2008]. Wnt is a ligand that binds to the Frizzled (Fz)/LRP receptor and activates one of three pathways (Figure 1): (1) cell proliferation/ differentiation (also known as the canonical Wnt pathway) [Gordon and Nusse 2006; Papkoff et al, 1996], (2) cytoskeletal polarity [Strutt, 2003], and (3) cell adhesion [Veeman et al, 2003]. As evidence to this central role, several components in the canonical Wnt signaling pathway have been observed to be mutated and uncontrollably activated in cancer [Polakis, 2007]. Our primary focus is on the canonical Wnt signaling pathway.

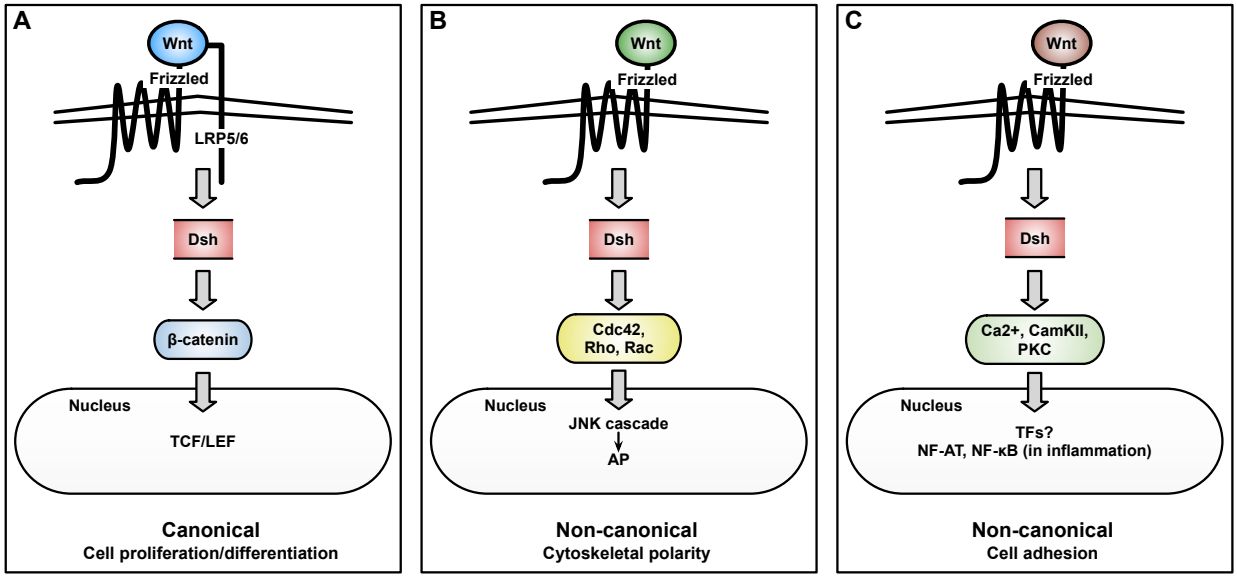

Figure 1. Pathways triggered by Wnt.

A. Canonical Wnt pathway. Wnt ligands bind to Frizzled and LRP5/6 receptors and activate β-catenin through Dsh. In complex with the TCF/LEF transcription factor, β-catenin subsequently activates several genes involved in cell proliferation and/or differentiation. **B**. Planar cell polarity pathway. Ligand Wnt (e.g. Wnt11) binds to Frizzled receptor and activates Cdc42 and G-proteins like Rac and Rho kinases, resulting in activation of the JNK cascade and AP transcription factor responsible for cytoskeletal polarity and convergent extension (Strutt, 2003; Habas et al, 2003; Schlessinger et al, 2007; Choi and Han, 2002). **C**. Wnt/Ca^{2+} pathway. Ligand Wnt (e.g. Wnt5a), with the help of G-proteins, promotes the release of Ca^{2+} and activation of CamKII and PKC (Kuhl et al, 2000). The final nuclear targets are transcription factors that are involved in either cell adhesion or NF-AT, NF-κB in the case of inflammatory responses (Sen and Ghosh, 2006).

Canonical Wnt pathway

Through the canonical pathway (Figure 2), Wnt regulate genes involved in cell proliferation and differentiation. The pathway can exist in two states, ON (Fig. 2A) or OFF (Fig. 2B) (reflected by the activity of β-catenin) depending on the presence or absence of external

Wnt.

Figure 2A illustrates the default OFF state of the cell in the absence of Wnt signal. In this scenario, the destruction core complex comprising of scaffold proteins Axin and Adenomatous Polyposis Coli (APC), kinases Glycogen Synthase Kinase-3β (GSK3β), Casein Kinase-1α (CK1α), and other proteins including phosphatase PP2A (not shown in figure), sequesters β-catenin [Behrens et al, 1998; Itoh et al, 1998, Hamada et al, 1999]. Bound β-catenin is then phosphorylated by GSK3β and CK1 [Yanagawa et al, 2002; Liu et al, 2002; Amit et al, 2002] and targeted for ubiquitination and hence degradation. This keeps the level of free β-catenin low. In the absence of β-catenin, Groucho and other repressor proteins keep the downstream T cell-specific transcription factor (TCF) inactive in the nucleus.

Figure 2B depicts the course of events in the presence of Wnt signal. Wnt binds to the receptors Frizzled (Fz) and low-density lipoprotein receptor-related protein (LRP5/6). This ligand-receptor complex recruits Dsh and the components of the destruction core complex, Axin, GSK3β and CK1α to the receptor. Kinases, CK1 and GSK3β, phosphorylate the LRP receptor and keeps the core destruction box membrane bound allowing β-catenin to accumulate in the cytoplasm. β-catenin translocates to the nucleus and binds to TCF thereby activating it [Nusse 1999]. Several target genes of the canonical Wnt pathway are then transcribed, including cell cycle, development and differentiation related genes cMyc [He 1998], CyclinD1 [Tetsu et al, 1999; Shtutman et al, 1999], Wnt3a [Zhang 2009], Axin2 [Yan, 2001; Lustig, 2002; Jho, 2002], LGR5 [Barker, 2007], TCF1 [Roose 1999], BMP4 [Kim 2002; Baker 1999] and many others.

At the core of the signaling events in the presence of Wnt, the phosphorylation states of the scaffold protein Axin and kinase GSK3β play an important role in the net activity of the

destruction core complex and its binding to β-catenin. The details of these phosphorylation events are described in sections below and are central to our model of this pathway.

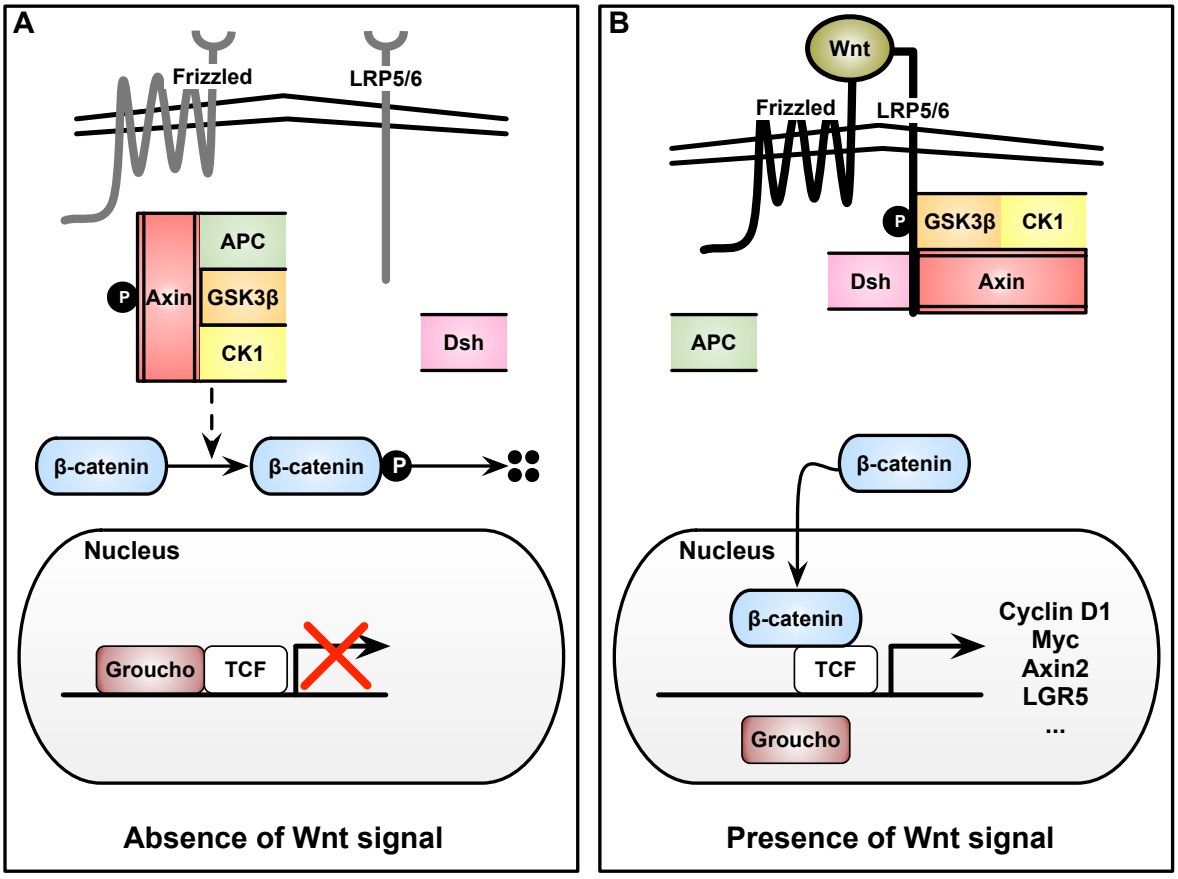

Figure 2. Canonical Wnt pathway.

A. In the absence of Wnt ligand, the destruction core complex comprising Axin, APC, GSK3β and CK1 is intact and causes ubiquitination and degradation of transcription factor activator, β-catenin. Groucho-bound TCF transcription factor is inactive in the nucleus resulting in lack of transcription. **B**. In the presence of Wnt, the Frizzled and LRP5/6 receptors cluster and get activated. Dsh recruits the destruction core complex including Axin, GSK3β and CK1 to the LRP5/6 receptor tail leading to phosphorylation of specific serine residues on the tail. β-catenin is now free to accumulate due to absence of ubiquitination. Accumulated β-catenin moves to the nucleus, relieves inhibition from the TCF complex and allows active transcription of target genes including CyclinD1, Myc, Axin2 and several

others.

Deregulation of the canonical pathway, a common molecular signature of colon cancer, occurs due to mutations and inactivation of APC. This results in accumulation of β-catenin and hence inappropriate activation of cell cycle and growth genes like cMyc and CyclinD1.

Modeling of the Wnt signaling pathway

The Wnt pathway has been extensively studied using molecular genetics and biology to elucidate the key players and the mechanism of their interactions. A better understanding of such pathways can be gained by studying the dynamics of their interactions using mathematical modeling. This approach has been successfully applied for several control systems including cell cycle [Tyson et al, 2003], apoptosis [Spencer and Sorger, 2011], segment polarity [Chaves and Albert, 2008], and circadian rhythm [Hogenesch and Ueda, 2011]. In recent years, several groups have performed quantitative studies and modeling of the Wnt signaling pathway [summarized in Kofahl and Wolf, 2010] focusing on the dynamics of the destruction core complex [Lee et al, 2003], robustness in the Wnt pathway [Kruger and Heinrich, 2004], fold-change response to levels of β-catenin [Goentoro and Kirschner, 2009], oscillations in β-catenin concentrations depending on Axin concentrations [Wawra et al, 2007], and multi-scale models of colorectal cancer involving some details of the Wnt pathway [reviewed in Van Leeuwen et al, 2007]. In the mathematical model built by Lee et al. (referred to as Lee2003 subsequently) the destruction core cycle (involving Axin, APC, GSK3β and Dsh) is the central and most important module of the network. They showed, in combination with fine experimental measurements and validation, that

the dynamics of the Wnt pathway and accumulation of β-catenin could be captured by considering the reactions of the core complex [Lee et al, 2003].

An earlier model of the Wnt signaling pathway: Lee2003 model

Lee *et al* (2003) have built a detailed mathematical model of the destruction core pathway of the canonical Wnt signaling pathway, deriving evidence and rate constants from experiments. The core of the destruction complex consists of APC, Axin, GSK3β and β-catenin. We highlight several aspects about the working of the Wnt pathway based on their detailed analysis.

- The two scaffold proteins of the destruction complex, **APC** and **Axin**, largely differ in their abundances. While APC is always present at a high level, Axin is present in limiting concentration. Therefore, *the functioning of the Wnt signaling system (reflected in the half-life of β-catenin) may actually depend on the low Axin concentration.*
- The kinase **GSK3β** phosphorylates and activates APC and Axin in the destruction core complex, which are required for β-catenin ubiquitination and degradation. The signal (Wnt) causes Dsh activation, leading to the dissociation of GSK3β from the core complex that degrades β-catenin. This finally results in dissociation of APC from the core complex and degradation of Axin. Therefore, the presence of Wnt signal prevents β-catenin degradation, and β-catenin levels become high.

Due to these observations, we propose that tracking *GSK3β and Axin* might be sufficient to capture the dynamics of the canonical pathway.

In the present work, we build on the core module used in the Lee2003 paper, first by simplifying it and then by incorporating additional key regulatory interactions. We show that the

Wnt signaling pathway represented by our model displays bistability, in agreement with preliminary experimental results [Thorne and Lee, unpublished results to be described in detail in the next section], and that the dynamics predicted by our model captures the essence of the whole pathway.

Initial experiments suggesting bistability

The phosphorylation and stabilization of Axin by GSK3β, and activation of GSK3β by dephosphorylation by Axin comprises a positive feedback in the destruction core complex in the Wnt signaling pathway [Yamamoto et al, 1999; Kimelman and Xu 2006; MacDonald et al, 2009; Thorne and Lee, unpublished results]. Lee and Tyson identified this motif and proposed that this core module of the Wnt signaling pathway would exhibit bistability (personal communication). The details of the experimental evidence for the positive feedback and the mathematical model are described under Results and Discussion.

This hypothesis for bistability in the Wnt/β-catenin network has been tested and validated by a battery of experiments by Thorne and Lee (unpublished results). They have demonstrated experimentally that cells display all-or-none behavior in response to signal, Wnt3a (one of the known ligands of the canonical Wnt pathway; Figure 3). These experiments were performed in RKO cells, which are human intestinal cancer cells that contain no mutations in Wnt pathway components and have low membrane bound β-catenin, allowing easy quantification of the dynamic cytoplasmic pool of β-catenin. It can be seen clearly that for low signals, there are either no or very few cells that express β-catenin, whereas for higher signals, almost all cells show high levels of β-catenin. For intermediate concentrations, some cells have low levels of β-

catenin whereas others have high levels. However, for a given cell, there appears to be an all-or-none accumulation in β-catenin.

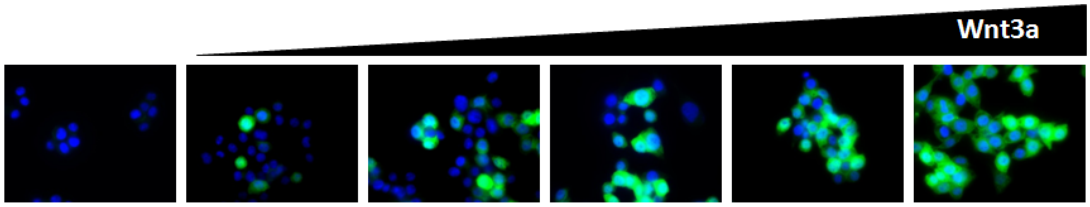

Figure 3. β-catenin accumulation appears all-or-none in RKO cells.

(Thorne and Lee, unpublished.) Immunofluorescent images of β-catenin levels in each RKO cell in response to increasing Wnt3a concentrations shows an all-or-none response. DNA are stained blue by DAPI and β-catenin is tagged with green fluorescent protein.

Thorne and Lee also show that in a population of RKO cells, when single cells are analyzed, β-catenin displays a bimodal distribution for intermediate Wnt3a signal (Figure 4A; personal communication). In this experiment, the β-catenin levels for each of the 20,000 cells in a population have been determined using flow cytometry and plotted for increasing concentrations of Wnt signal. Although the whole population of RKO cells shows a graded response of β-catenin accumulation to signal, Wnt (Thorne and Lee, personal communication), single-cell flow cytometry experiments show bimodality. This can be observed in Figure 4A, as the signal strength is increased, the size of the population with low β-catenin decreases, and the size of the population with high β-catenin increases. At intermediate values of the signal, there are two discrete population of cells, one with low β-catenin and one with high β-catenin levels. Such bimodal behavior is also observed for intermediate concentrations in a gradient treatment

with LiCl (Figure 4B), a molecule that mimics Wnt signaling by inhibiting GSK3β [Klein and Melton, 1996; Lee et al, 2003]. In fact the two β-catenin peaks are more clearly visible upon LiCl treatment than Wnt3a treatment.

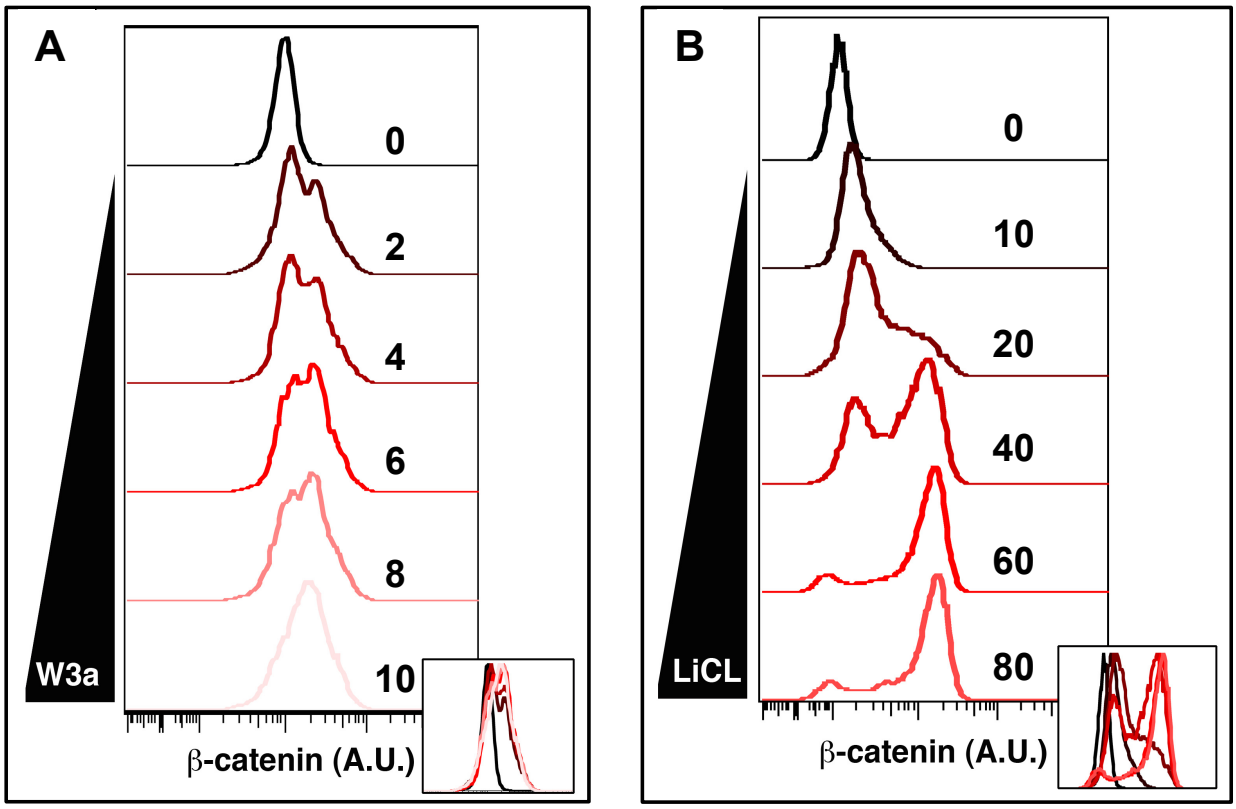

Figure 4. β-catenin shows bimodal response to increasing Wnt3a and LiCl.

(Thorne and Lee, unpublished.) A. Flow cytometry graphs of β-catenin levels in response to increasing Wnt3a concentrations (0-10 in relative units). **B**. Flow cytometry graphs of β-catenin levels in response to increasing LiCl concentrations (10-80 mM). Histograms represent β-catenin levels in a population of 20,000 counted cells. Inset in A, B correspond to overlay of histograms for different values of Wnt3a and LiCl, respectively.

RKO cells also exhibit a toggle-like switching behavior – hysteresis – in response to increasing and decreasing signal strengths of Wnt3a, resulting in different thresholds for the activation (accumulation) and inactivation (degradation) of β-catenin (Figure 5). The experiment shows that the threshold level of Wnt3a to stimulate β-catenin accumulation (level=4, top panel in Figure 5) is higher than the threshold level of Wnt3a needed to maintain β-catenin (level=1 in bottom panel in Figure 5).

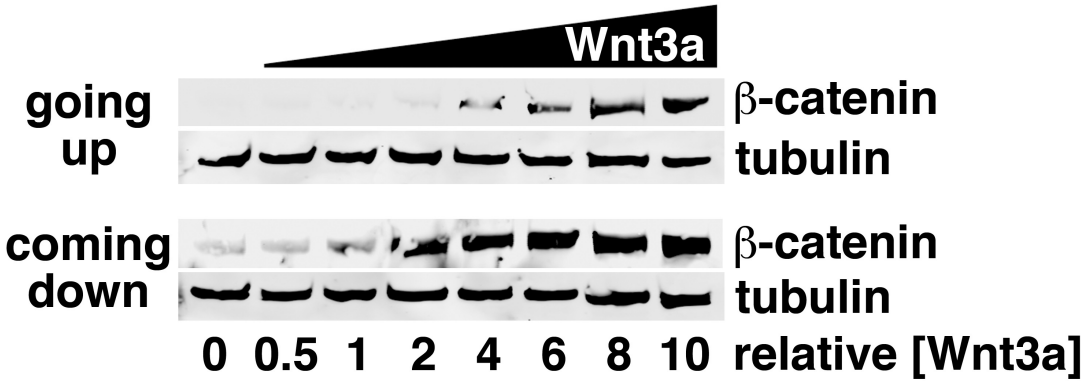

Figure 5. β-catenin response to stimulus exhibits hysteresis.

(Thorne and Lee, unpublished.) Western blot for β-catenin is shown for varying signal strengths. In the top 'going up' panel, increasing level of Wnt3a signal is applied to unstimulated cells, and in the bottom 'coming down' panel, stimulus is washed away and various doses of Wnt3a are applied to the prestimulated cells.

These properties of bimodality (Figure 4) and hysteresis (Figure 5) along with previously observed all-or-none behavior (Figure 3) are highly suggestive of a bistable system of β-catenin response to Wnt signal. To test if stabilizing Axin would disrupt the positive feedback and hence bistability, Thorne and Lee treated the RKO cells with the small molecule IWR-1 that stabilizes

Axin by blocking its ubiquitination and degradation [Chen et al, 2009]. They observed that addition of IWR-1 results in seemingly a loss of bistability leading to a graded response in β-catenin accumulation (Figure 6; Thorne and Lee, personal communication).

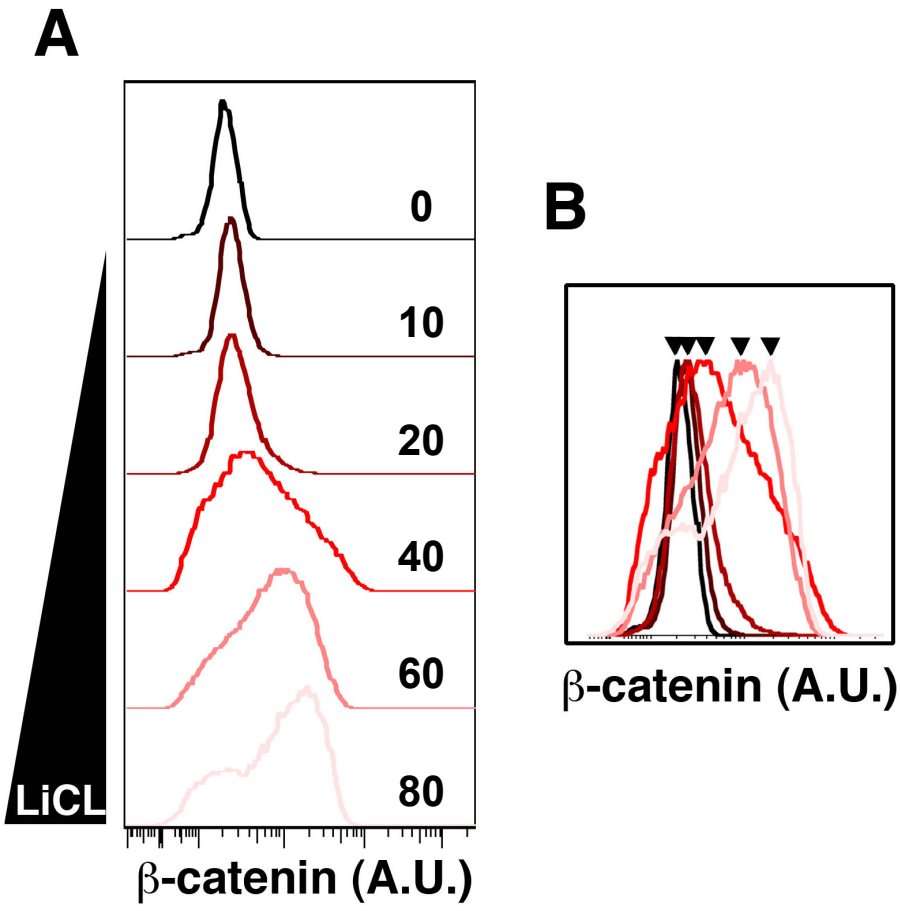

Figure 6. Effect of Axin stabilizer, IWR-1, on β-catenin accumulation.

(Thorne and Lee, unpublished.) **A**. RKO cells were treated with IWR-1 (5 uM) 1 hour before LiCl stimulation. Flow cytometry graphs of β-catenin levels in response to increasing LiCl concentrations (10-80 mM) are plotted. Histograms represent β-catenin levels in a population of 20,000 counted cells. **B**. Overlay of histograms from (A).

We have incorporated the initial evidence for the positive feedback motif and the effect of LiCl and IWR-1 in our model in order to emulate these experimental results as well as make predictions that would validate the initial hypothesis of bistability in the Wnt signaling pathway.

Results and Discussion

Model of the destruction core cycle in the Wnt signaling pathway

As explained in the previous section, for the purpose of the model, we only take into account the interactions involving Axin and GSK3β (modifying Lee2003) and consider additional interactions between these molecules as suggested by recent experimental evidences (Figures 3-6; Thorne and Lee, unpublished results). To summarize, the regulation of the pathway occurs at the core destruction complex composed of APC, Axin and GSK3β in response to external Wnt concentrations. When Wnt is absent, scaffold proteins APC and Axin activate the kinase GSK3β, which together can bind and phosphorylate free β-catenin in the cytosol, signaling it for destruction by the proteasome. When enough Wnt is produced in the extracellular matrix (by other cells), it binds to receptors Fz and LRP5/6, which in turn modify Dsh in the cytosol. Dsh binds to and destabilizes the destruction complex disabling it from binding to β-catenin. As free β-catenin concentration builds up, it translocates to the nucleus, binds to its transcription factor partner, TCF, and activates gene expression.

We build our model on the basis of the following interactions that have experimental validation:

1. Unphosphorylated Axin is rapidly degraded [Yamamoto et al, 1999; Thorne and Lee, unpublished results].
2. GSK3β phosphorylates and stabilizes Axin by preventing its degradation [Yamamoto et al, 1999; Kimelman and Xu 2006; MacDonald et al, 2009].

3. High Axin concentration stimulates the dephosphorylation of serine (at amino acid residue #9) in GSK3β. Phosphorylation at Ser9 residue has an inhibitory effect on the kinase activity of GSK3β; thus Axin activates GSK3β [Thorne and Lee, unpublished results].
4. PP2A likely plays a prominent role in removing phosphates on GSK3β or Axin depending on the activity of the pathway [Thorne and Lee, unpublished results].
    a. Low or no Wnt signal: PP2A targets GSK3β to keep it active.
    b. High signal: PP2A targets Axin, thereby destabilizing it, in turn, keeping GSK3β in its phosphorylated and inhibited form.
5. In vitro data shows that the phosphatase and kinase acting on GSK3β are PP2A and Casein kinase 1 alpha (CK1α), respectively [Thorne and Lee, unpublished results].

We capture these experimental findings in the form of a molecular wiring diagram shown in Figure 7. To highlight the role of individual proteins, we designate Axin and GSK3β as independent components in the network although Axin and GSK3β are part of the same complex and are mutual modifiers of each other.

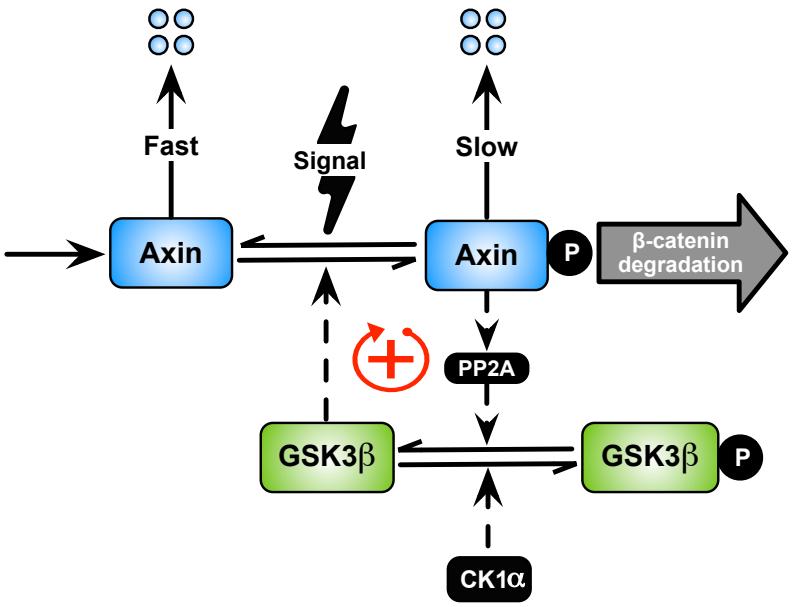

Figure 7: Mathematical model for the β-catenin accumulation in response to Wnt signal through the canonical pathway.

In our model, the primary species are Axin and GSK3β. Icons with 'P' in a black circle represent the phosphorylated forms of the molecules. Although not shown, Axin and GSK3β are part of the same complex that also includes APC (a scaffold protein), PP2A (a phosphatase), and CK1α (a kinase). GSK3β phosphorylates Axin. CK1α and PP2A (activated by Axin) are the kinase and phosphatase for GSK3β, respectively. Phosphorylated Axin (Axin-P, bound to other core complex members) is assumed to be the active complex that causes ubiquitination and degradation of β-catenin. Wnt/Signal acts on the active complex, Axin-P, modifying it to a form that can no longer acts on β-catenin. Equations, parameters and initial conditions for the model are defined in the Materials and Methods section.

Presented below is a synopsis and assumptions of our model.

1. GSK3β is phosphorylated by the kinase CK1α and becomes less active.
2. GSK3β-P is dephosphorylated by Axin-P-activated PP2A.
3. Axin is phosphorylated and becomes more stable and active by non-phosphorylated GSK3β.

4. We keep track of Axin's synthesis and degradation since its turnover rate is comparable to the timescales of our model. On the other hand, GSK3β level is considered to be approximately constant as it is degraded very slowly [Lee2003].
5. The signal (Wnt) converts Axin-P (the active and more stable form) into Axin (less active and less stable form), resulting in lowering the amount of active destruction core complex.
6. We consider Axin-P to be the 'functional response' to the pathway, since this complex leads to the ubiquitination/degradation of β-catenin. When Axin-P is high, β-catenin is low and the pathway is off. When Axin-P is low, the pathway is on (β-catenin high).
7. The intensity of the signal is represented by a parameter *Sig,* which governs the rate of the reaction from Axin-P to Axin. In reality, it is Dsh, another component of the core complex that gets modified by the signal, leading to lesser amount of active complex. To simplify, we assume that the signal directly reduces the amount of active Axin in the complex (Axin-P) by a dephosphorylation event.

Bistability and hysteresis in the regulation of the destruction core complex and β-catenin accumulation: theory and experiments

We translate the above model (Figure 7) into a set of ordinary differential equations and solve them numerically (see Materials and Methods section for details).

A phase plane diagram of a dynamical system depicts the system's trajectories, and stable and unstable steady states in a state space of varying concentrations of the controlling variables. A nullcline for each variable is the set of points in the phase plane where the time derivative of that variable is zero (i.e. in the x, y plane, the nullcline for x is the curve for $dx/dt=0$ and for every

point on that curve, the vector field is vertical, since *dx/dt*=0 but *dy/dt* may be non-zero. Similarly there would be a *y*-nullcline). The points of intersection of the nullclines mark the steady states of the system. In order to determine the steady states in our molecular system, we plot the phaseplane for the two variables in our model, Atot and Ap corresponding to the total and phosphorylated Axin, respectively. The variable Ap corresponds to the active degradation complex wherein Axin is phosphorylated and stable, and GSK3β is dephosphorylated and active. High Ap means that the destruction complex is active thereby β-catenin is degraded. Conversely, low Ap indicates high levels of β-catenin. The curves in the diagram correspond to nullclines of Atot and Ap, respectively (Figure 8A). The nullcline for Atot (red line) is a straight line (see equations in section on Materials and Methods at the end of the chapter), whereas the nullcline for Ap (black lines) is N-shaped and its value depends on signal strength. For a given set of parameters, the points of intersection between the N-shaped curve and the straight line reveal the steady states present. We observe that in the absence of signal, the system has only one stable steady state with high levels of Ap (and hence low β-catenin) (curve corresponding to Signal=0 in Figure 8A); and for high signals (curve corresponding to Signal=3 in Figure 8A), the steady state is located at Ap=0, denoting that β-catenin concentrations are high and accumulating. The system is bistable for intermediate values of signal, Wnt (curves corresponding to Signal=1, 2 in Figure 8A), there are 3 steady states, two stable steady states (one with low Ap and one with high Ap values) and one unstable steady state at intermediate Ap values. This is in line with the experimental observation (as explained below) that the Wnt signaling pathway displays bimodality for intermediate values of the Wnt signal (Figure 4A).

To gain further insight into the fate of β-catenin accumulation in response to Wnt, we draw a signal-response curve (one-parameter bifurcation diagram; Figure 8B). A one-parameter bifurcation diagram shows the possible long-term behavior (steady states) of a system as a function of a parameter (signal) in the system. In this diagram, we track the system's response (concentration of the active destruction core complex, Ap) as a function of the signal (Wnt). Therefore, plotting steady state values of Ap against the signal strength (including strengths marked in Fig. 8A), we get the one-parameter bifurcation graph in Figure 8B. Together, these graphs would help describe the dynamics of free β-catenin. In the plot, the top and bottom curves in the profile correspond to stable steady states, whereas the connecting curve between SN1 and SN2 corresponds to an unstable steady state in the system. SN1 and SN2 are the two bifurcation points where the stable and unstable steady states come together and annihilate each other (Figure 8B). They are called the saddle node bifurcation points. The region of signal that lies between SN1 and SN2, where all three steady states (curves in Figure 8B) coexist defines the bistable regime for the system. In this region, the cells can either have high or low Ap (and hence low or high β-catenin). All points starting with initial conditions (for Ap) above the unstable steady state (line connecting SN1 and SN2) would be sucked into the basin of attraction of the higher stable steady state, while the points with initial conditions below the unstable steady state would be attracted towards the lower stable steady state. Each initial condition in the figure could correspond to a cell with different starting conditions and its final fate (level of Ap and hence level of β-catenin) would depend on the initial conditions of the system and its position with respect to the unstable steady state.

Although represented in our model as a deterministic system, in reality, the cells are

highly stochastic in nature, and there is a lot of variability in their individual behavior and response to signal. Due to this heterogeneity, at a given signal strength, for a population of cells, the level of Ap will show a bimodal distribution. Consider case 1 in Figure 8B, when the signal is low and the system is bistable with two stable steady states and one unstable saddle point. For this value of the signal, the majority of cells would have higher levels of Ap and only a few would have low Ap levels. This is due to the disparity in the basins of attraction for these two steady states (see bimodal distribution corresponding to case 1 in Figure 8B). Similarly, the logic can be followed for cases 2 and 3 in the bifurcation diagram and the corresponding bimodal distributions in Figure 8B. For increasing values of the signal parameter, the distribution favors lower levels of Ap, which corresponds to high β-catenin. Therefore, we infer that as signal strength increases, more and more cells in the population have lower Ap resulting in the accumulation of β-catenin. However, each individual cell would show β-catenin accumulation in an all-or none fashion (depending on its initial Ap level based on whether it was above or below the unstable steady state).

Hysteresis is a general property of dynamical systems with mutual activation (or antagonism) that follows bistability. It manifests in our model in the following manner. The value of Wnt signal that induces a transition from high to low Ap (low to high β-catenin) is quite different from the value needed to induce the reverse transition (SN2 and SN1 in Figure 8B, corresponding to ‘going up’ and ‘coming down’ panels in Figure 5). Once the system has been switched on (high β-catenin) by moving the signal across the bifurcation point, it cannot be switched off by reducing the signal back across the activation threshold in the opposite direction.

In contrast, non-hysteretic (ultrasensitive) switches behave differently, switching on and off at the same value of the signal [Tyson et al. 2003].

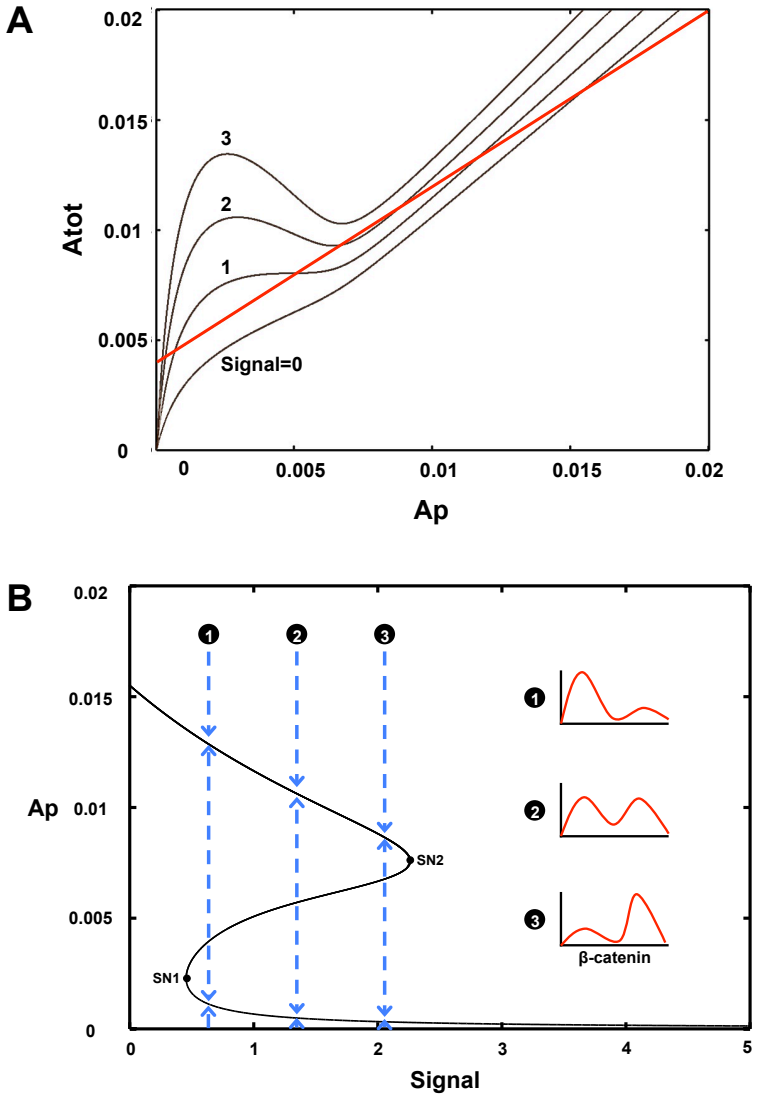

Figure 8. β-catenin shows bistability w.r.t varying Wnt signal.

A. Phaseplane analysis for different signal strengths. Only the Ap nullclines (black curves) shift in response to signal. The Atot nullcline (straight red line) does not depend on the signal parameter. **B**. One-parameter bifurcation diagram showing steady state values for the active destruction core complex, Ap, as a function of the signal (Wnt).

High levels of Ap correspond to low or no β-catenin, and low Ap corresponds to high β-catenin. The steady state that lies on the line connecting SN1 and SN2 is the unstable steady state. This line separates the set of initial conditions of Ap that would lead to one stable steady state or the other. (SN1 and SN2 are points where stable and unstable steady states collide and disappear. They are called saddle node bifurcation points) The blue arrows marked 1, 2 and 3 indicate the stable steady state that the system would finally reach based on the initial conditions for three specific signal strengths. Bimodal distributions with populations having either high or low β-catenin are drawn corresponding to these three cases.

These results and interpretation are thus consistent with the experiments described in the previous section, showing all-or-none behavior (Figure 3), bimodality for intermediate levels of signals (Figure 4A) and hysteresis (Figure 5) as captured by the saddle node bifurcations in the signal-response curve in Figure 8B.

Bistability and hysteresis, rather than a simple and sharp sigmoidal response, ensures that the system is not overly sensitive to the signal and that there is sufficient hysteresis and memory to prevent switching back and forth between the two states in the presence of small perturbations. The source of bistability is a positive feedback. In our small model, it is the loop corresponding to GSK3β phosphorylation of Axin, which in turn causes the dephosphorylation and activation of GSK3β, leading to further Axin phosphorylation and stabilization (highlighted by the red arrow in Figure 7).

There is also evidence for an alternate source for positive feedback upstream of destruction core complex in the form of receptor clustering of LRP5/6 in response to Wnt signal [Bilic et al, 2007]. However, we have only considered the former source of positive feedback and bistability in our model. We expect the addition of the latter motif to our network or replacing the current motif with the latter to result in similar overall dynamics of the system.

Bistability in response to LiCl, a synthetic activator of the Wnt signaling pathway

In the experiments performed by Thorne and Lee in Figure 4B, LiCl is used as a synthetic activator of the Wnt pathway as it inhibits GSK3β similar to the ligand Wnt3a, and leads to β-catenin accumulation [Klein and Melton, 1996; Lee et al, 2003]. This observation was emulated using our mathematical model (Figure 9). LiCl=1 in our model corresponds to 20mM LiCl in experiments.

Two-parameter bifurcation diagram for β-catenin accumulation in response to increase in Signal strength and LiCl concentration: Similar to the analysis for Wnt signal, we plot the phase plane of the system for various concentrations of LiCl (Figure 9A), and the corresponding one- (Figure 9B) and two-parameter bifurcation diagrams (Figure 9C).

In the one-parameter bifurcation diagram (Figure 9B), signal (Wnt) strength is zero, and we follow how the steady state of the control system changes as LiCl is varied. We obtain two saddle node points SN1 and SN2, which defines the bistable region (green region in Figure 9B). For the two-parameter diagram (Figure 9C), we follow the two saddle nodes SN1 and SN2 as signal strength is increased. Then Wnt signal is applied, the control system responds and the location of the saddle nodes change (i.e. they will occur at different LiCl concentration). As Figure 9C shows, the bistable region is shifted to lower LiCl concentration. That means, in the presence of signal, less LiCl is needed to trigger β-catenin accumulation (from high Ap, low β-catenin state to low Ap, high β-catenin state).

The two-parameter bifurcation diagram in Figure 9C indicates that in the parameter space of signal strength and LiCl, our model shows that there are three regions that the control system

can reside in: (i) the monostable region with high Ap (orange region) when both signal and LiCl are low (this is the region where β-catenin is degraded), (ii) the bistable region (green region) for intermediate values of Signal and LiCl (region where the control system will display bimodal β-catenin distribution), and (iii) monostable region with low Ap (blue region) when either LiCl (>3) or signal (>2) is high (region where β-catenin accumulates).

The predictions derived from the two-parameter diagram of our model (Figure 9C) are consistent quantitatively with the experiments by Thorne and Lee described in Figure 4A (bimodal distribution of β-catenin in the presence of signal) and Figure 4B (bimodal distribution of β-catenin in the presence of LiCl), and the model agrees qualitatively (though not quantitatively) to the experiment shown in Figure 5 (hysteresis).

Experiment in Figure 4A shows the behavior of the system in presence of signal alone. The system is monostable (with low β-catenin) when Wnt3a is 0, bistable (with two populations of cells having high and low β-catenin, respectively) when Wnt3a ranges from 2-8, and monostable again (with low β-catenin) when Wnt3a is greater than 10. In our model, the horizontal axis in Figure 9C corresponds to no LiCl and varying signal strength. If we assign signal=1 (in our model) to be equivalent to Wnt3a=4 (in experiments), then our prediction that the system is bistable in the region where signal=0.5-2.2 (corresponding to Wnt3a=2-8.8) would agree quantitatively with experimental observations.

Experiment in Figure 4B shows the behavior of the system in the presence of LiCl alone (absence of signal). The system is bistable in the region of LiCl=20-60mM (Figure 4B). These conditions correspond to the vertical axis in Figure 9C. Our model shows that the bistable region is from LiCl = 0.6 to 3. If we assign LiCl=1 in model to 20mM (in experiments), the predicted

region of bistability would be from 12-60mM, which would be in perfect agreement with the observations made (Figure 4B).

The model is also in qualitative agreement with the hysteresis experiment shown in Figure 5 in the absence of LiCl. If the previous assignment of signal=1 corresponding to Wnt3a=4 is considered, the region of bistability (when LiCl is absent and signal is applied corresponding to the horizontal axis in Figure 9C) would have to be roughly bounded by Wnt3a values of 2 and 8.8. Figure 5 indicates that the control system shows hysteresis behavior that the threshold values of signal to trigger β-catenin accumulation is higher than the threshold value of signal to keep β-catenin accumulated. However, the 'going up' and 'coming down' thresholds in Figure 5 are ~6 and ~1. They are slightly shifted in values and are not in quantitative agreement with the simulation results or the experimental results shown in Figure 4A.

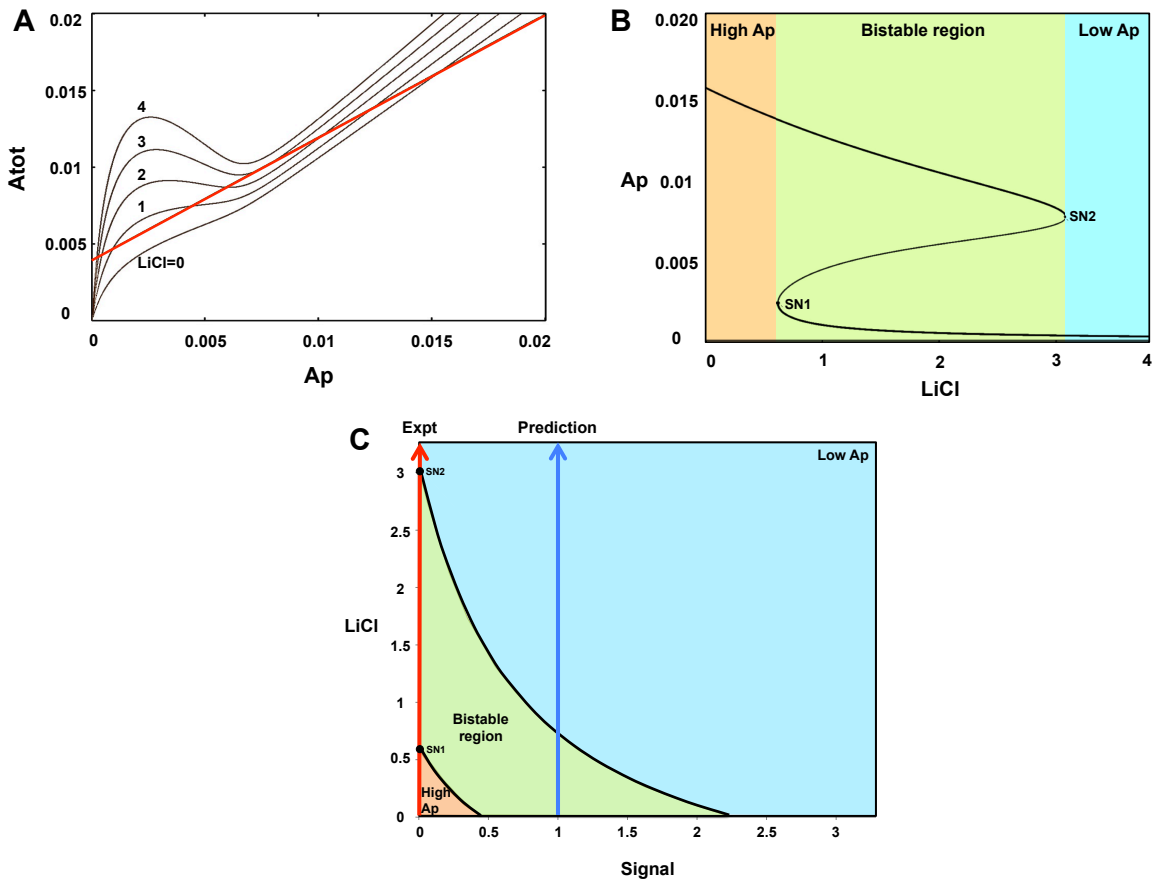

Figure 9. β-catenin shows bistability w.r.t varying LiCl concentration.

A. Phaseplane for different concentrations of LiCl (Signal=0). **B**. One-parameter bifurcation diagram showing the active destruction core complex, Ap, as a function of LiCl concentration drawn at constant signal=0. **C**. Two-parameter bifurcation diagram of LiCl vs. Signal (IWR=0). The vertical red arrow corresponds to the experiment described in Figure 4B, the horizontal red arrow corresponds to the experiments described in Figures 4A and 5, and the vertical blue arrow corresponds to a prediction made (described in the main text). In both B and C, the orange, green and blue regions correspond to high Ap (low β-catenin), bistable and low Ap (high β-catenin) regions respectively. Notations used are similar to Figures 8A and B, respectively).

In addition to mirroring the experiments, the model also predicts the behavior of the system in response to increasing LiCl, but in the presence of an intermediate level of Wnt signal

(blue arrow in Figure 9C). If the experiment starts with signal strength high enough for the model to be bistable (corresponding to Wnt3a=4 in Figure 4A for which β-catenin shows bimodal distribution) even with no LiCl ('green' region in Figure 9C), then increasing LiCl concentration would cause the system to eventually leave the bistable regime and reach the monostable steady state of low Ap and high β-catenin ('blue' region in Figure 9C). At this stage, even if LiCl is washed off, the system will remain in the low Ap state (as a single peak), and β-catenin would remain stable throughout while traversing from the monostable to the bistable region, with low Ap in both.

β-catenin response to Axin-stabilizer, IWR-1

As mentioned earlier, Thorne and Lee tested the role of Axin's stability in positive feedback and bistability of Wnt signaling (Figure 6). They treated RKO cells with the small molecule IWR-1 that stabilizes Axin by blocking its ubiquitination and degradation [Chen et al, 2009]. Based on the distribution of β-catenin levels in the population, they inferred that addition of IWR-1 did result in seemingly a loss of bistability leading to a graded response in β-catenin accumulation (Figure 6; Thorne and Lee, personal communication).

Therefore, using our mathematical model, we next address the effect of IWR on β-catenin accumulation. Figure 10 shows the two-parameter bifurcation diagram (LiCl vs. IWR-1) of the control system in the absence of signal. In the absence of IWR, the scenario would be as described in the previous section (Figure 4B, red arrow at IWR=0 in Figure 10). Increasing LiCl would cause the system to traverse from the region with high Ap through the bistable regime to the region with low Ap.

However, contrary to current experimental observations, we believe that addition of IWR would not remove bistability. Instead we believe that the bistable region becomes wider and shifts towards higher concentration of LiCl. We consistently only observe a shift in the location of the bistable region towards higher concentrations of LiCl (red arrow at IWR=1 in Figure 10). Indeed, if one looks at the data closely, although the fourth and fifth tracing show no bimodal distribution, one can still notice two peaks in the very last tracing in Figure 6 (LiCl=80mM), where the system is exposed to the highest LiCl concentration. Based on our bifurcation analysis (Figure 10), we expect to see a bimodal distribution of β-catenin for LiCl=2-10 (LiCl=40-200mM), corresponding to the last three tracings in Figure 6.

These results were followed up with experiments by our collaborators (Thorne and Lee), because they were in contradiction with the first set of findings (Figure 6). The second set of experiments was in agreement with our predictions (data not shown, personal communication). We further predict that an additional increase in the concentration of LiCl in the same experiment would make the system exit the bistable region resulting in low Ap and high concentration of β-catenin (horizontal blue arrow following the red arrow at IWR=1 marked as 'Prediction 1' in Figure 10).

The two-parameter bifurcation diagram also shows that the region with high Ap widens for higher values of IWR ('orange' region in Figure 10), and this agrees with the experimental observations (Figures 4B, 6). This means that in the presence of IWR, higher concentrations of LiCl are needed to enter the bistable regime. Comparing Figures 4B and 6, in the LiCl experiment without IWR-1, the population of cells starts to display bimodality even at 20mM of LiCl, whereas in the experiment in the presence of IWR-1, the system is still monostable for

LiCl=20mM with high Ap. In the absence of IWR-1, for LiCl=80mM, the system is monostable with low Ap, whereas in the presence of IWR-1, the system is in the bimodal region. Our model, therefore, recapitulates this shift in the onset of bistability in response to IWR-1 (starting of 'green' region in Figure 10).

Yet another prediction from this analysis is about the behavior of the system with increasing concentration of IWR at a constant, sufficiently high LiCl (e.g. the end point of the experiment in Figure 4B): when IWR is increased, we speculate that the system will transition from the low Ap state (with β-catenin accumulated), through the bistable region, to end up in the state of high Ap (with β-catenin degraded) (vertical blue arrow marked as 'Prediction 2' in Figure 10). Experimental confirmation of this behavior would validate our model.

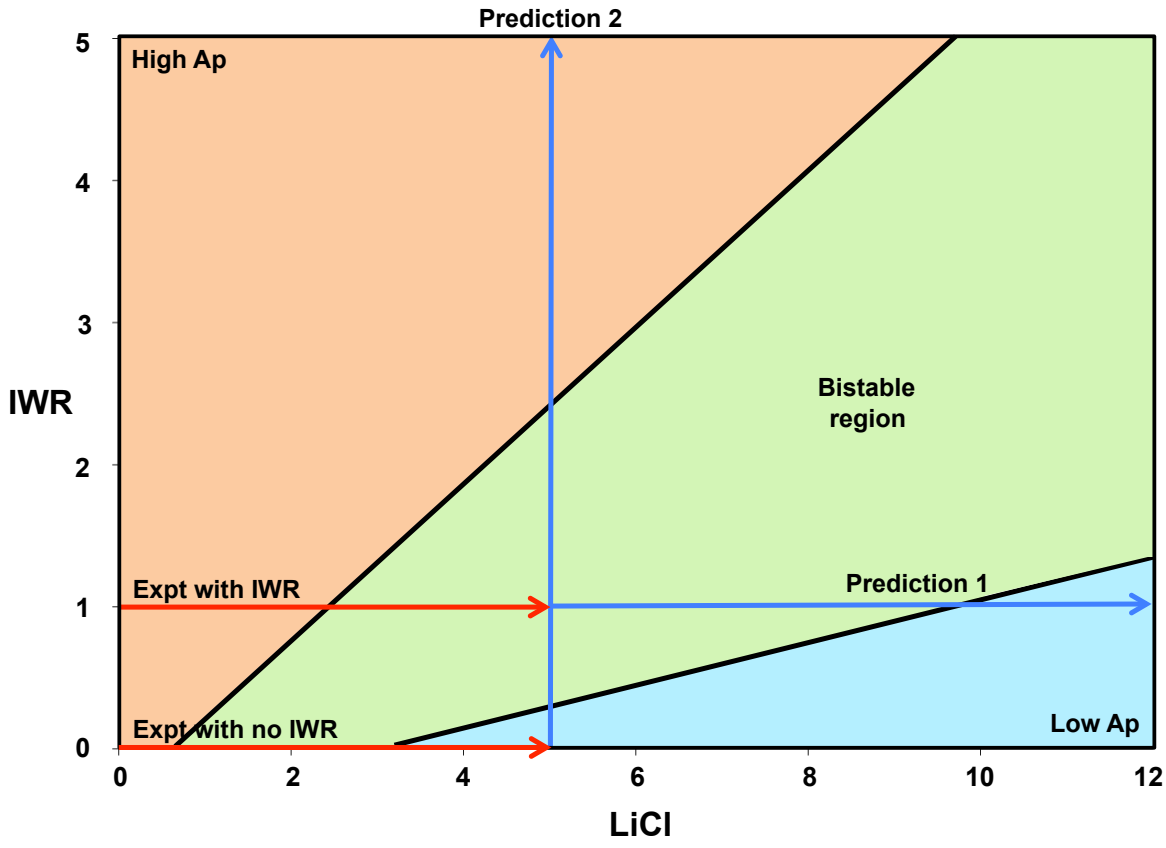

Figure 10. Effect of Axin stabilizer, IWR.

The figure shows a two-parameter bifurcation diagram of IWR vs. LiCl (signal=0). The orange, green and blue regions correspond to high Ap, bistable and low Ap regions, respectively. The red and blue arrows correspond to experiments and predictions, respectively. The two red arrows at IWR equal to 1 and 0 correspond to the experiments described in Figures 6 and 4B in the presence and absence of IWR, respectively. The horizontal and vertical blue arrows correspond to predictions 1 and 2 respectively and have been described in the main text.

Along with the two-parameter bifurcation diagram (Figure 10), the one-parameter bifurcation diagram for Ap vs. Signal for different values of IWR (Figure 11A) makes it evident that increase in IWR-1 concentration makes the bistable region larger and shifts it to higher concentrations of Wnt signal. A similar prediction is made about shift to higher LiCl levels using

a one-parameter bifurcation diagram w.r.t LiCl (data not shown). This prediction has been confirmed by some preliminary experiments shown in Figure 11B. The blue, red and green curves corresponding to three different concentrations of IWR can be compared across Figures 11A and B. It can be noted from the figure that for higher concentration of IWR-1, the threshold for the accumulation of β-catenin shifts to a higher value of the signal, Wnt3a. This compares well with the shift in thresholds for the accumulation of β-catenin (corresponding to thresholds for high Ap to low Ap transition) for different values of IWR in the model (Figure 11A,B). The different thresholds for moving from high to low Ap in Figure 11A correspond to the activation thresholds for the accumulation of β-catenin shown in the inset in Figure 11B. We observe that these activation thresholds shift to the right for higher IWR values.

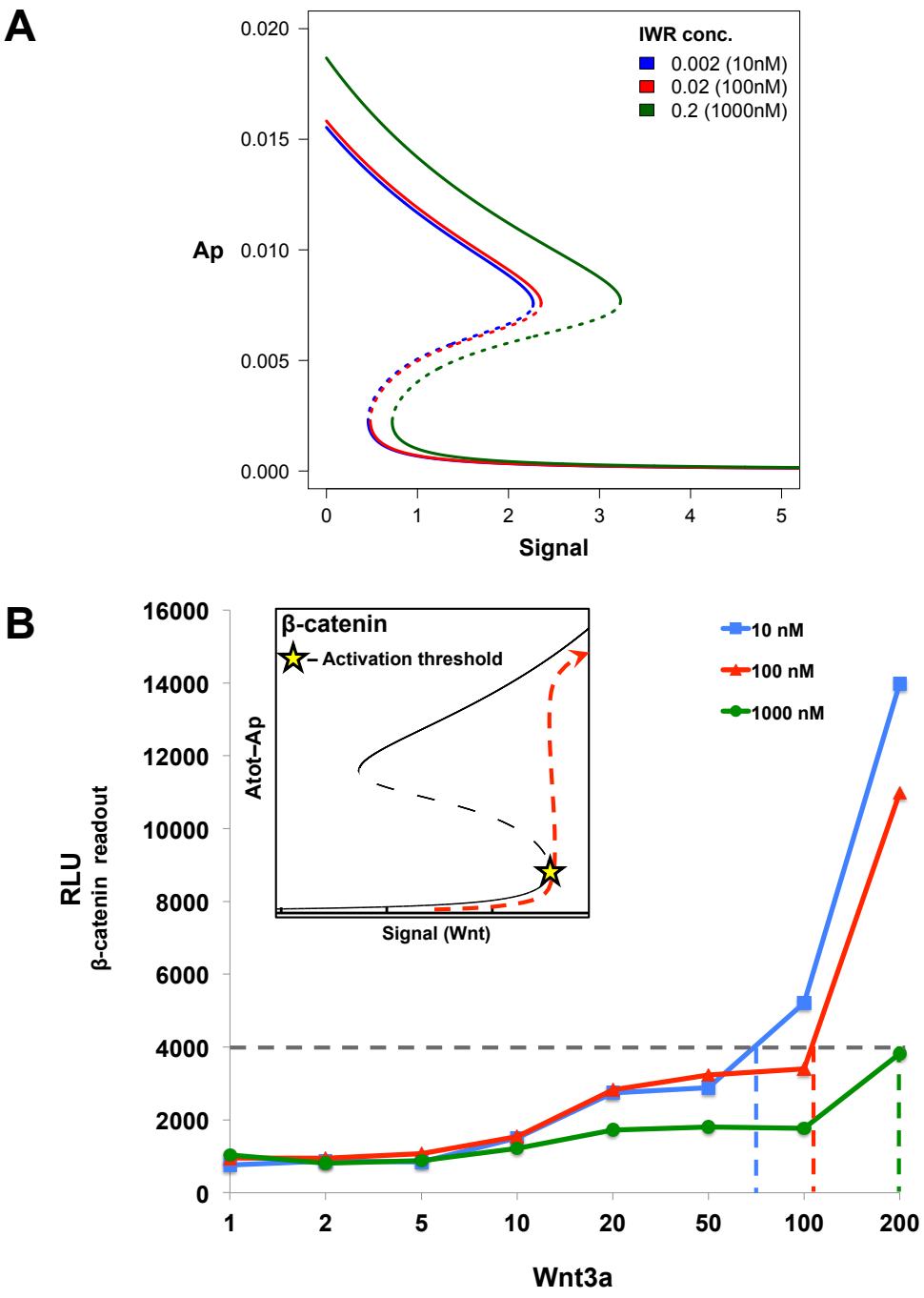

Figure 11. Effect of IWR on dose-response curves w.r.t Signal (Wnt).

A. Model. One-parameter bifurcation diagram showing the active destruction core complex, Ap, as a function of Signal for three different concentrations of IWR. **B.** Experiment (Redrawn with raw data from Thorne and Lee, unpublished results, used with permission). RKO cells were treated with different concentrations of IWR-1 (10,

100, 1000 nM) and dose-response curves were plotted against Wnt3a. Relative Light Units (RLU) of a luciferase gene driven by the TCF promoter, a target of β-catenin, is plotted on the y-axis. The dotted lines are drawn to identify the value of Wnt3a corresponding to the activation threshold at which β-catenin starts to accumulate happens for different concentrations of IWR-1. The inset includes a cartoon to show what we mean by the activation threshold w.r.t β-catenin accumulation.

Conclusions and Future directions

Our model in tandem with experimental evidences performed in RKO cells (by Thorne and Lee, personal communication) suggests the existence of a bistable switch in the Wnt/β-catenin pathway in contrast to the traditional interpretation of a graded response. We show that the dynamics of a simplified representation of the core control system captures that of the characteristic features of the whole pathway. The β-catenin responses with respect to the ligand, Wnt3a (Figures 3, 4A,B), as well the synthetic activator, LiCl (Figure 5), are captured by the model in quantitative detail. The model also predicted the β-catenin response with regard to the Axin stabilizer, IWR-1 for different concentrations of LiCl (that proved to be correct as well despite initial disagreement between the two) and signal, Wnt.

The predictions described in the text (Figures 9, 10) remain to be validated in RKO cells as well as a more physiologically relevant cell type like the HCEC (Human Colonic Epithelial Cells). Confirming our predictions would further validate the model and allow us to add further details related to the dynamics of the model. These details could include a second positive feedback loop based on receptor clustering or a negative feedback arising from Wnt targets such as Axin2. On the experimental front, it might also be useful to perform knockout/knockdown studies perturbing one or more of these feedback loops to understand their compound effects on the overall dynamics of β-catenin accumulation. Addition of other components of the Wnt pathway described in Lee2003 may improve the model and aid in making more physiologically relevant predictions.

Materials and Methods

Mathematical model

The model is described by a set of ordinary differential equations for total and phosphorylated Axin. The unphosphorylated and active form of GSK3β is governed by a Goldbeter-Koshland function that gives rise to ultrasensitivity (Goldbeter and Koshland, 1981). The initial conditions for the system are taken from experiments (Lee et al, 2003).

Equations and kinetic constants

Function definition (GK=Goldbeter-Koshland function)

$$BB(Va, Vi, Ja, Ji) = Vi - Va + Ja * Vi + Ji * Va$$

$$GK(Va, Vi, Ja, Ji) = 2 * Ji * \frac{Va}{(BB(Va, Vi, Ja, Ji) + \sqrt{(BB(Va, Vi, Ja, Ji)^2 - 4 * (Vi - Va) * Ji * Va))}}$$

Equation for GSK3β

$$G = Gtot * GK(khg * Ap, kpg * Kin, Lg * Gtot, Lg * Gtot)$$

Equations for different forms of Axin

$$\frac{dAp}{dt} = (kpa' * Gtot + kpa * G) * \frac{(Atot - Ap)}{(1 + LiCl)} - (kha' + kha * Sig + kd2) * Ap$$

$$\frac{dAtot}{dt} = ks1 - kd1 * \frac{Atot}{(1 + IWR)} + (kd1 - kd2) * \frac{Ap}{(1 + IWR)}$$

aux $percentG = \frac{G}{Gtot}$

Parameters

$Sig = 0, LiCl = 0, IWR = 0$
$ks1 = 8 \cdot 10^{-5}, kd1 = 0.02, kd2 = 0.004$
$kha' = 0.04, kha = 0.06$
$kpa' = 0.0002, kpa = 0.016$
$khg = 0.03, kpg = 0.002, Lg = 0.002, Kin = 0.1$
$Gtot = 50$

Initial Conditions

$Ap = 0.02, Atot = 0.02$

Computer simulations

We used the computer programs XPPaut (developed by G. Bard Ermentrout) and Oscill8 (developed by Emery Conrad), to solve the differential equations numerically, plot the phase planes and also draw one and two-parameter bifurcation diagrams.

References

Amit S, Hatzubai A, Birman Y, Andersen JS, Ben-Shushan E, Mann M, Ben-Neriah Y, Alkalay I. Axin-mediated CKI phosphorylation of beta-catenin at Ser 45: a molecular switch for the Wnt pathway. Genes Dev. 2002 May 1;16(9):1066-76.PubMed [citation] PMID: 12000790, PMCID: PMC186245

Baker JC, Beddington RS, Harland RM. Wnt signaling in Xenopus embryos inhibits bmp4 expression and activates neural development. Genes Dev. 1999 Dec 1;13(23):3149-59.PubMed [citation] PMID: 10601040, PMCID: PMC317181

Barker N, van Es JH, Kuipers J, Kujala P, van den Born M, Cozijnsen M, Haegebarth A, Korving J, Begthel H, Peters PJ, Clevers H. Identification of stem cells in small intestine and colon by marker gene Lgr5. Nature. 2007 Oct 25;449(7165):1003-7. Epub 2007 Oct 14.PubMed [citation] PMID: 17934449

Behrens J, Jerchow BA, Würtele M, Grimm J, Asbrand C, Wirtz R, Kühl M, Wedlich D, Birchmeier W. Functional interaction of an axin homolog, conductin, with beta-catenin, APC, and GSK3beta. Science. 1998 Apr 24;280(5363):596-9.PubMed [citation] PMID: 9554852

Bilic J, Huang YL, Davidson G, Zimmermann T, Cruciat CM, Bienz M, Niehrs C. Wnt induces LRP6 signalosomes and promotes dishevelled-dependent LRP6 phosphorylation. Science. 2007 Jun 15;316(5831):1619-22.PubMed [citation] PMID: 17569865

Chaves M, Albert R. Studying the effect of cell division on expression patterns of the segment polarity genes. J R Soc Interface. 2008 Aug 6;5 Suppl 1:S71-84. PubMed PMID: 18434279; PubMed Central PMCID: PMC2706454.

Chen B, Dodge ME, Tang W, Lu J, Ma Z, Fan CW, Wei S, Hao W, Kilgore J, Williams NS, Roth MG, Amatruda JF, Chen C, Lum L. Small molecule-mediated disruption of

Wnt-dependent signaling in tissue regeneration and cancer. Nat Chem Biol. 2009 Feb;5(2):100-7. Epub 2009 Jan 4.PubMed [citation] PMID: 19125156, PMCID: PMC2628455

Choi SC, Han JK. Xenopus Cdc42 regulates convergent extension movements during gastrulation through Wnt/Ca2+ signaling pathway. Dev Biol. 2002 Apr 15;244(2):342-57.PubMed [citation] PMID: 11944942

Croce JC, McClay DR. Evolution of the Wnt pathways. Methods Mol Biol. 2008;469:3-18.PubMed [citation] PMID: 19109698, PMCID: PMC3052202

Goentoro L, Kirschner MW. Evidence that fold-change, and not absolute level, of beta-catenin dictates Wnt signaling. Mol Cell. 2009 Dec 11;36(5):872-84.PubMed [citation] PMID: 20005849, PMCID: PMC2921914

Gordon MD, Nusse R. Wnt signaling: multiple pathways, multiple receptors, and multiple transcription factors. J Biol Chem. 2006 Aug 11;281(32):22429-33. Epub 2006 Jun 22. Review. No abstract available. PubMed [citation] PMID: 16793760

Habas R, Dawid IB, He X. Coactivation of Rac and Rho by Wnt/Frizzled signaling is required for vertebrate gastrulation. Genes Dev. 2003 Jan 15;17(2):295-309.PubMed [citation] PMID: 12533515, PMCID: PMC195976

Hamada F, Tomoyasu Y, Takatsu Y, Nakamura M, Nagai S, Suzuki A, Fujita F, Shibuya H, Toyoshima K, Ueno N, Akiyama T. Negative regulation of Wingless signaling by D-axin, a Drosophila homolog of axin. Science. 1999 Mar 12;283(5408):1739-42.PubMed [citation] PMID: 10073940

He TC, Sparks AB, Rago C, Hermeking H, Zawel L, da Costa LT, Morin PJ, Vogelstein B, Kinzler KW. Identification of c-MYC as a target of the APC pathway. Science. 1998 Sep 4;281(5382):1509-12.PubMed [citation] PMID: 9727977

Hogenesch JB, Ueda HR. Understanding systems-level properties: timely stories from the study of clocks. Nat Rev Genet. 2011 Jun;12(6):407-16. Epub 2011 May 10. Review. PubMed PMID: 21556016.

Itoh K, Krupnik VE, Sokol SY.Axis determination in Xenopus involves biochemical interactions of axin, glycogen synthase kinase 3 and beta-catenin. Curr Biol. 1998 May 7;8(10):591-4.PubMed [citation] PMID: 9601644

Jho EH, Zhang T, Domon C, Joo CK, Freund JN, Costantini F. Wnt/beta-catenin/Tcf signaling induces the transcription of Axin2, a negative regulator of the signaling pathway. Mol Cell Biol. 2002 Feb;22(4):1172-83.PubMed [citation] PMID: 11809808, PMCID: PMC134648

Kim JS, Crooks H, Dracheva T, Nishanian TG, Singh B, Jen J, Waldman T. Oncogenic beta-catenin is required for bone morphogenetic protein 4 expression in human cancer cells.Cancer Res. 2002 May 15;62(10):2744-8.PubMed [citation] PMID: 12019147

Kimelman D, Xu W. beta-catenin destruction complex: insights and questions from a structural perspective. Oncogene. 2006 Dec 4;25(57):7482-91. Review.PubMed [citation] PMID: 17143292

Klein PS, Melton DA. A molecular mechanism for the effect of lithium on development. Proc Natl Acad Sci U S A. 1996 Aug 6;93(16):8455-9.PubMed [citation] PMID: 8710892, PMCID: PMC38692

Kofahl B, Wolf J. Mathematical modelling of Wnt/β-catenin signalling. Biochem Soc Trans. 2010 Oct;38(5):1281-5.PubMed [citation] PMID: 20863299

Krüger R, Heinrich R. Model reduction and analysis of robustness for the Wnt/beta-catenin signal transduction pathway. Genome Inform. 2004;15(1):138-48.PubMed [citation] PMID: 15712117

Kühl M, Sheldahl LC, Park M, Miller JR, Moon RT. The Wnt/Ca2+ pathway: a new vertebrate Wnt signaling pathway takes shape. Trends Genet. 2000 Jul;16(7):279-83. Review.PubMed [citation] PMID: 10858654

Lee E, Salic A, Krüger R, Heinrich R, Kirschner MW. The roles of APC and Axin derived from experimental and theoretical analysis of the Wnt pathway. PLoS Biol. 2003 Oct;1(1):E10. Epub 2003 Oct 13. Erratum in: PLoS Biol. 2004 Mar;2(3):E89. PubMed [citation] PMID: 14551908, PMCID: PMC212691

Liu C, Li Y, Semenov M, Han C, Baeg GH, Tan Y, Zhang Z, Lin X, He X. Control of beta-catenin phosphorylation/degradation by a dual-kinase mechanism. Cell. 2002 Mar 22;108(6):837-47.PubMed [citation] PMID: 11955436

Liu P, Wakamiya M, Shea MJ, Albrecht U, Behringer RR, Bradley A. Requirement for Wnt3 in vertebrate axis formation. Nat Genet. 1999 Aug;22(4):361-5.PubMed [citation] PMID: 10431240

Lustig B, Jerchow B, Sachs M, Weiler S, Pietsch T, Karsten U, van de Wetering M, Clevers H, Schlag PM, Birchmeier W, Behrens J. Negative feedback loop of Wnt signaling through upregulation of conductin/axin2 in colorectal and liver tumors. Mol Cell Biol. 2002 Feb;22(4):1184-93.PubMed [citation] PMID: 11809809, PMCID: PMC134640

MacDonald BT, Tamai K, He X. Wnt/beta-catenin signaling: components, mechanisms, and diseases. Dev Cell. 2009 Jul;17(1):9-26. Review.PubMed [citation] PMID: 19619488, PMCID: PMC2861485

Nusse R. WNT targets. Repression and activation. Trends Genet. 1999 Jan;15(1):1-3. Review.PubMed [citation] PMID: 10087922

Papkoff J, Rubinfeld B, Schryver B, Polakis P. Wnt-1 regulates free pools of catenins and stabilizes APC-catenin complexes. Mol Cell Biol. 1996 May;16(5):2128-34.PubMed [citation] PMID: 8628279, PMCID: PMC231200

Polakis P. The many ways of Wnt in cancer. Curr Opin Genet Dev. 2007 Feb;17(1):45-51. Review.PubMed [citation] PMID: 17208432

Roose J, Huls G, van Beest M, Moerer P, van der Horn K, Goldschmeding R, Logtenberg T, Clevers H. Synergy between tumor suppressor APC and the beta-catenin-Tcf4 target Tcf1. Science. 1999 Sep 17;285(5435):1923-6.PubMed [citation] PMID: 10489374

Saif MW, Chu E. Biology of colorectal cancer. Cancer J. 2010 May-Jun;16(3):196-201. Review.PubMed [citation] PMID: 20526096

Schlessinger K, McManus EJ, Hall A. Cdc42 and noncanonical Wnt signal transduction pathways cooperate to promote cell polarity. J Cell Biol. 2007 Jul 30;178(3):355-61. Epub 2007 Jul 23.PubMed [citation] PMID: 17646398, PMCID: PMC2064837

Sen M, Ghosh G. Transcriptional outcome of Wnt-Frizzled signal transduction in inflammation: evolving concepts. J Immunol. 2008 Oct 1;181(7):4441-5. Review.PubMed [citation] PMID: 18802045

Sheldahl LC, Slusarski DC, Pandur P, Miller JR, Kühl M, Moon RT. Dishevelled activates Ca2+ flux, PKC, and CamKII in vertebrate embryos. J Cell Biol. 2003 May 26;161(4):769-77.PubMed [citation] PMID: 12771126, PMCID: PMC2199364

Shtutman M, Zhurinsky J, Simcha I, Albanese C, D'Amico M, Pestell R, Ben-Ze'ev A. The cyclin D1 gene is a target of the beta-catenin/LEF-1 pathway. Proc Natl Acad Sci U

S A. 1999 May 11;96(10):5522-7.PubMed [citation] PMID: 10318916, PMCID: PMC21892

Spencer SL, Sorger PK. Measuring and modeling apoptosis in single cells. Cell. 2011 Mar 18;144(6):929-36. Review. PubMed [citation] PMID: 21414484

Strutt D. Frizzled signalling and cell polarisation in Drosophila and vertebrates. Development. 2003 Oct;130(19):4501-13. Review. PubMed [citation] PMID: 12925579

Tetsu O, McCormick F. Beta-catenin regulates expression of cyclin D1 in colon carcinoma cells. Nature. 1999 Apr 1;398(6726):422-6.PubMed [citation] PMID: 10201372

Tyson JJ, Chen KC, Novak B. Sniffers, buzzers, toggles and blinkers: dynamics of regulatory and signaling pathways in the cell. Curr Opin Cell Biol. 2003 Apr;15(2):221-31. Review. PubMed PMID: 12648679.

Veeman MT, Axelrod JD, Moon RT. A second canon. Functions and mechanisms of beta-catenin-independent Wnt signaling. Dev Cell. 2003 Sep;5(3):367-77. Review.PubMed [citation] PMID: 12967557

Wawra C, Kühl M, Kestler HA. Extended analyses of the Wnt/beta-catenin pathway: robustness and oscillatory behaviour. FEBS Lett. 2007 Aug 21;581(21):4043-8. Epub 2007 Jul 27.PubMed [citation] PMID: 17678900

Yamamoto H, Kishida S, Kishida M, Ikeda S, Takada S, Kikuchi A. Phosphorylation of axin, a Wnt signal negative regulator, by glycogen synthase kinase-3beta regulates its stability.J Biol Chem. 1999 Apr 16;274(16):10681-4.PubMed [citation] PMID: 10196136

Yan D, Wiesmann M, Rohan M, Chan V, Jefferson AB, Guo L, Sakamoto D, Caothien RH, Fuller JH, Reinhard C, Garcia PD, Randazzo FM, Escobedo J, Fantl WJ, Williams

LT.Elevated expression of axin2 and hnkd mRNA provides evidence that Wnt/beta-catenin signaling is activated in human colon tumors. Proc Natl Acad Sci U S A. 2001 Dec 18;98(26):14973-8.PubMed [citation] PMID: 11752446, PMCID: PMC64968

Yanagawa S, Matsuda Y, Lee JS, Matsubayashi H, Sese S, Kadowaki T, Ishimoto A. Casein kinase I phosphorylates the Armadillo protein and induces its degradation in Drosophila. EMBO J. 2002 Apr 2;21(7):1733-42.PubMed [citation] PMID: 11927557, PMCID: PMC125941

Yochum GS, McWeeney S, Rajaraman V, Cleland R, Peters S, Goodman RH. Serial analysis of chromatin occupancy identifies beta-catenin target genes in colorectal carcinoma cells. Proc Natl Acad Sci U S A. 2007 Feb 27;104(9):3324-9. Epub 2007 Feb 21.PubMed [citation] PMID: 17360646, PMCID: PMC1805576

Zhang Z, Deb A, Zhang Z, Pachori A, He W, Guo J, Pratt R, Dzau VJ. Secreted frizzled related protein 2 protects cells from apoptosis by blocking the effect of canonical Wnt3a. J Mol Cell Cardiol. 2009 Mar;46(3):370-7. Epub 2008 Dec 9.PubMed [citation] PMID: 19109969, PMCID: PMC2710029

Conclusions

Over the past 25 years, geneticists and molecular biologists have uncovered many molecular details of the regulation of cell cycle events, including the START transition in budding yeast. We have attempted to reconcile all these findings into a comprehensive model of the START transition. Our model successfully accounts for the observed phenotypes of more than 100 START mutants and for the known subcellular localization and translocation of transcription factors (SBF and MBF) involved in the START transition. Our model also provides a basic mechanism for size control. We believe that cell biologists and molecular geneticists can benefit from our work by using our validated model to make novel predictions and by testing the predictions. In the future, the model can be expanded by inclusion of new experimental findings. The model can also be simplified to represent a generic mechanism underlying START, or it can be extended to represent the R-point in the mammalian cell cycle. Another fertile avenue for future work is the addition of mechanistic details necessary to explain nutritional conditions that modulate the size control mechanism.

The Wnt signaling pathway is another regulatory process that plays a key role in cell proliferation and development. We have built a simple mathematical model to characterize an important dynamical property of this pathway, bistability. The model explains the response of the downstream transcriptional coactivator, β-catenin, to signal (Wnt), to a Wnt mimic (LiCl) and to a stabilizer (IWR-1) of the core protein, Axin. We have made predictions from the model, and experimental validations are currently underway. These validations would corroborate our model and help in discerning the dynamics of the signaling pathway. These follow-up experiments will most likely reveal

further details and stimulate development of an improved model of the Wnt signaling pathway.

Copyright Clearance Center

Confirmation Number: 10744453
Order Date: 12/18/2011

Customer Information

Customer: Janani Ravi
Account Number: 3000479779
Organization: Janani Ravi
Email: janani@vt.edu
Phone: +1 (540)8089055
Payment Method: Credit Card ending in 0488

Order Details

MOLECULAR BIOLOGY OF THE CELL. ONLINE

Billing Status:
Charged to Credit Card

Order detail ID:	59644300
ISSN:	1939-4586
Publication year:	2004
Publication Type:	Other
Publisher:	AMERICAN SOCIETY FOR CELL BIOLOGY
Rightsholder:	AMERICAN SOCIETY FOR CELL BIOLOGY
Author/Editor:	Katherine C. Chen

Permission Status: **Granted**

Permission type:	Republish or display content
Type of use:	Dissertation
Requested use:	Dissertation
Republishing organization:	Virginia Tech
Organization status:	Non-profit 501(c)(3)
Republication date:	12/25/2011
Circulation/ Distribution:	1
Type of content:	Figure/ diagram/ table
Description of requested content:	Integrative Analysis of Cell Cycle Control in Budding Yeast
Page range(s):	2
Translating to:	No Translation
Requested content's publication date:	05/15/2004
Payment Method:	CC ending in 488

$ 3.50

Total order items: 1

Order Total: $3.50

AMERICAN SOCIETY FOR MICROBIOLOGY LICENSE TERMS AND CONDITIONS

Dec 19, 2011

This is a License Agreement between Janani Ravi ("You") and American Society for Microbiology ("American Society for Microbiology") provided by Copyright Clearance Center ("CCC"). The license consists of your order details, the terms and conditions provided by American Society for Microbiology, and the payment terms and conditions.

All payments must be made in full to CCC. For payment instructions, please see information listed at the bottom of this form.

License Number	2812720947249
License date	Dec 19, 2011
Licensed content publisher	American Society for Microbiology
Licensed content publication	Journal of Bacteriology
Licensed content title	Asymmetrical division of Saccharomyces cerevisiae.
Licensed content author	P G Lord, A E Wheals
Licensed content date	Jun 1, 1980
Volume	142
Issue	3
Start page	808
End page	818
Type of Use	Dissertation/Thesis
Format	Electronic
Portion	Figures/tables/images
Number of figures/tables	2
Order reference number	
Title of your thesis / dissertation	Mathematical modeling of pathways involved in cell cycle regulation and differentiation
Expected completion date	Dec 2011
Estimated size(pages)	185
Billing Type	Invoice
Billing address	Perry Street, Derring Hall 5076 BLACKSBURG, VA 24061 United States
Customer reference info	